

University of Louisville

ThinkIR: The University of Louisville's Institutional Repository

Electronic Theses and Dissertations

5-2015

Development of a surrogate bruising detection system to describe potential bruising patterns associated with common childhood falls.

Raymond Dsouza
University of Louisville

Follow this and additional works at: <https://ir.library.louisville.edu/etd>



Part of the [Mechanical Engineering Commons](#)

Recommended Citation

Dsouza, Raymond, "Development of a surrogate bruising detection system to describe potential bruising patterns associated with common childhood falls." (2015). *Electronic Theses and Dissertations*. Paper 2019.
<https://doi.org/10.18297/etd/2019>

This Doctoral Dissertation is brought to you for free and open access by ThinkIR: The University of Louisville's Institutional Repository. It has been accepted for inclusion in Electronic Theses and Dissertations by an authorized administrator of ThinkIR: The University of Louisville's Institutional Repository. This title appears here courtesy of the author, who has retained all other copyrights. For more information, please contact thinkir@louisville.edu.

DEVELOPMENT OF A SURROGATE BRUISING DETECTION SYSTEM TO
DESCRIBE POTENTIAL BRUISING PATTERNS ASSOCIATED WITH
COMMON CHILDHOOD FALLS

By

Raymond Dsouza
B.S., University of Pune, India, 2004
M.S., University of Louisville, 2008

A Dissertation
Submitted to the Faculty of the
J.B. Speed School of Engineering
of the University of Louisville
in Partial Fulfillment of the Requirements
for the Degree of

Doctor of Philosophy
in Mechanical Engineering

Department of Mechanical Engineering
University of Louisville
Louisville, Kentucky

May 2015

Copyright 2015 by Raymond Dsouza

All rights reserved

DEVELOPMENT OF A SURROGATE BRUISING DETECTION SYSTEM TO
DESCRIBE POTENTIAL BRUISING PATTERNS ASSOCIATED WITH
COMMON CHILDHOOD FALLS

Submitted by:
Raymond Dsouza

A Dissertation Approved On

April 20, 2015

by the following Dissertation Committee:

Dr. Gina Bertocci
Dissertation Director

Dr. Karen Frost

Dr. Mary Clyde Pierce

Dr. Michael J. Voor

Dr. Sean Shimada

ACKNOWLEDGEMENTS

This study was funded by the National Institute of Justice (Grant No.# 2008-DD-BX-K311) and by the Office of Juvenile Justice and Delinquency Prevention (Grant No.# 2009-DD-BX-0086), Office of Justice Programs, US Department of Justice. Post-mortem CT data was provided courtesy of the University of New Mexico Radiology-Pathology Center for Forensic Imaging, supported by National Institute of Justice Grant 2010-DN-BX-K205. Data and images from the clinical database were provided by Dr. Mary Clyde Pierce and Kim Kaczor. Points of view or opinions expressed herein are those of the authors and do not necessarily represent the official position or policies of the US Department of Justice.

First and foremost, I would like express my deepest gratitude to my mentor and advisor, Dr. Gina Bertocci for firstly providing me with the opportunity to conduct research in this field, followed by her unrelenting guidance, patience, and support through all this time. The determination and drive to make this distant vision a reality would not have been possible without her. I am forever grateful.

Next I would like to acknowledge Dr. Mary Clyde Pierce and Kim Kaczor for their help in not only providing data from their clinical database, but also for sharing their wealth of knowledge and clinical perspective to enrich this study.

I would like to thank the rest of my dissertation committee, Dr. Karen Frost, Dr. Michael J. Voor, and Dr. Sean Shimada for their time, guidance and valued input to improve on this study.

My gratitude also goes out to Dr. Angela Thompson for her continued assistance and support in not just overcoming everyday hurdles in research, but also in this study by helping with our statistical assessment of the data and help in converting CT image files to a 3D solid model.

Most of all, I am fully indebted to my parents, Rex and Iona and my brother Rodney; a family without which I would have never been presented these opportunities to take advantage of. Their continued love and support through thick and thin over the years have inspired me to do my very best. Lastly I need to thank my fiancée, Jessica, for not only putting up with me through this journey but also being encouraging and supportive in every way possible.

ABSTRACT

DEVELOPMENT OF A SURROGATE BRUISING DETECTION SYSTEM TO DESCRIBE POTENTIAL BRUISING PATTERNS ASSOCIATED WITH COMMON CHILDHOOD FALLS

Raymond Dsouza

April 20 2015

Child abuse is a leading cause of fatality in children aged 0-4 years. An estimated 1,700 children die annually as a result of child abuse of which three-quarters (75.7%) of the children were younger than 4 years old¹. Infants (younger than 1 year) had the highest rate of fatalities among the group. Many of the serious injuries and fatalities could have potentially been prevented if clinicians and child protective services were able to better distinguish between injuries associated with abuse versus those caused by accidents. Missed cases of child abuse have been shown to be as high as 71% of all admitted cases, where children are presented at hospitals for their injuries and not evaluated as being abused². Additionally, when child abuse is legally pursued for criminal charges, a little more than half of the cases move forward to prosecution as opposed to being screened out for reasons including the need for further investigation or insufficient evidence³. Therefore there is a need to provide clinicians, child protective services and law enforcement personnel with improved knowledge related to the types of injuries that are possible from common household

accidents that are often reported to be the underlying cause of injury in child abuse.

Bruising is an early sign of abuse, and can be an effective indicator of child abuse. Although not life threatening, bruising injuries or bruising patterns provide a “roadmap” documenting a child’s exposure to impact. Previous research has relied upon the use of instrumented anthropomorphic test devices, or test dummies, to investigate injury risk in common childhood falls and accidents in addition to head injury and bone fracture risk in children ⁴⁻⁷. However, the ability to predict bruising patterns occurring in association with falsely reported events in child abuse does not exist, and could prove extremely useful in the distinction between abusive and accidental injuries.

This study required the modification of an existing pediatric test dummy to allow for the prediction of potential bruising locations and bruising patterns in children during common household fall events that are often stated as false scenarios in child abuse. The scope of this project included the development of a “sensing skin” that was adapted to a commercial pediatric test dummy. This modified test dummy was then used in mock laboratory experiments replicating common household injury events while the “sensing skin” measured and recorded levels of impact force and locations of impact on the human surrogate. The data from the “sensing skin” was acquired and compiled in a computerized visual body map image displaying the areas of contact or impact locations. This body map image provided a “roadmap” of the human surrogate’s contact exposure during the specific fall event and defined a compatible impact

roadmap-specific event combination. Impact roadmap-event combinations for various common household falls provide an indication of where potential bruising could occur. This knowledge of potential bruising patterns could aid clinicians in distinguishing between abusive and accidental injuries for specific fall types.

TABLE OF CONTENTS

	<u>Page</u>
ACKNOWLEDGEMENTS.....	iii
ABSTRACT	v
LIST OF TABLES	xiv
LIST OF FIGURES	xvi
CHAPTER I: INTRODUCTION	1
SPECIFIC AIMS.....	2
BACKGROUND AND SIGNIFICANCE.....	5
Child Abuse Statistics	5
Failure to Diagnose Child Abuse.....	6
Failure to Prosecute Substantiated Child Abuse Cases.....	9
Bruising in Children Associated with Accidents and Abuse.....	11
Bruising Associated with Accidents.....	12
Bruising Associated with Abuse	13
Use of Anthropomorphic Test Devices (ATDs) in Child Abuse Research	16
Levels of force associated with bruising.....	18
Force/Pressure Sensor Technologies	22
Resistive Pressure Sensors	22
Force Sensing Resistor (FSR)	22

Capacitive Pressure Sensors.....	24
Optical Sensors.....	25
Force/Pressure Sensors for Artificial Skin Applications	26
SUMMARY	35
CHAPTER II: EVALUATE AND IDENTIFY FORCE SENSORS	36
OVERVIEW	36
METHODS	37
Establish Design Criteria for Sensors	37
Establish Design Criteria for Sensing Skin.....	39
Evaluate Commercial Sensors.....	39
Data Acquisition	40
Design and Fabrication Techniques of In-House Developed Sensors	40
Prototype Sensing Skin Design.....	41
RESULTS.....	42
Commercial Sensors.....	42
Sensing Skin	43
Evaluate Commercial Sensors.....	43
Static Testing:	44
Dynamic Testing:	45
Design and fabrication techniques of in-house developed sensors	47
In-House Integrated Sensor Matrix Design and Fabrication	49
Prototype Sensing Skin Development.....	54
Conclusions.....	58

CHAPTER III: FORCE SENSING SKIN DESIGN AND DEVELOPMENT	59
OVERVIEW	59
INTRODUCTION.....	60
METHODS	61
System Overview	61
Sensor Overview.....	63
Data Acquisition System (DAQ).....	64
Image Mapping	65
RESULTS.....	66
Adapted Sensing Skin.....	66
Sensor Characteristics	68
Computerized Body Mapping Image System	71
DISCUSSION AND CONCLUSION	73
LIMITATIONS.....	75
CHAPTER IV: POTENTIAL BRUISING PATTERNS IN REARWARD FALLS ...	78
OVERVIEW	78
INTRODUCTION.....	79
METHODS	80
Test Setup.....	81
Data Acquisition and Analysis.....	83
Motion Capture	84
Statistical Methods	85
RESULTS.....	85

Fall Dynamics	85
Rearward Falls – Upright Initial Position	85
Rearward Falls – Posteriorly Inclined Initial Position.....	87
Contact Forces.....	88
Contact Regions	90
Linoleum over concrete.....	90
Carpet over wood.....	91
DISCUSSION AND CONCLUSION	92
Dynamics	92
Forces	94
Contact Regions	96
LIMITATIONS.....	102
CHAPTER V: POTENTIAL BRUISING PATTERNS IN BED FALLS	105
OVERVIEW	105
INTRODUCTION.....	106
METHODS	108
Test Setup.....	108
Data Acquisition and Analysis.....	110
Motion Capture	112
Statistical Methods.....	112
RESULTS.....	112
Fall Dynamics	112
Facing Forward – 24 in bed height (FF24).....	113

Facing Forward – 36 in bed height (FF36).....	114
Facing Rearward – 24 in bed height (FR24)	116
Facing Rearward – 36 in bed height (FR36).....	117
Contact Forces.....	119
Contact Regions	121
Facing Forward – 24 in and 36 in bed height.....	121
Facing Rearward – 24 in and 36 in bed height	122
DISCUSSION AND CONCLUSION	126
Dynamics	127
Forces	129
Potential Bruising Regions	132
Clinical Skin Findings in Accidental and Abuse Cases	138
Clinical Cases – Bed Falls	139
Clinical Cases – Change Table Falls	142
Clinical Cases – Abuse	145
Abuse Case Histories Provided	149
Evaluation of Abusive Bruising Locations	149
LIMITATIONS.....	151
CHAPTER VI: SUMMARY AND CONCLUSIONS	154
Key Findings and Clinical Implications	156
Future work	160
REFERENCES	162
APPENDIX A.....	169

APPENDIX B.....	177
APPENDIX C.....	180
CURRICULCUM VITA.....	187

LIST OF TABLES

	PAGE
Table 1. Characteristic locations of bruises in children as seen in accident and abuse.	14
Table 2 : Sensor Design Criteria and Comparative Matrix.....	42
Table 3: Dynamic testing of sensors with impulse hammer	45
Table 4: Time delay recorded for every sensor evaluated during dynamic testing.	46
Table 5: In-House Printed Sensor Performance Versus Design Criteria	53
Table 6: Evaluated fall scenarios, ATD center of gravity (CG) position and impact surfaces.....	84
Table 7: Mean (8 trials) peak contact force ($N \pm CI$) for each body region in various fall scenarios	88
Table 8: Comparison of head impact forces, ATD head properties and initial conditions for various fall studies.....	96
Table 9: Comparison of potential bruising locations in our study to observed bruising in previous clinical studies	101
Table 10: Initial joint angles for the side lying ATD	110
Table 11: Evaluated fall scenarios with surface height, ATD initial position and impact surface.	111
Table 12: Mean (5 trials) peak contact force ($N \pm CI$) for each body region in various fall scenarios	119
Table 13: Overview of body planes with and without contact with the impact surface as observed in all conducted experimental falls.	124
Table 14: Overview of body regions with and without contact with the impact surface for all conducted experimental falls.....	125

Table 15: Comparison of head impact forces, ATD head properties and initial conditions for various fall studies..... 132

Table 16: Comparison of potential bruising locations in our study to observed bruising in previous clinical studies 137

Table 17: Regions with and without contact in experimental 24 inch facing forward and facing rearward falls, highlighting bruising locations recorded in clinical cases (shown as “#”) involving bed falls identified as *definite accident* or *likely accident* in children 10-14 months of age.. 141

Table 18: Regions with and without contact in experimental 36 inch facing forward and facing rearward falls, highlighting bruising locations recorded in clinical cases (shown as “#”) involving change table falls identified as *definite accident* or *likely accident* in children 10-14 months of age. 144

Table 19: Experimental results of the 24 inch facing forward and facing rearward falls, comparing regions with, and without contact highlighting bruising locations (shown as “#”) recorded in clinical cases involving furniture falls identified as abuse in children 10-14 months of age. 149

LIST OF FIGURES

	PAGE
Figure 1: The two laminated layers that make up a Force Sensing Resistor	23
Figure 2: Conductive side space and trace designs to be implemented through milling of copper clad substrate.	48
Figure 3: Milled copper clad conductive side with various space and trace patterns.	48
Figure 4: Drawing of forearm conductive side of integrated sensor matrix incorporating 8 individual sensors and associated wiring and terminal end connection.	50
Figure 5: Conductive side forearm sensor matrix printed using solid ink on copper clad sheeting and etched.	52
Figure 6: Neoprene patterns (top and bottom layers) cut for the prototype matrix sensor that would wrap around the forearm.	54
Figure 7: Prototype sensor matrix showing the placement of the sensors in relation to the forearm and associated wiring.	55
Figure 8: Piezoelectric film sensors designed by Measurement Specialties Inc.	56
Figure 9: Prototype matrix using piezo-film sensors showing the placement of the sensor matrix.	56
Figure 10: Comparison of forearm sensing skin prototypes	57
Figure 11. Conceptual model of surrogate bruising detection system (Patent No.: US 8,292,830 B2).	62
Figure 12 : The sensor matrix schematic incorporating 8 individual sensors and associated wiring that constitute the forearm sensor matrix (A). The sensor design etched on copper clad laminate, constituting the conductive side of the forearm sensor matrix illustrating the individual sensors and associated leads coming together at the terminal point where the ZIF connector was soldered (B).	66

Figure 13: The forearm sensor matrix enveloped in neoprene, ready to be adapted to the ATD.	68
Figure 14: Load versus voltage calibration profile for the forearm sensor (A). FSR sensor repeatability testing schematic indicating a load applied to the sensing skin fitted on the ATD forearm (B).....	70
Figure 15: Loads of 10 lbs (n=6), 20 lbs (n=6) and 30 lbs (n=6) exerted by the MTS versus load measured by the FSR to demonstrate sensor repeatability (error bars show one standard deviation).....	70
Figure 16: 3D body mapping images of the forearm (overlying the outline of individual sensors shown in white) (A) and complete ATD (B) capable of displaying varying colors dependent on the level of force imparted to specific regions of the body. Test results show peak force on the forearm sensor matrix associated with a squeezing action (A), and peak force on the abdominal region sensor matrix associated with a fist blow (B).	72
Figure 17: ATD in an upright initial position (scenario 1) for simulated rearward fall experiments	82
Figure 18: Frame sequences showing video capture of the upright initial position fall onto the carpet surface and SBDS body map images at corresponding time intervals. The body map images show the posterior ATD where the colors and intensities vary depending on the level of force (N) imparted to specific regions during the fall event.....	86
Figure 19: Frame sequences showing video capture of the inclined initial position fall onto the carpet surface and SBDS body map images at corresponding time intervals. The body map images show the posterior ATD where the colors and intensities vary depending on the level of force (N) imparted to specific regions during the fall event.....	88
Figure 20: Maximum impact force across 8 trials for each initial position scenario as recorded by the SBDS for rearward falls onto linoleum over concrete surface. The body map images show the posterior ATD where the colors and intensities vary dependent on the level of force (N) imparted to specific regions during the fall event.	91
Figure 21: Maximum impact force in across 8 trials for each initial position scenario as recorded by the SBDS for rearward falls onto carpet on wood surface. The body map images show the posterior ATD where the colors and intensities vary dependent on the level of force (N) imparted to specific regions during the fall event.....	92

Figure 22: Lateral comparative overlay of 11-month-old child (3D reconstruction of CT imaging) and 12-month-old CRABI ATD (transparent; blue) highlighting morphological differences in head profile.	100
Figure 23: CRABI anthropomorphic test device (ATD) in side-lying, facing forward initial position for bed fall experiments. The pendulum actuator providing the initial force to the posterior torso of the ATD is located behind the ATD.	109
Figure 24: Frame sequences showing video capture of the FF24 bed fall onto the padded carpet surface at corresponding time intervals.	113
Figure 25: SBDS body map image corresponding to the FF24 bed fall impact where the colors and intensities vary depending on the level of force imparted to specific regions during the fall event.....	114
Figure 26: Frame sequences showing video capture of the FF36 bed fall onto the padded carpet surface at corresponding time intervals.	115
Figure 27: SBDS body map image corresponding to the FF36 bed fall impact where the colors and intensities vary depending on the level of force imparted to specific regions during the fall event.....	115
Figure 28: Frame sequences showing video capture of the FR24 bed fall onto the padded carpet surface at corresponding time intervals.	116
Figure 29: SBDS body map image corresponding to the FR24 bed fall impact where the colors and intensities vary depending on the level of force imparted to specific regions during the fall event.....	117
Figure 30: Frame sequences showing video capture of the FR36 bed fall onto the padded carpet surface at corresponding time intervals.	118
Figure 31: SBDS body map image corresponding to the FR36 bed fall impact where the colors and intensities vary depending on the level of force imparted to specific regions during the fall event.....	118
Figure 32: Maximum impact force across 5 trials as recorded by the SBDS for the FF24 fall scenario. The body map images show the anterior, posterior, left lateral and right lateral aspects of the ATD. The colors and intensities vary dependent on the level of force (N) imparted to specific regions during the fall event.	122
Figure 33: Maximum impact force across 5 trials as recorded by the SBDS for the FF36 fall scenario. The body map images show the anterior, posterior, left lateral and right lateral aspects of the ATD. The colors and intensities vary dependent on the level of force (N) imparted to specific regions during the fall event.	122

Figure 34: Maximum impact force across 5 trials as recorded by the SBDS for the FR24 fall scenario. The body map images show the anterior, posterior, left lateral and right lateral aspects of the ATD. The colors and intensities vary dependent on the level of force (N) imparted to specific regions during the fall event.	123
Figure 35: Maximum impact force across 5 trials as recorded by the SBDS for the FR36 fall scenario. The body map images show the anterior, posterior, left lateral and right lateral aspects of the ATD. The colors and intensities vary dependent on the level of force (N) imparted to specific regions during the fall event.	124
Figure 36: Lateral (A) and overhead (B) views of a comparative overlay of an 11-month-old child (3D reconstruction of CT imaging) and the 12-month-old CRABI ATD (transparent; blue) highlighting morphological differences in head profile.	133
Figure 37: A comparative overlay of an 11-month-old child (3D reconstruction of CT imaging) and the 12-month-old CRABI ATD head (transparent; blue) highlighting approximate head sensor locations (red) as comprised in the SBDS.	134
Figure 38: Cumulative humagram highlighting skin findings from the BCDR database cases involving bed falls identified as <i>definite accident</i> or <i>likely accident</i> in children 10-14 months of age.	140
Figure 39: Cumulative humagram highlighting skin findings from the BCDR database cases involving change table falls identified as <i>definite accident</i> or <i>likely accident</i> in children 10-14 months of age.	143
Figure 40-A: Cumulative humagram highlighting skin findings from the BCDR database Case–A identified as <i>definite abuse</i> or <i>likely abuse</i> in a child 10-14 months of age. Legend - Bruise indicates discrete bruises. Petechiae describes red spots under the skin surface caused by intradermal hemorrhage. Multi-confluent indicates a bruised region where a discrete bruised area is difficult to identify; thus the area surrounding the bruised region was recorded. Patterned implies a distinct bruise imprint left by an impacting object.	146
Figure 40–B: Humagram highlighting skin findings from the BCDR database Case–B identified as <i>definite abuse</i> or <i>likely abuse</i> in a child 10-14 months of age. Legend - Bruise indicates discrete bruises. Petechiae describes red spots under the skin surface caused by intradermal hemorrhage. Multi-confluent indicates a bruised region where a discrete bruised area is difficult to identify; thus the area surrounding the bruised region was recorded. Patterned implies a distinct bruise imprint left by an impacting object.	147

Figure 40–C: Humagram highlighting skin findings from the BCDR database
Case–C identified as *definite abuse* or *likely abuse* in a child 10-14
months of age. Legend - Bruise indicates discrete bruises. Petechiae
describes red spots under the skin surface caused by intradermal
hemorrhage. Multi-confluent indicates a bruised region where a discrete
bruised area is difficult to identify; thus the area surrounding the bruised
region was recorded. Patterned implies a distinct bruise imprint left by
an impacting object 148

CHAPTER I: INTRODUCTION

Child abuse is a leading cause of fatality in children aged 0-4 years. An estimated 1,700 children died in 2013 as a result of child abuse of which four-fifths (75.7%) of the children were younger than 4 years old¹. Infants (younger than 1 year) had the highest rate of fatalities among the group. Many of the serious injuries and fatalities could have potentially been prevented if clinicians and child protective services were able to better distinguish between injuries associated with abuse versus those caused by accidents. Missed cases of child abuse have been shown to be as high as 71%, where children present to hospitals for their injuries and not evaluated for abuse². Additionally, when child abuse is legally pursued for criminal charges, little more than half of the cases move forward to prosecution as opposed to being screened out for reasons including the need for further investigation or insufficient evidence³. Therefore there is a need to provide clinicians, child protective services and law enforcement personnel with improved knowledge related to the types of injuries that are possible from common household accidents that are often reported to be the underlying cause of injury in child abuse.

Bruising is an early sign of abuse, and can be an effective indicator of child abuse. Although not life threatening, bruising characteristics and bruising

patterns provide a “roadmap” documenting a child’s exposure to impact. Previous research has relied upon the use of instrumented anthropomorphic test devices, or test dummies, to investigate injury risk in common childhood falls and accidents in addition to head injury and bone fracture risk in children ⁴⁻⁷. However, the ability to predict bruising patterns occurring in association with falsely reported events in child abuse does not exist, and could prove extremely useful in the distinction between abusive and accidental injuries.

The purpose of this study was to provide objective data about potential bruising locations in children in common household falls. Impact locations documented during specific fall experiments identify regions where a bruise could potentially develop, but not necessarily occur. Regions where potential bruising might occur could aid clinicians in distinguishing between abusive and accidental injuries where false histories of household falls are given. The study goal was accomplished by conducting multiple fall experiments replicating common household falls, using a custom developed contact and force sensing system adapted to a child surrogate test dummy. Three specific aims were established to achieve the goal of this study.

SPECIFIC AIMS

1. Design and develop a sensing skin adapted to a child surrogate capable of capturing and recording potential bruising locations and impact force when used in simulated injurious events.

2. Describe potential bruising patterns (impact locations) in children associated with rearward falls.

3. Describe potential bruising patterns (impact locations) in children associated with bed falls.

The hypotheses for this study are listed below:

Hypothesis 1 – Different initial condition bed falls (height and position) will lead to differences in impact locations recorded in number of planes.

Hypothesis 2 – Different initial condition bed falls (height and position) will lead to differences in impact locations recorded in number of body regions.

Hypothesis 3 – During bed falls, impacts to the ear region will be less than 10%.

This study included three methodological components to accomplish the established goal and address the specific aims. In the first component we adapted an existing pediatric anthropomorphic test device (ATD) with custom developed force sensors integrated into a conformable skin. The sensors were coupled to a data acquisition system through which recorded force data was displayed on a computerized body mapping image system. The surrogate bruising detection system (SBDS) was developed to allow for the assessment of potential bruising locations while using the ATD to simulate falls. Impact locations documented during specific fall experiments identify regions where a bruise could potentially develop, but not necessarily occur.

The second component utilized the SBDS to simulated rearward fall experiments that were performed onto two different impact surfaces (padded carpet and linoleum tile over concrete) with two different initial positions (standing upright and posteriorly inclined). Potential bruising regions and fall dynamics were investigated.

The final component utilized the SBDS to simulated bed fall experiments that were performed from two initial heights (24 in and 36 in) with two different initial positions (facing forward and facing rearward). Potential bruising regions and fall dynamics were investigated and comparisons were made to skin findings clinical fall data obtained from accidental and abuse cases. A key distinction is that the experimental falls identify all regions of contact with the impact surface during a specific, controlled fall scenario where a bruise could potentially develop, but not necessarily occur. Our experimental results do not predict bruising; rather only identify fall specific contact locations where potential bruising may occur.

BACKGROUND AND SIGNIFICANCE

Child Abuse Statistics

The Federal Child Abuse Prevention and Treatment Act (CAPTA), (42 U.S.C.A. §5106g), as amended by the Keeping Children and Families Safe Act of 2003, defines child abuse and neglect as ⁸:

- Any recent act or failure to act on the part of a parent or caretaker which results in death, serious physical or emotional harm, sexual abuse or exploitation; or
- An act or failure to act which presents an imminent risk of serious harm.

Child abuse and neglect continues to be an omnipresent public health problem that can devastate the lives of children. In 2011 an estimated 2 million reports of suspected maltreated, abuse or neglect were assessed by Child Protective Services ⁹. Of these, approximately 680,000 children were found to be victims of abuse or neglect. Children in the age group of birth to 1 year had the highest rate of victimization at 21.2 per 1,000 children in the national population. Additionally more than one-half of the child victims were girls (51.1%) and 48.6 percent were boys ⁹. An estimated 1,760 children died as a result of child abuse or neglect of which 75.7% of the children were younger than 4 years old¹.

Death and injury resulting from child maltreatment have staggering financial costs including medical care, lost future earnings and diminished quality of life ¹⁰. The direct and indirect costs of child abuse in the US are estimated at

\$104 billion per year ¹¹. Direct costs include health care services, child welfare services, law enforcement services and judicial system costs totaling \$33 billion a year. Indirect costs associated with child abuse include those associated with special education, mental health care, continued health care and lost productivity to society, totaling \$71 billion a year.

For adult survivors of child abuse, there are persistent, long-term adverse outcomes to the individual, families and society including higher risk of chronic disease (heart, liver and lung disease), unhealthy behaviors (smoking, alcohol and drug abuse, sexual promiscuity), and mental health problems (depression, re-victimization) ¹².

Failure to Diagnose Child Abuse

Of the 1,760 children that die each year due to child abuse, many are seen at medical facilities for their injuries prior to death, but early signs of abuse are often missed or dismissed as not caused by deliberate trauma. This could be due to inadequate training or knowledge in the recognition of abusive injuries or inadequate evidence for a conclusive diagnosis of abuse.

Subtle presentations of child abuse pose diagnostic challenges for pediatricians and emergency room physicians. Potentially life-threatening child abuse in the youngest, most vulnerable children can be missed when signs and symptoms are subtle.

Touloukian ¹³ presented five fatal cases of abused children with blunt abdominal trauma and found that each injury and complication was potentially curable, provided early treatment was rendered. However, these cases were not suspected as child abuse cases because the physicians were provided misleading histories of the injuries from the parent or guardian. Touloukian emphasizes the concept that the syndrome of abuse is a progressive event, beginning with deprivation and if unchecked, continuing to maltreatment and ultimately death of the child. Jackson et al ¹⁴ reviewed traumatic injuries in children under the age of 2 years at King's College Hospital in London (England). The study ¹⁴ found 18 of 100 cases to have been missed cases of child abuse and concluded that it was highly likely that other hospitals had missed cases on child abuse on their hands as well. O'Neill et al ¹⁵ reviewed the cases of 110 abused children that were seen at Vanderbilt University Medical Center (Nashville, Tennessee) over a 5 year period and found that eighty percent of the children had signs of repeated injury. Additionally more than 67% of the abused children had more than one new injury when first seen at the hospital. Supplemental cases of child abuse that were missed by physicians were reported by Diamond et al ¹⁶. Alexander et al ² found that 71% of abused children that were seen at the University of Iowa hospitals and clinics (Iowa City) had prior history of abuse or neglect. Ewing-Cobbs et al ¹⁷ discovered signs of preexisting brain injury in 45% of children with inflicted traumatic brain injury compared with none in children with accidental traumatic brain injury. A retrospective study done by Jenny et al ¹⁸ found that physicians had missed the diagnoses of head injuries

in abused children by 31% and the number of physician visits before the trauma was recognized varied between two and nine. Benzel et al ¹⁹ reviewed 23 patients that were victims of abuse and incurred neurological injury as a result of the abuse, seen at Louisiana State University Medical Center over a four year period. The study found that 9 of the 23 (39%) abused children with head injuries were known to have been seen by other physicians because of similar problems or other injuries consistent with child abuse.

Early recognition of child abuse is paramount to saving not only the life of the affected child but also possibly the lives of siblings. In a study done by Smith et al ²⁰, approximately 45 children from a total sample of 134 child abuse cases were found to have a sibling who had also been maltreated. Additionally, 10 abused children from the sample had siblings that had died, of which some were under suspicious circumstances.

Failure to diagnose child abuse is not only detrimental to the child because of the possibility of continued abuse, but also poses legal issues for the doctor in charge of the child's well-being. If a health professional fails to diagnose and report suspected maltreatment, they become financially liable if the child is further abused or killed and can be sued for medical malpractice ²¹.

Such studies suggest a need for pediatricians and health practitioners to be vigilant to the possibility of abuse when evaluating children with atypical accidental injuries.

Failure to Prosecute Substantiated Child Abuse Cases

During the fiscal year 2011, of the 3.4 million referrals, involving the alleged maltreatment of 6.2 million children, approximately 61 percent (60.8%) of referrals were screened for investigation or assessed by CPS agencies⁹. Of the 61%, approximately 20 percent of the investigations or assessments determined a child to be a victim of abuse⁹. While substantiation is typically a predicate to legal prosecution, substantiation does not ensure prosecution to follow. According to the research done by Tjaden et al²², in examining 833 cases of substantiated child maltreatment, only 21% were found to result in dependency court filings and 4% of the cases were found to result in criminal court filings. Criminal prosecution was also significantly and positively linked to the severity of the maltreatment, such that prosecutors were more likely to prosecute cases involving severe maltreatment, violence and death of the victim. It was also found that the victims' age was a contributing factor to the prosecution of the case, as it is easier to question the ability of a younger child recalling events accurately than that of an older child. Additionally the prosecutors are compelled to pursue only those cases where there is a high likelihood of conviction. Finally, approximately 70% of the cases that were criminally prosecuted resulted in convictions, of which 92% were obtained through guilty pleas. Approximately 75% of the defendants convicted of child abuse, received probation or a deferred sentence instead of being incarcerated²².

The prosecution of child abuse cases was studied by Cross et al³ by conducting a meta-analysis consisting of 21 studies to examine the rates of

criminal justice decisions in child abuse. It was found that a little more than half of the cases that were referred for criminal charges were moved forward for prosecution as opposed to being screened out. Reasons for not filing criminal charges include the need for further investigation, insufficient evidence and victim issues related to age and willingness to testify. From the cases carried forward, the plea rate was consistently high, exceeding 83%. The trial rates varied from 3% to 67% with a mean of 18% and the conviction rate was 94% (mean) for the cases carried forward. Lastly, the incarceration rate of those convicted varied from 24% to 96% with a mean of 54%³.

Recently, Sedlack et al.²³ followed the justice system path and examined the trajectory of 225 child abuse cases investigated by Child Protective Services. 210 of these cases were referred to law enforcement (93%) for criminal investigation of which 160 cases (71%) were opened for investigation; the remaining 50 cases were dropped by law enforcement or were of unknown status. Insufficient evidence was the most common reason the Prosecutor decided to drop a case. For these cases, the Prosecutor's office also cited the age of the victim and the child's best interest as part of the explanation for not pursuing them in criminal court. A total of thirty-six (36%) percent (n=81) of the investigated cases led to sheriff arrests. Further, 80 of these cases in addition to 9 non-arrest cases (a total of 89 (40%)) were sent on to the prosecutor's office. Of these 89 cases, 72 were filed as felonies, 10 were filed as misdemeanors and 7 received no filing.²³

Bruising in Children Associated with Accidents and Abuse

“The skin is the most commonly injured organ system and the easiest to examine”²⁴. Skin is generally composed of three primary layers from outer to inner surfaces: epidermis, dermis and hypodermis (or subcutaneous adipose). The subcutaneous layer has a majority in the number of capillaries and is also composed of fat which makes this layer easily deformable. During an injury, capillary networks of the 2 inner surfaces are most affected, causing the preponderance of hemorrhages in the subcutaneous layer of tissue. These damaged blood vessels, caused either through impact or a “pressure increase exceeding the injury threshold of the vessel wall”, and would result in blood loss into surrounding tissue²⁵. The vascular disruption in the lower layers without a rupture to the epidermis, results in pooling or accumulation under the surface of the skin which shows up as a bruise²⁶. Although not a life-threatening injury, bruising can be an early indicator of abuse that is easily recognized without the need for diagnostic tests.

Bruising in children is known to be the earliest, most visible and one of the most common outcomes of child abuse^{20,25,27,28}. Despite providing a “roadmap” describing the environment that a child has been exposed to, bruising is often overlooked in the assessment of a child’s injuries when attempting to differentiate between abusive and non-abusive injuries. It is crucial to accurately distinguish bruising patterns on children that arise from everyday play activities and accidents versus those from intentional causes such as abuse. Early

identification of bruises resulting from child abuse can allow for intervention and prevent further abuse.

The scientific literature provides strong evidence that differences in bruising patterns (location, number, size) exist in children exposed to accidents versus those exposed to physically abusive conditions. Maguire et al ²⁹ compiled evidence in support of this hypothesis in his comprehensive review of the scientific literature to determine whether patterns of bruising in childhood are diagnostic or suggestive of abuse. In doing so, Maguire sourced 6984 papers with scientific literature spanning 53 years, relating bruising associated with accidents, as well as bruising patterns associated with abuse. After review, 23 papers met their criteria for full analysis by a panel of 15 reviewers, all with child protection expertise. Seven papers addressed bruising in non-abused children, 14 discussed bruising due to abuse and two more discussed both abused and non-abused children. These key studies as well as Maguire's conclusions are described below.

Bruising Associated with Accidents

Maguire et al ²⁹ identified seven studies ³⁰⁻³⁶ meeting inclusion criteria that addressed bruising patterns in non-abused children. From these studies, Carpenter observed, increased bruising with increased family size ³⁰. Bruises were characteristically small ^{30,31,33} with an increased number of bruises noted in the summer ³². All bruises were less than 10 mm ³⁰ and 15 mm ³³ in any dimension. Also bruising was directly correlated to motor developmental stages

^{30,34,36} of the children. It was shown that bruising in a child who has no independent mobility was very uncommon ^{30,34}. The prevalence and mean number of bruises increased with age and developmental stage ^{30,32,34} of the child. The most common sites of bruising in children who are walking are the knees and shins ³⁴⁻³⁶. Additionally bruises occurred mostly (93%-100%) over bony prominences ^{30,34}. Accidental bruises were commonly seen on the front of the body and those to the head were usually on the forehead ³⁰. Accidental bruising was uncommon to the back, buttocks, forearm, face, abdomen or hip, upper arm, posterior leg or foot in children of any developmental stage ^{30,34,36}. Lastly, bruising to the ears ³¹ and hands (all 7 studies) did not occur for the studies considered.

Bruising Associated with Abuse

Maguire ²⁹ also described studies focusing primarily on bruising in abused children. Bruising was found to be very common in abused children ^{20,37-39}. The mean number of bruises in abused children varied from 5.7 to 10, while controls had a mean number of 1.5 bruises ^{31,39}. Additionally, the measured length of bruises were found to be greater in abused children ³¹. It was also found that the head was the most common site of bruising in abused children ^{20,31,38,40}. Multiple bruises to the head and face were found to occur in fatal child abuse cases as shown by de Silva ⁴⁰. Bruising to the ear, face, head, neck, trunk, buttocks and arms was seen significantly more in abused children than controls ^{31,39}. Bruising to children with abusive fractures was found to the head and neck ³⁸, and

abused children were found to have bruises on non-bony prominence areas ⁴¹. Also a common feature in abused children was clustering of bruises ^{42,43}. These bruises were thought to be associated with a defensive maneuver and were often found on the arm, thigh and trunk. Additionally, bruises often carried the imprint of an implement used to inflict injury ^{43,44}. Table 1 shows a summary of the characteristic locations of bruises in children incurred by abuse and accident as described in the studies above.

Table 1. Characteristic locations of bruises in children as seen in accident and abuse.

Accident	Abuse
Knees	Posterior Torso
Shins	Buttocks
Forehead	Forearm
Hips	Face
Shoulders	Abdomen
Elbows	Hip
Ankles	Upper Arm
	Foot
	Torso
	Ears
	Thigh

Collectively these above mentioned studies strongly suggest that bruising patterns associated with child abuse differ substantially from those occurring as a

result of an accident in terms of body region affected, number and size of bruises. Frequency of bruises, age of the child and the child's developmental ability are also important factors that must weigh in to determining whether bruises are associated with abusive or accidental trauma. Considering these differences, it is reasonable to assert that bruising patterns can provide a guideline and be used as an indicator in attempting to differentiate between abuse and accidental trauma.

One study that attempted to quantify this difference by developing a new scoring system for bruise patterns which could help identify children who may be abused was conducted by Dunstan et al ³¹. In this study, clinicians studied the bruising patterns of children, up to the age of 13, attending a specialist children's center over a four year period. Dunstan found a significant difference in the number of bruises across all body regions when comparing children injured through abuse to those injured in accidents. Details of bruises in each of 12 regions of the body - anterior chest and abdomen, back, buttocks, left and right arms, left and right legs, left and right face, left and right ears, and head and neck - were recorded for 133 physically abused children and 189 control children aged between one and 14 years. In each body region the numbers of bruises were recorded together with the maximum dimension of each bruise, and whether or not each bruise had a specific shape, such as being linear or shaped like a hand. A total of 763 bruises were found in 133 abused children, while 282 bruises were found in 189 control children in this study. There were clear statistical differences in the number of bruises present in abused versus non-abused children for all

body regions except for the legs. Dunstan also investigated location of bruising in his study and found that bruising to the head and neck was common in abused children, but rare in children that had been accidentally injured. Dunstan further determined that head and neck bruises in victims subjected to accidental trauma were no larger than 0.1 cm in mean total length, whereas abused children were found to have head and neck bruises of a mean total length of 5.1 cm. Therefore, Dunstan's scoring system considered areas such as the head and neck to weigh more emphasis than the legs or arms, because children who had not been abused, rarely had signs of bruising in this region. Dunstan concluded, "the extent of bruising tends to be a good discriminator between children that were abused and those who were not". In addition, the discrimination was even more accurate if bruises with a recognizable shape were detected. Lastly, it was also found that ear bruising was a good indicator of abuse in his study. Ear bruising was present in 16 percent of abused children, but was not present in any of the control children in his study resulting in a statistically significant difference ³¹.

Use of Anthropomorphic Test Devices (ATDs) in Child Abuse Research

Anthropomorphic Test Devices (ATD), often referred to as crash test dummies; are human surrogates that simulate the dimensions, weight and dynamic response of the human body. In the recent past, ATD's have been used to study pediatric injury risk in falls, as well as the shaken baby syndrome ^{4-7,45-47}. In the absence of human volunteers, these surrogates provide a means of studying biomechanical response, estimating injury risk and understanding injury

mechanisms associated with various potentially injurious events. A number of previous studies have used pediatric ATD's representing both 12 month old (CRABI ATD) and 3 year old (Hybrid II and III ATD) children in simulating free falls and bed falls to investigate the risk of femur fractures and head injury ⁴⁻⁷.

One of the first human surrogate studies in the child abuse field was conducted by Duhaime et al ⁴⁶ who investigated the shaking baby syndrome using a modified doll representative of a 1 month old infant, instrumented with accelerometers placed in the neck. Prange et al investigated free falls from different heights onto different surfaces using a customized infant surrogate (representative of a 1.5 month old infant) to determine the rotational response of the head of an infant ⁴⁷. Additionally, Prange et al studied inflicted impacts to the head and repeated Duhaime's shaking baby experiments using the customized surrogate ⁴⁷. The Hybrid II 3 year old ATD was used in studying biomechanical measures such as head, chest and pelvis accelerations, femur loads and head injury criteria (HIC) in fall experiments from bed heights ⁴ and feet first impact falls from short distances onto different impact surfaces ⁵. Deemer et al used a Hybrid III 3 year old ATD to study pediatric head and femur injury risk in the influence of wet surfaces and fall heights in feet-first falls ⁶.

Despite limitations in ATD biofidelity that may exist, these studies have allowed for comparative analyses of injury scenarios (e.g. shaking versus free fall) to assess relative risk of injury. However, as ATD's were developed to assess injury risk in high energy events, the ATDs biofidelity in lower energy falls

have not been validated and hence must be considered a limitation when drawing conclusions from these experimental studies.

Levels of force associated with bruising

As described earlier, skin is generally composed of three primary layers of which the subcutaneous layer has a majority in the number of capillaries and is also composed of fat which makes this layer easily deformable. The application of blunt force causes a preponderance of hemorrhages in the subcutaneous layer of tissue resulting in blood loss into surrounding tissue, which shows up as a bruise²⁵.

There seems to be no precise answer to the question of how much force can cause a bruise. This is primarily due to the fact that there are many contributing factors that affect the development of a bruise which is a very complex issue in itself. Extrinsic factors such as the amount of force applied, rate of force application, distribution of the force over larger/smaller areas are some of the parameters that can affect the presence or absence of a bruise. Additionally, intrinsic factors related to the architecture of the skin such as tissue thickness, toughness of skin, fat content, vessel fragility, presence and depth of underlying bone add to the complexity of the issue. Additionally, factors pertinent to an individual such as hemoglobin levels, systemic blood pressure, vascular diseases and vasoactive drugs can also have a great influence on the variability of bruises induced for varying loads. However it can be said with some degree of

certainty that smaller forces will result in smaller sized bruises while larger forces will cause larger bruises.

Information in the literature related to force levels required to cause a bruise is very limited. Hrysonmallis⁴⁸ studied thigh contusions as related to common sports related injuries. Hrysonmallis evaluate the relative effectiveness of protective cricket thigh guards by developing a model. This study utilized data generated from impacts on human volunteers and cadavers to select a surrogate soft tissue component for developing the thigh model. The data collection consisted of measuring accelerations caused by dropping a known mass (2.23 kg steel hemispherical impactor with a 73 mm diameter) fitted with an accelerometer from a known height onto the anterior part of the mid thigh of the volunteers and the cadaver. From the pilot work done by Hrysonmallis, it was established that a drop height of 100 cm onto living tissue (volunteers) often lead to a mild contusion and was considered as the threshold level for injury. The data collected in this study⁴⁸ was used to select a surrogate tissue that was integrated into the thigh model. The surrogate tissue was attached to a stainless steel beam that represented the femur and was instrumented with a transducer to measure local peak forces induced during testing. This thigh model was used to provide a measure of the impact force attenuation capacity of varying protective equipment.

Desmoulin et al⁴⁹ studied bruising mechanics in a living human subject by using an impact recording system. The equipment consisted of an impactor, a limb mount, force plate and potentiometer. For each impact, the limb was placed

on the limb mount on the force platform directly underneath the impact apparatus. A total of twelve impacts evenly spaced along the length of the limb were performed. Of these, six were performed using a 1.9 kg weight on one leg (3 shin, 3 calf) and six impacts using a 2.6 kg weight on the other leg (3 shin, 3 calf). Twenty four hours after impact, the impact area was examined for contusions and if present, its location, size, color, and shape were noted. Eight of the twelve impacts produced bruising. Peak force, peak pressure, displacement, tissue stiffness, impact velocity, force impulse, pressure impulse, and energy density all did not vary significantly under the two categories of bruise or no bruise. However, energy absorbed by the limb did vary significantly according to the two criteria. For energy absorbed by the limb, a contusion threshold of 6.5 J was found.

Mc Brier et al ⁵⁰ conducted a study where they created and validated an injury producing device that could generate multiple levels of injury starting from a contusion, all the way up to fractures by using experimental animals. The device consisted of a free falling mass (276g) with the ability of adjusting desired fall heights. The mass was directed to fall onto a location, where the experimental animal's extremities could be secured. A load cell was installed in the base of the impactor to measure the loads transmitted through the animal's extremities being impacted. The animal testing consisted of 20 caged, sedentary, male Wistar rats, 3 to 4 months old. Prior to injury, animals were euthanized via carbon dioxide inhalation and then the hind limbs were positioned in the device with the hind limb fully extended inside the leg holder and clamped into position.

Measurements taken included peak displacement, peak velocity, peak load, impulse, and energy. After the impact, the animal was scanned with magnetic resonance imaging (MRI) to evaluate the level of injury induced by the different drop heights (40, 50, 60, or 70 cm). Based on the data collected, it was found that for the weights dropped from a height between 40 and 50 cm produced mild to moderate level of injury, which could be reproduced. When the drop height was increased to 60 cm or higher moderate to severe levels of severity were sustained. Heights of 70 cm or greater were likely to result in fractures of the tibia and fibula.

In a study done by Hamdy et al ⁵¹, the factors affecting experimental bruises in animals were studied by observing the visible and chemical changes that were associated with bruise healing. The study used cattle and rabbits as the experimental animals. Each cow was bruised with approximately the same force, using a 7 lb hammer which traveled at about 3 ft/sec. The rabbits received ten blows from a rubber pressure tube that was 1.5 inch thick, traveling at approximately 4 ft/sec. The results from this study showed that there was an influence of previous bruising on the rate of healing as the time required for complete healing was shorter for every subsequent bruise administered. Additionally, the rate of healing in different animals was shown to be very similar across cattle, hogs, sheep and rabbits. Lastly, bruises subjected to younger animals were seen to heal more rapidly than those seen in older animals.

Force/Pressure Sensor Technologies

There are a wide range of force/pressure sensors available which have various operating principles and functional ranges. Additionally, they can have different shapes, sizes and could be constructed from a variety of materials. The majority of the sensors available are based on resistive, capacitive, or optical technologies. These sensor technologies and others are described below:

Resistive Pressure Sensors

The operating principle of this type of sensor is the transformation of a change in the physical pressure applied to the sensor to a relative change or modulation of the sensors electrical resistance. Mostly, resistive sensors measure an increase in force/pressure with a corresponding decrease in the resistivity measured across the sensor. The use of flexible materials that have defined force-resistance characteristics have received considerable attention in touch and tactile sensor applications. Manufacturers such as Interlink, IEE, Teckscan and Verg Inc provide force sensing sensors based on resistive technology.

Force Sensing Resistor (FSR)

A type of resistive sensor is a force sensing resistor which is made up of two parts, usually flexible polymer sheets that are either screen printed (thick

film) or deposited (thin film) with conductive lines. Figure 1 shows the two layers that usually make up a FSR.

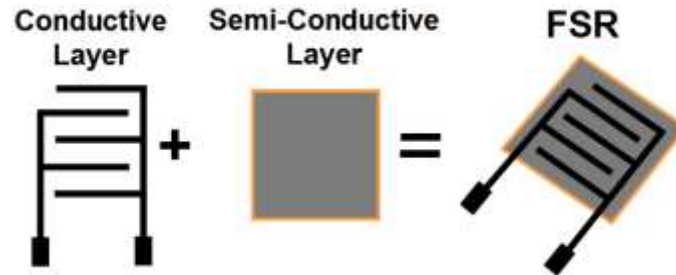


Figure 1: The two laminated layers that make up a Force Sensing Resistor

The first part is a pressure sensitive ink or semi-conductive sensing material that is applied to one side of the film. The sensing film could consist of both electrically conducting and non-conducting particles suspended in a matrix such that it changes resistance in a predictable manner following application of force to its surface. The particle sizes and order are formulated to improve response characteristics, reduce the temperature dependence, and improve mechanical properties. The second part is a set of conductive (usually silver or silver/graphite) interconnected contacts applied to one side of the film. These two parts or films are then placed over each other so that the printed sides of the two films interact to create a FSR. The semi conductive material serves to make an electrical path between the sets of conductors on the other film. Applying a force to the surface of the sensor, causes the sensing film conductive particles to touch the conducting electrodes and this in turn changes the resistance of the sensor. Depending on the properties of the semi-conductive sensing film, a sensors response (conductivity) can approximate a linear function of applied force. As

with all resistive based sensors a force sensitive resistor requires a relatively simple interface and can operate satisfactorily in most environments

There are two operating principles in FSR's. One is the Shunt-Mode and the other is the Thru-Mode. Shunt-Mode was described above in the operation of the FSR, which consists of the two substrate layers, commonly made of polyester film, with one layer being coated with the force-sensitive ink and the other substrate layer being screen printed with conductive electrode fingers. The two substrates are positioned facing each other, such that the conductive fingers and sensing ink can interact with each other. When a force is applied to the sensor, shunting or short circuiting takes place. The more force applied to the sensor, the more conductive the output. A Thru-Mode FSR is also constructed with two layers of substrate such as polyester film. However, in this case, there are two conductive pads with the interconnected finger like electrodes that are screen printed on each of the two substrates. Additionally, the force-sensing ink is then screen printed over the conductive pads. These two printed substrates are then placed facing each other such that they form a laminate of the two substrate layers, forming the force sensor. The more force applied to the ThruMode sensor, the more conductive the output.

Capacitive Pressure Sensors

Similar to resistive sensors, capacitive sensors use a three layered structure which forms the basic capacitive circuit. Two electrode surfaces with a specific contact area are separated by a dielectric medium which could comprise

of a compressible non-conducting elastomer. The capacitive sensor functions via the applied force either changing the distance between the capacitive plates or the effective surface area of the capacitor. This change in capacitance can be as low as a few pF (picofarad) which requires highly sensitive equipment to register or sense the read out. In such a sensor if the two conductive plates and the dielectric medium, are made of flexible materials, then the entire sensor can be flexible while having good repeatability and sensitivity in its force-to-capacitance characteristics. Manufacturers such as Pressure Profile Systems and Xsensor incorporate capacitive technology for their force sensors.

Optical Sensors

Optical technology provides an alternative method of producing pressure sensors. The operating principles of optical-based sensors are known to fall into two categories: intrinsic and extrinsic. Extrinsic sensors are those where the light leaves the transmitting fiber to be changed by the system being measured, before it continues to the detector through the return or receiving fiber. Intrinsic sensors are different in that the light beam doesn't leave the optical fiber but is changed in optical phase, intensity, or polarization by the measured system while still contained within it fiber. Intrinsic and extrinsic optical sensors can be used for touch, force or pressure sensing. For robotic touch and force-sensing applications, the extrinsic sensors are more commonly used due to their simplicity in construction and data processing.

Tactex controls Inc (Tactex controls Inc., Victoria, BC V9A 3K5, Canada) has developed a force/pressure sensitive sensor (Kinotex®) based on optics related to the way light scatters within cellular foam. The sensor consists of two plastic optical fibers, one transmitter fiber and one receiver fiber that are embedded in cellular foam. An LED light source is used to impart light along the transmit fiber into the foam sensing surface. When pressure is applied to the foam, the intensity of the back-scattered light increases, which is monitored by the receive fiber sent back to a photo-diode for processing.

Force/Pressure Sensors for Artificial Skin Applications

Pressure sensing technology has been a key factor and a primary area of interest in robotics from the early development of robots designed for human interaction ^{52,53}. Artificial skin or electronic skin is the key aspect in obtaining complete artificial intelligence in robots ^{52,53}. Important factors of tactile sensors used in robotic applications include the sensors being thin, flexible and resilient, properties which are similar in nature to the pressure sensors we are considering with this project. A review of the relevant literature describing pressure sensors developed and utilized in electronic skin sensor applications is provided below:

Shimojo et al ⁵⁴ developed a sensor that uses pressure conductive rubber as the primary material in the sensor. Pressure-conductive rubber was selected because of its good flexibility, workability, and ease of use. This rubber is a product of The Yokohama Rubber Co., Ltd. (Corporate Head Office: 6-11, Shimbashi 5-chome, Minato-ku, Tokyo 105-8685, Japan) and consists of carbon

particles, which function as an electro-conductive material which is dispersed uniformly in a silicone rubber matrix. The conductive mechanism of the pressure-conductive rubber seems to be due to the following principle. In a state with no pressure acting, the carbon particles within the pressure-conductive rubber are positioned apart from each other; consequently, the resistance value is infinitely large. However, when pressure is increased, the thickness of the rubber decreases, therefore the carbon particles come in closer contact which reduces the measured resistance. In this study, a single layer composite structure was adopted by stitching wires into the pressure conductive rubber. The sensors consisted of electrodes that were configured in the horizontal direction by stitching wires into the front and back surfaces of the rubber, alternating back and forth, and similarly, the columns of wires were configured in the vertical direction.

Each sensing element was formulated by the intersection of the row and column wires. The wire was stitched at 3-mm intervals in the horizontal and vertical directions. Additionally, the stitch pattern was manually sewn with a needle, so the wire positions were not exactly linear. Electrical isolation of the sensor was (required because the exposed wires on both sides of the pressure-sensitive rubber) achieved by the artificial leather and a silicone rubber film. The total thickness of the sensor was approximately 0.5 mm with the sensor being 44 mm long and 12mm wide. The sensing area consisted of 163 sensels with a 3 mm pitch. The sensors pressure sensitivity was analyzed and reported in the range of 0 – 30 psi. The endurance of the pressure-conductive rubber was tested

by applying a repeated force (12 N) at a cycle rate of 3 Hz with a flat-head rod (diameter: 5 mm). The testing resulted in no change of the rubber's characteristics after one million cycles of loading. Additionally, there was no variation in the resistance value measured after repeated cyclic loading (over one million times) that proves good endurance for the sensor. The sensors response time was measured by subjecting the sensor to an impulse hammer and comparing the waveform of the resistance change from the load applied to the sensor to that recorded from the impulse hammer. The respective timing of peak values of both waveforms from sensor and impact hammer (15 N over a time period of less than 10 ms) were compared, which resulted in a delay of approximately 1 ms. Therefore the sensors response time was estimated to be 1 ms. The entire sensing system consisted of the sensor, scanning circuit and control, and the PC. The sensors were lastly attached to a four-finger robot hand and was analyzed for grasping different shaped objects (column, sphere, cone shaped). The experimental data collected, resulted in successfully characterizing the grasping operation in terms of grasping pressures and transitions in parts of the robot hand in contact and not in contact while holding different object shapes⁵⁴.

Ohmura et al ⁵⁵ presented a study related to the design and testing of a tactile sensor skin capable of conforming to curved surfaces . The tactile sensing elements operated on the basis of light optics and consisted of a photo-reflector covered by a layer of urethane foam. The foam was not only used as a light reflector for the working of the sensor, but also guaranteed mechanical

compliance and protection for the sensing elements and associated circuitry. These sensors worked by measuring the light scattered by the urethane foam upon deformation (The scattered light is concentrated by the deformation). Their sensor was listed as a variant of the optical sensors used by KINOTEX (Tactex controls Inc., Victoria, BC V9A 3K5, Canada). However, KINOTEX sensors, were described as being affected by problems related to flexibility and size because of the number of fiber optic cables at a LED and a photo detector. This study suggested ways to solve both problems by not using fiber-optic cables and instead bonding a photo-reflector directly onto the urethane foam. Ohmura used photo-reflectors with a size of 3.2 mm× 1.7 mm× 1.1 mm. The only disadvantage of this system deals with high power consumption when using a large number of photo-reflectors (each is rated at 50mA). The study claimed that this issue could be avoided by restricting the number of powered-on LEDs through time-sharing control.

The study proposes each module consisting of tactile sensor elements be mounted to a bendable substrate. Additionally the distance between each tactile sensor element can also be adjusted to user desired spacing. Ohmura's tactile sensor sheet consisted of 32 tactile sensor elements connected to a serial bus of a computer. Eight tactile sensor elements shared one analog-digital converter and each set of eight tactile sensor elements were simultaneously controlled by the micro-controller (responsible to switch on and off the LEDs corresponding to the individual tactile elements).

The sensors operation in a zero load condition was shown by the output of the photo-reflector being saturated or maximum. For increasingly larger pressures, the change of voltage decreased and eventually flattened out. The sensors characteristics were analyzed for pressure ranges of 0 – 73 psi and were found to be nonlinear in nature with a high sensitivity. However these characteristics could be controlled by changing the variety and thickness of the urethane. The sampling time was defined as the sum of the time required for communication and of the time of transition duration of a tactile sensor after switching the LED on. The time required for sampling four sensors was evaluated to be approximately 0.2 ms. The complete tactile sensor was deemed suitable for a large scale, dynamic whole-body application such as in robotic humanoids.

Meyer et al ⁵⁶ presented the design of a pure textile, capacitive pressure sensor designed for integration into clothing to measure pressure on human body. The intended applications for these sensors include any field requiring a soft and bendable sensor where high resolution is needed, such as rehabilitation, pressure-sore prevention or motion detection due to muscle activities. The pure textile pressure sensor consisted of a three-layer structure forming a capacitor with a pressure sensing dielectric textile (thickness of 3 mm and a compressibility of 50 % at 1.8 N/cm²) placed between two electrodes. Arrays of individually connected textile electrodes were embroidered using silver coated yarn that made up the sensor matrix. A square area of 2x2 cm was found to be an appropriate sensor size for measuring the local pressure resolution and maintain accuracy of measurement. The dielectric material separating the textile

electrodes consisted of a compressible textile. Two additional layers of conductive textile shielding were placed over the outer layers of the capacitive array sensor. Using the described design concept, Meyer assembled and tested these pressure sensors with 1, 8, 16, and 30 sensing elements. The compressibility and thickness of the dielectric textile were found to influence the pressure range and the resolution capabilities of the sensor making it easily adjustable for different pressure ranges. To measure the capacitance from the sensor array, it was connected to an analog to digital converter and then linked to a computer. Meyer used an iterative algorithm to adjust for hysteresis caused in the foam textile due to cracking and deformations in the inner molecular structure and calculated the output of the sensors for each time step. The pressure was measured with a maximal error of 0.5 N/cm^2 (0.72 psi) in the range of 0 to 4 N/cm^2 (5.8 psi) when the textile spacer was utilized. The error increased for higher pressures up to 10 N/cm^2 (14.5 psi), since the compression-pressure curves slope increased.

Meyer used the developed sensor to detect the activity of the muscles of the upper arm during a lifting motion. The sensor was fixed on the biceps and triceps with an elastic band placed on the muscle where the highest variation in pressure was observed. When the muscle contracted, it increased the pressure of the stretched band which was measured while continuously lifting a weight of 2 kg. The experiment proved that not only could the motion of the arm can be detected but also independent motions of the bicep and triceps could be evaluated. Lastly Meyer concluded that integrating these sensors directly into a

piece of clothing could help evaluate breathing in addition to the physical state of the wearer of the clothing. Other applications stated were integrating the sensors into a cushion for pressure sore detection.

Sergio et al ⁵⁷ also developed a textile based capacitive sensor which consisted of an array of capacitive elements whose capacitance varied according to exerted pressure on the sensors. The rows and columns of the array sensors were conductive fibers patterned on two opposite sides of elastic synthetic foam, which acts as the dielectric. The output of these pressure sensitive fabric arrays were linked to an operational amplifier for amplifying the output signal which was then digitized by an A/D converter. The data was collected by a data acquisition board and then digitally processed by digital filters, for noise compensation and gamma correction to produce pressure images displayed in real time at about 3 F/s onto a PC monitor. The emphasis in this study was on the detection of light pressures being applied over a relatively wide area. Advantages of these sensors were listed as simple capacitive sensing elements that could be used as robust sensors even when exposed to strong mechanical stresses.

Inaba et al ⁵⁸ conducted a study to develop a full body tactile sensor suit using electrically conductive fabric and string. The tactile sensing mechanism is based on a layered fabric FSR approach using electrically conductive fabric and strings. The structure of the tactile sensor consisted of six layers. The top and bottom most layers were soft cloth layers to cover the sensing element and the wiring layer. The sensing element of the sensor was made of three layers consisting of the wiring, grid switch pattern and the spacer material respectively.

The last layer was a conductive fabric used for grounding purposes. The sensitivity of this sensor depended on the size of the net hole and the thickness and structure of the grid pattern spacer layer. The lower value of recorded pressures during testing was 70 g/mm^2 (hg) or 1.35 psi. This sensor was incorporated into the structure of an entire suit for a full-body humanoid robot. This suit consisted of four sections including, left and right sides of sleeves, front body and back body. The suit had a total of 160 sensing regions varying in size from 10 cm x 5 cm to 5 cm x 5 cm areas and was tested on a remote-brained robot. The signals from the sensor suit were integrated into a visual image by a video multiplexer and processed on a remote computer. The suit provided the robot with the ability to sense touch. The robot sensor suit was deemed a promising research tool to advance behavior based control of robots through body interactions.

Someya et al ⁵⁹ developed a large-area, flexible pressure sensor matrix using organic field-effect transistors for artificial skin applications. The pressure sensor structure consisted of a multiple layers sandwiched together to form the organic transistor with pressure sensitive rubber laminated to the bottom to form the FSR. The transistor consisted of a base film (substrate) which was ultra-high heat-resistant polyethylene naphthalate (PEN) with a thickness of 100 μm . This film was sandwiched between two layers of polyethylene terephthalate (PET) to help in the later drilling process. Through this film, holes were drilled and the PET layers were then removed by an organic solvent. Then both sides of the PEN base layer were coated with 150 nm thick gold layers with 5 nm thick chromium

adhesion layer in order to make an electronic connection between electrodes on the two sides of the base film. Next, polyimide was spin-coated to form a 500 nm thick gate dielectric layer which was drilled into so as to have contact with the other layers. Also pentacene and gold layers were added to complete the organic transistor design. Lastly, the pressure-sensitive rubber sheet and the copper electrodes were laminated to the bottom of the base film to integrate pressure sensors with the transistor.

The sensors were arranged in a matrix with a spacing of 2.54 mm. Higher densities could be obtained by reducing device dimensions or using a shorter channel length in the transistor design. The accuracy of the pressure sensor reading over large areas was limited mainly by the performance of organic transistors, whereas the sensitivity was limited by the performance of the pressure-sensitive conducting rubber. The developed pressure sensor could detect a few tens of kilopascals, claimed to be comparable to the sensitivity of discrete pressure sensors. An important characteristic of this sensor related to its flexibility as it was found that the device was electrically functional even when being wrapped around a cylindrical bar with a 2 mm radius. Additionally, the time response of the pressure-sensitive rubber was close to hundreds of milliseconds, and the individual sensors did not respond to higher frequencies. The scan speed of the entire sensor cell array (16 x16) was limited by the performance of individual transistors and was independent of the frequency response of the pressure sensors. The cycle time of each transistor was measured to be around 30 ms in this study, from which the total time to access the 16 x16 transistors

was estimated to be 480 ms. This implies that for a larger device with a large number of sensor cells, the organic transistors will be the limiting factor of the frequency response. For artificial skin in particular, the integration of pressure sensors and organic peripheral electronics allowed the sensor to be mechanical flexibility, have a large area, and low cost which was demonstrated in this study.

SUMMARY

Previous studies have shown that bruising patterns resulting from abuse are significantly different than those resulting from accidents. However, this distinguishing feature of abuse inflicted bruising is often overlooked in the clinical setting, as well as in forensic investigations in part because there is no objective information about potential bruising patterns seen in accidental falls which are often used as false histories by perpetrators. There needs to be agreement between a child's bruising and the biodynamics of the stated cause. It is this evaluation of biodynamic compatibility based upon the bruising "roadmap" that our study aims to address by predicting potential bruising patterns occurring in falls which are sometimes used as false histories in children subjected to abuse.

CHAPTER II:

EVALUATE AND IDENTIFY FORCE SENSORS THAT MEETS THE DESIGN REQUIREMENTS OF THE FORCE SENSING SKIN

OVERVIEW

Unexplained bruising is an early sign of child abuse. Bruising locations on the body can be an effective delineator in abusive versus accidental trauma. However, the ability to predict potential bruising locations associated with falsely reported injury causing events (e.g. bed falls, stair falls) in child abuse does not exist. An existing pediatric ATD can be used to recreate common household fall events that are often stated as false scenarios in child abuse. However the ATD's standard instrumentation that includes multiple accelerometers and load cells does not allow for independent force measurements over discrete body segments or regions as would be required to assess potential bruising locations while using the ATD to simulate falls. To overcome this, we propose to develop a "sensing skin" that will consist of multiple individual force sensors arranged so as to be adapted to a commercial pediatric test dummy, capable of capturing and recording potential bruising locations and impact force when used in simulated injurious events

The scope of this study includes establishing design criteria for the force sensors, and the sensing skin and evaluation and identification of force sensors that meet the established design requirements.

METHODS

Establish Design Criteria for Sensors

Design criteria and target values for each criterion that must be met by sensing skin were established and represented in a comparison matrix. The design criteria for the sensors included, but not limited to the following factors:

- Force or pressure sensing range – The sensors should be able to detect low as well as high impact forces (associated with falls)
- Sensitivity – The ability for the sensor to read small increments in force over its entire range is favorable
- Response time – A quick response time is required to record forces during impact events.
- Conformability and compliance – The sensor should be able to conform to all curved surfaces of the ATD without affecting sensor operation.
- Weight – Individual sensor weight should be low, since the sensors will cover the entire ATD surface area.

- Power consumption – Low power consumption is desired, because with the large number of sensors required to cover the ATD surface, the power requirements would be multiplied.
- Size and thickness – Individual sensor size should be small enough so as to capture a high number of discrete sensing locations but at the same time not be so small that the number of sensors required to cover the entire ATD exceeds the limits of the data acquisition system. A thin sensor is desired to limit the bulk added to the ATD.
- Toughness – High robustness against impact and shear forces is desired because of the impact loads applied to the sensors.
- Hysteresis and creep – Lower values of hysteresis will be required for minimal differences between loading and unloading measurements of the sensors. Lower creep values will be required in static applications where the sensor value should not vary with time on the application of constant load. As our application is dynamic and we are primarily interested in the loading curve, these properties have a low priority in our design.
- Cost – Lastly the sensors should be relatively inexpensive considering the larger number of sensors required to envelope the ATD surface; the associated costs could exceed the budget limitations.

All available and applicable sensor systems were evaluated and compared to determine how well they compare to established sensor criteria.

Establish Design Criteria for Sensing Skin

The design criterion for the sensing skin includes but is not limited to the following factors:

- Flexibility – Skin needs to adapt to the irregular conforms of the 12 month old ATD surface
- Friction – A high contact friction is required between the skin and ATD surface so as to prevent relative motion between the two surfaces. This will facilitate in maintaining sensor positions on the ATD surface
- Protective – The skin should help limit sensor damage through the intended dynamic impact testing of the system (drop tests)
- Thickness and weight – In an effort to reduce overall bulk of system, the skin needs to limit the amount of bulk or thickness as well as weight added to the ATD so as to not drastically change the ATD's dynamics

Evaluate Commercial Sensors

Commercially available, distributed and discrete sensors were evaluated against established design criteria for potential use in the sensing skin. We expect the sensors used to form the sensing skin to be either resistive or capacitive type force sensors. The sensors force sensing range and sensitivity was evaluated by exerting a known load/pressure on the sensor and then measuring the corresponding output. A comparison between measured loads and applied load provided the measurement error for each tested sensor.

Data Acquisition

The output from each evaluated sensor was recorded using Labview 8.2 (National Instruments) running on a PC (operating system- Windows XP sp3) equipped with a National Instruments data acquisition card (NI PCI-MIO-16E-4) connected to a 68-Pin I/O terminal block (NI CB-68LP). A simple VI (virtual instrument) developed in Labview helped in evaluating and data logging of the sensors output.

The sensors were tested under static load conditions by applying a known load/weight over a known surface area. Additionally, dynamic testing of the sensors was performed by subjecting the sensors to an impact with the means of an impulse hammer (PCB, #086C02). The output from the impulse hammer was recorder along with the sensors output in Labview. These two output signals were then compared to evaluate the error in sensor force measurement and the delay in response time for evaluated sensors.

If commercial sensors fail to meet design criteria, in-house sensor design and fabrication needs to be explored.

Design and Fabrication Techniques of In-House Developed Sensors

The FSR's conductive side was produced in house, however the semiconductive side was custom ordered to our specifications from an industry leading manufacturer (Sensitronics): The methodology of producing individual force sensing resistive sensors (FSRs) in- house were explored by multiple processes described below:

1. Milling of conductive patterns onto a flexible copper-coated substrate using a rapid circuit board plotter.
2. Photolithography, where a matrix of individual sensor patterns are transferred from a photo mask onto a copper substrate, which is then etched to produce a desired space and trace pattern (University of Louisville Micro/Nano Technology Center).
3. Printing the sensor matrix pattern directly onto flexible copper clad substrate using a solid ink laser printer, followed by a copper etching process.

Various space and trace designs of the conductive side were generated using the above in-house methodologies. Additionally, several different semi-conductive materials will be joined with the conductive side designs for evaluation purposes. Cabling and cabling interface strategies (between the sensor matrix and cable, and between the cable and data acquisition hardware components) were evaluated for in-house generated integrative sensor matrices.

Prototype Sensing Skin Design

After conducting the sensor evaluation, the candidate sensor(s) were integrated into a protective skin to form the sensing skin that can be easily adapted to the ATD's body segments. The sensors were glued with an adhesive bonding agent into the protective skin and made to conform to the desired area of coverage. The individual sensor elements were wired together such that each sensor would have individual leads that could connect to the data acquisition

system. We have originally conceptualized the skin to be similar to a neoprene wet suit.

RESULTS

Commercial Sensors

A comprehensive review of pressure sensors manufacturers that design and develop pressure sensors relevant to our application yielded companies such as Tekscan, Trossen robotics, Pressure Profile Systems and Sensitronics. These manufacturers' sensors were further evaluated during the course of this study. The above listed manufacturers' sensor specifications and characteristics were arranged in a matrix alongside the desired characteristics that would be required from the sensors in our application. Additionally, a preliminary ranking based on the importance of each listed criteria that should be met by sensing skin prototypes are represented in the comparison matrix listed below in Table 2:

Table 2 : Sensor Design Criteria and Comparative Matrix

Sensor Technology	Tekscan	Trossen	PPS	Sensitronics	Criteria
Sensing Range (psi)	0 – 75	0 – 175	0 – 508	0 – 125	≥ 110
Resolution (sensors per cm ²)	0.6	≥ 0.6	5	≥ 0.6	1
Sensor Elements	96	1	≤ 10,240	1	-
Sensitivity (psi)	-	1.5 – 150	-	1 – 125	≥ 1
Error	11% ²	-	-	-	≤ 5%
Response time (msec)	-	1 – 2	-	1	2

Sensor Technology	Tekscan	Trossen	PPS	Sensitronics	Criteria
Hysteresis	-	-	-	-	≤ 5%
Conformability	-	-	Stretch 10%	-	-
Temperature Range (°C)	-	-30 to 70	-20 to 50	-15 to 200	-20 to 50
Scan Rate	500 Hz ¹	-	10 kHz	-	Variable
ADC Resolution	8-bit ¹	-	12-bit	-	Variable
Weight	10 gm	-	-	-	0.1 gm/sensor
Thickness (mm)	0.15 ¹	0.2–1.25	3	0.2 – 1.25	1
Active Area (mm x mm)	203 x 76	38 x 38	407 x 508	510 x 610	Variable
Lifetime cycles	-	>10 ⁶	-	> 10 ⁶	> 50,000
Cost	~\$300	~\$ 10	~\$1500	~\$500	≤ \$ 1.00

Sensing Skin

We had envisioned the sensing skin to be similar to a wet suit enveloping the ATD, which is why we opted to use neoprene which is a synthetic rubber material designed to be flexible, durable has a high coefficient of friction with the ATD surface and will serve well to protect the sensors during dynamic testing. The neoprene is 1.0mm in thickness and double nylon backed.

Evaluate Commercial Sensors

Sensors based on capacitive and optical technology are typically unable to sustain impact without damage to the sensor structure. Thus we eliminated these types of sensors from further consideration and focused our evaluation on force

sensing resistive sensors (FSRs). Commercially available discrete resistive force sensors were evaluated for potential use in the sensing skin. If commercial sensors failed to meet design criteria, in-house sensor design and fabrication would need to be explored.

Static Testing:

Commercially available resistive sensors from Sensitronics, Trossen Robotics, Tekscan and Distance Lab were evaluated under static loading conditions. Measurements of the individual sensors included physical dimensions, resistance range while unloaded and with maximum registered load, sensor rise time and static load measurement error were recorded for all samples attained. A listing of the commercially available sensors testing is shown in Appendix 1.

The results demonstrate nonlinear response characteristics for all the sensors. This is observed as the measured percent error varied nonlinearly as the load on the sensor increased or decreased. Also the sensors with smaller physical dimensions could tolerate higher pressures while still recording a change in resistance, which translated into a higher sensing range capability (Trossen circular small, Sensitronics circular small and Sensitronics square small sensors had greater pressure measuring ranges varying from 0-37 psi, 0-140 psi and 0-50 psi respectively than the rest of the samples).

Dynamic Testing:

Dynamic testing of the sensors was performed by subjecting the sensors to an impact force with the means of an impulse hammer. The output from the impulse hammer and sensor output were compared to evaluate the measurement error in sensing force. The average of 5 trials for the sensors output and impulse hammers output along with the corresponding mean percent error is shown in Table 3 for all the sensor samples tested.

Table 3: Dynamic testing of sensors with impulse hammer

SENSOR	Mean Applied Pressure (psi)	Mean Recorded Pressure (psi)	Mean % Error
	Impulse Hammer	Sensor	
Distance Lab	9.25	11.44	-23.67 %
FlexiForce-Tekscan	88.31	55.31	37.36 %
Trossen-Circle	12.11	15.10	-24.65 %
Trossen-Small Circle	10.94	8.27	24.44 %
Trossen-Square	10.96	8.30	24.35 %
Sensitronics – Circle	13.81	14.65	-6.09 %
Sensitronics –Circle Prototype	56.50	61.71	-9.22 %
Sensitronics –Small Circle	81.34	98.11	-20.60 %
Sensitronics –Square	14.50	14.36	0.95 %
Fabric – 1 Layer Velostat	71.11	57.94	18.51 %
Fabric – 4 Layer Velostat	75.76	59.61	21.31 %

The dynamic testing results exhibited mean percent error of all sensors to vary from approximately -25% to 37%. The Sensitronics square sensor showed the least mean percent error (0.95%) of all the tested sensors. The dynamic testing was within a range of 10 to 90 psi; thus, testing through different load ranges could yield different results. Additionally, during dynamic testing, the output signals from the impulse hammer and sensors were compared to evaluate the delay in response time for evaluated sensors. Table 4 provides the recorded time delay between the impulse hammer and the sensors.

Table 4: Time delay recorded for every sensor evaluated during dynamic testing.

SENSOR	Time delay between hammer and sensor (ms)
Distance Lab - 1 Layer Velostat	-1.7
FlexiForce-Tekscan	-0.2
Trossen-Circle	-1
Trossen-Small Circle	-1
Trossen-Square	-1.1
Sensitronics – Circle	-0.4
Sensitronics –Circle Prototype	-1.3
Sensitronics –Small Circle	-0.4
Sensitronics –Square	-0.6
Fabric – 1 Layer Velostat	-1.8
Fabric – 4 Layer Velostat	-1.2

A negative value of time delay implies that the sensors response to the input force was observed after the impulse hammers output was recorded. Our recorded time delay values from the testing are within the manufacturers specifications which states that the sensors response times should be 1-2 msec.

The testing revealed that the sensors met most of the design criteria except for sensor density, bulk and cost. Since off-the-shelf commercial sensors are very limited in sizes, building a matrix of individual sensors to cover the ATD surface would have led to an unacceptably high sensor density and sensing skin mass (see Results Objective 1.3). Additionally, commercial customized sensor matrices (i.e. a single substrate containing multiple sensors of varying sizes and shapes) designed to adapt to contoured body regions of the ATD were found to be cost prohibitive. Thus the design and fabrication of in-house developed sensors were explored.

Design and fabrication techniques of in-house developed sensors

1. Milling of conductive patterns onto a flexible copper-coated substrate using a rapid circuit board plotter.

The design of the first batch of sensors consisted of seven various space and trace configurations so as to allow us to test and optimize the sensor design. Figure 2 illustrates various space and trace conductive side designs considered. The sensor designs were created by milling the pattern with a rapid circuit board plotter onto a flexible substrate coated with copper (Pryalux® - DuPont™). Figure

3 illustrates the implementation of these designs resulting in milled copper clad conductive side prototypes.

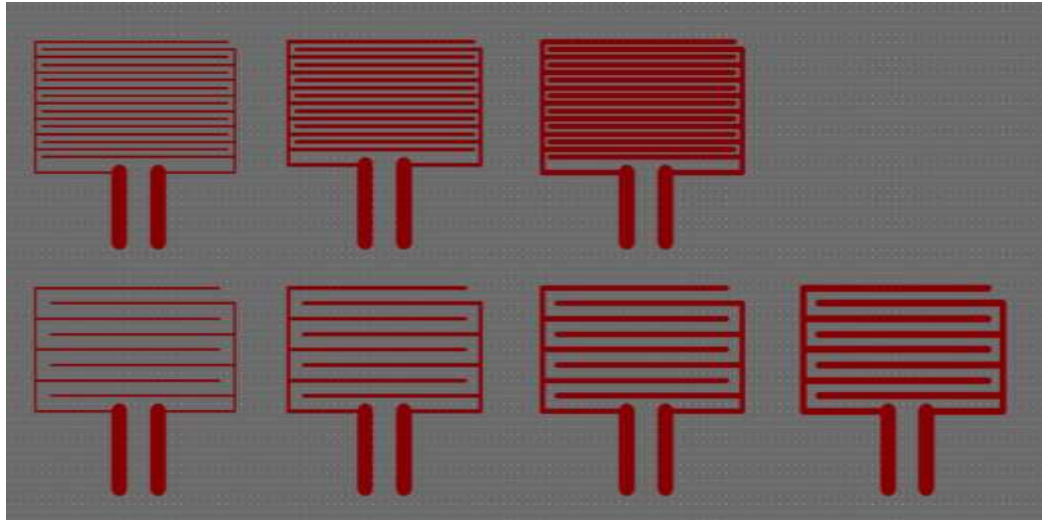


Figure 2: Conductive side space and trace designs to be implemented through milling of copper clad substrate.

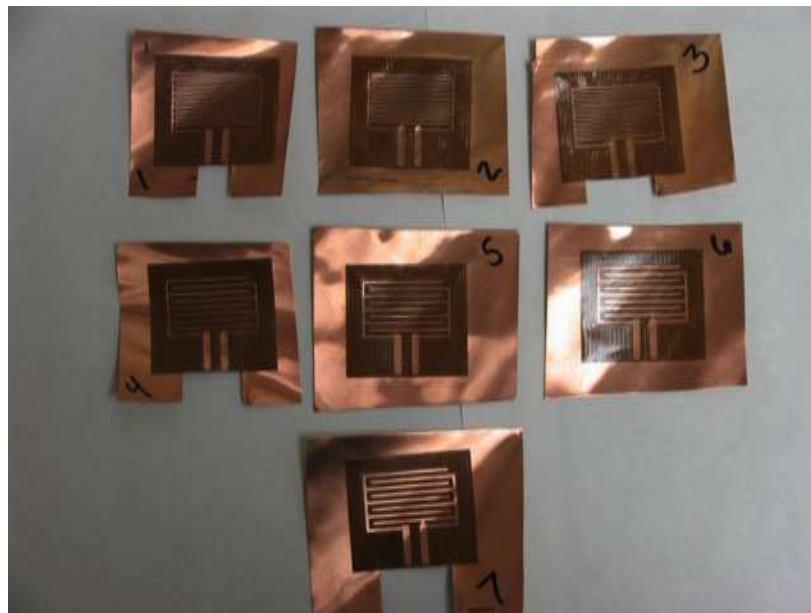


Figure 3: Milled copper clad conductive side with various space and trace patterns.

The in-house milled copper clad conductive side joined with various semi-conductive materials (to form an FSR sensor), along with commercial sensors showing promise based upon static testing results, were evaluated under dynamic loading conditions to characterize sensor change in resistance versus force application (Appendix B)

In-House Integrated Sensor Matrix Design and Fabrication

Even though the milled sensors produced desirable characteristics in comparison to commercial sensors, it was determined that matrices consisting of individual sensors would lead to excessive wiring and thus, excessive bulk and weight in our sensing skin (see Figure 13a and 13b). This increased bulk could interfere with sensor function when sensing skins from multiple body regions were introduced. Thus, we sought to develop a conductive side of an FSR sensor with multiple integrated sensors on a single substrate that also incorporated wiring to join the sensors. This approach would lead to a uniform thickness across the sensing matrix. Wiring for all sensors within the matrix were designed to have a common terminal point that would interface with external cabling.

A sensor matrix design incorporating eight (8) individual sensors and their associated wiring was generated for the ATD forearm (Figure 4). This matrix configuration was established with the intent of being able to wrap it, enveloped with neoprene protective layers, around the ATD forearm.

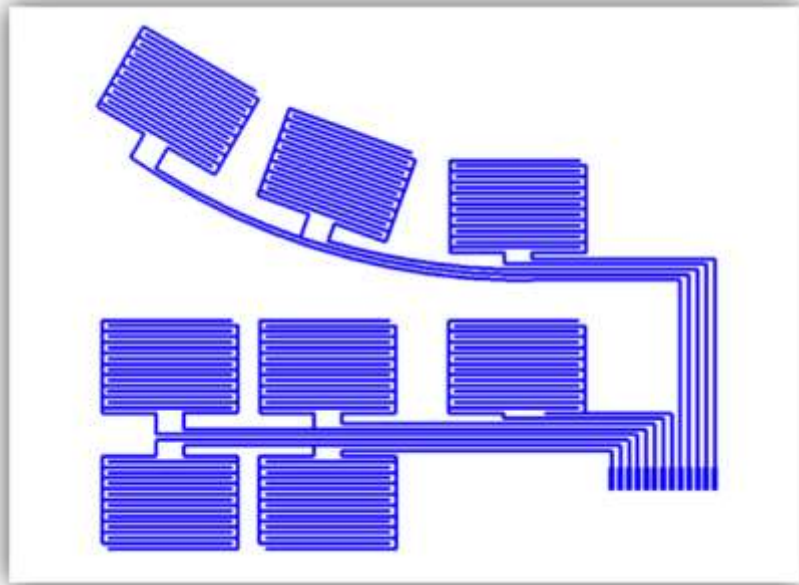


Figure 4: Drawing of forearm conductive side of integrated sensor matrix incorporating 8 individual sensors and associated wiring and terminal end connection.

In order to have this matrix design made by a contract manufacturer we approached several companies and the quotes to do so came in ranging from \$3,000 to \$18,000. This was just for a single forearm design, so extrapolating this cost to the entire ATD, even with our providing each ATD body region integrated matrix design, would lead to a cost prohibitive sensing skin. Thus we embarked upon attempting to fabricate this forearm sensor matrix design using affordable in-house capabilities.

The two approaches that were evaluated for their feasibility include

- 1) photolithography - typically used to transfer geometric patterns from a mask to the surface of a silicon wafer, and

2) Printing the sensor matrix pattern directly onto flexible copper clad using a solid ink laser printer, followed by a copper etching process.

Appendix C outlines the steps used to attempt to create the integrated sensor matrix conductive side using photolithography in the University of Louisville Micro/Nanotechnology Center (clean room). As described in Appendix C, this method was found to produce a pattern with discontinuities, and thus was deemed to be unacceptable. However, the direct printing of the conductive side pattern proved to be successful once we employed a solid ink laser printer. This method entailed direct printing of the pattern from a CAD-based drawing onto flexible copper clad sheeting fed into the printer. The copper clad sheeting with the pattern was then subjected to etching to remove unprotected copper, thereby retaining the wax-protected copper pattern (Figure 5). The final step was to protect the copper traces from corrosion by overlaying them with a tin coating. Joining the conductive side with a 1 M ohm semi-conductive material formed the FSR.

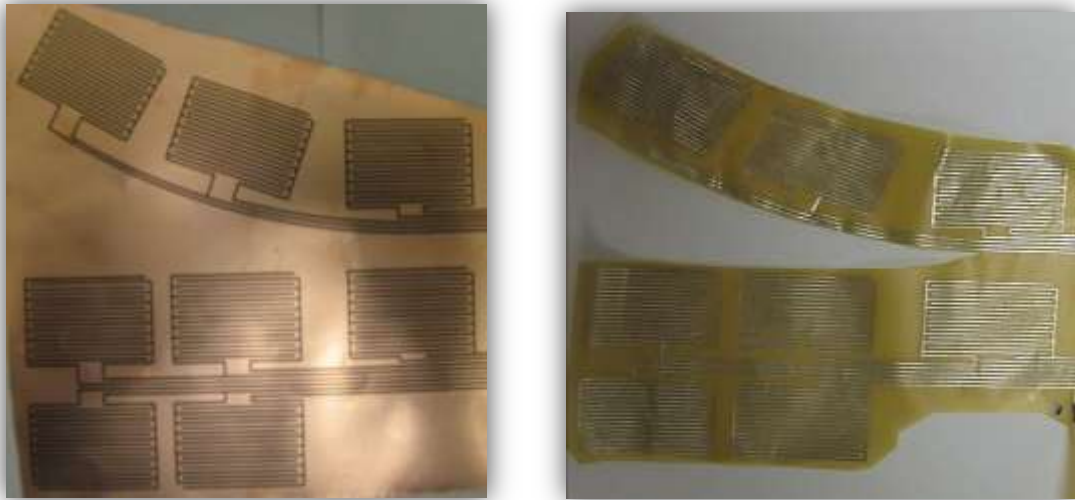


Figure 5: Conductive side forearm sensor matrix printed using solid ink on copper clad sheeting and etched.

In comparison to commercial fabrication of our forearm sensor matrix design (\$3000), our sensor material costs after purchasing a \$600 solid ink printer (also used to produce subsequent sensor matrices) were approximately \$20 and required approximately 5 hours for sensor fabrication. The in-house printed sensor was compared to initially established design criteria and was determined to have acceptable performance (Table 5).

Table 5: In-House Printed Sensor Performance Versus Design Criteria

Sensor Technology	U of L Printed Sensor	Design Criteria
Sensing range (kPa)	0–690	≥ 0–760
Sensing range (psi)	0 – 100	≥ 110
Resolution (sensors per cm ²)	>1	1
Sensor elements	Variable	-
Sensitivity (psi)	1 – 100	≥ 0 – 110
Error	-	≤ 5%
Response time (msec)	≤ 1	2
Hysteresis	-	≤ 5%
Conformability	6.25 cm radius	6.25 cm radius
Temperature range (°C)	-15 to 200	-20 to 50
Scan rate	250 kS/s	Variable
ADC resolution	16 Bit	Variable
Weight	0.2 gm/sensor	1 gm/sensor
Thickness (mm)	0.3 mm	1
Active area (mm x mm)	Variable	Variable
Lifetime in cycles	> 10 ⁶	> 50,000
Cost	\$ 0.41	≤ \$ 0.50

Prototype Sensing Skin Development

We initially created a prototype(s) forearm sensing skin using off-the-shelf commercial sensors available in limited sizes and shapes. Forearm prototype sensing skins were generated using individual FSR sensors from Sensitronics. A total of 17 square sensors were used in this matrix prototype, where all sensors were protected by inner and outer neoprene layers cut in a pattern that fit snugly when wrapped around the forearm (Figure 6). Ends of the neoprene were joined together to maintain placement on the forearm.



Figure 6: Neoprene patterns (top and bottom layers) cut for the prototype matrix sensor that would wrap around the forearm.

The FSR sensors forming the sensing skin prototype (Figure 7) were wired together so as to have a common lead that could be fed into the data acquisition system, where sensor data could be collected and processed using Labview.



Figure 7: Prototype sensor matrix showing the placement of the sensors in relation to the forearm and associated wiring.

As previously stated, off-the-shelf sensors were only available in limited small sizes and incorporating them in the sensing skin would create a large sensor density on ATD surface. For smaller ATD surfaces such as the forearm, this may be acceptable, however to get full coverage of larger surfaces such as the chest and back, this would translate to a large number of sensors increasing bulk and weight. We looked into an alternative technology of piezo electric sensors that were available in larger sizes than off-the-shelf FSR's. The piezoelectric film sensors were made by Measurement Specialties Inc (Figure 8) and function by producing an output voltage proportional to change in strain applied.



Figure 8: Piezoelectric film sensors designed by Measurement Specialties Inc.

Ten piezo electric sensors were used to develop an additional prototype sensor matrix for the forearm of the test dummy. The matrix consisted of the piezo film sensors wired together to a common lead and sandwiched between two layers of neoprene cut to fit the dummy's forearm (Figure 9).



Figure 9: Prototype matrix using piezo-film sensors showing the placement of the sensor matrix.

Additional forearm sensing skins were developed using individual in-house milled sensors (Figure 10 b), and using the in-house printed integrated sensor matrix (Figure 10 c). As evident in Figure 10, the in-house integrated sensor matrix prototype (Figure 13c) led to a sensing skin having a uniform thickness and reduced bulk. Additionally this prototype had the lowest mass, an important factor when adapting the sensing skin to the ATD so as to not alter the inertial characteristics of the ATD.




		
<p>Figure 10 a. Prototype sensing skin using individual commercial sensors.</p>	<p>Figure 10 b. Prototype sensing skin using individual in-house milled sensors.</p>	<p>Figure 10 c. Prototype sensing skin using in-house integrated sensor matrix.</p>

Figure 10: Comparison of forearm sensing skin prototypes

Conclusions

We successfully established design criteria and requirements for the force sensors, and sensing skin that would be required in the surrogate bruising detection system. Testing and the evaluation results proved that commercial off the shelf sensors were too bulky to work into our needs and custom sensors from industry manufacturers would not be cost effective to get full coverage of the ATD. This led us down the path to custom develop our own in-house force sensors after finalizing on a viable method of production. The in-house sensors would prove to be the candidate sensors that would be a primary component in our surrogate bruising detection system.

CHAPTER III:

DESIGN AND DEVELOPMENT OF A FORCE SENSING SKIN ADAPTED TO A CHILD SURROGATE TO IDENTIFY POTENTIAL BRUISING LOCATIONS

OVERVIEW

Unexplained bruising is an early sign of child abuse. Bruising locations on the body can be an effective delineator of abusive versus accidental trauma. However, the ability to predict potential bruising locations associated with falsely reported events (e.g. bed falls, stair falls) in child abuse does not exist. In our study we adapted an existing pediatric anthropomorphic test device (ATD) with custom developed force sensors integrated into a conformable skin. The sensors were coupled to a data acquisition system through which recorded force data was displayed on a computerized body mapping image system. A simulated abdominal blow demonstrated the modified ATD's capability to predict potential bruising location and impact force. To our knowledge no such system exists. This forensic tool can ultimately be utilized to develop a knowledge base of potential bruising "roadmaps" associated with accidental and abusive events.

INTRODUCTION

Child abuse is a leading cause of fatality in children aged 0-4 years. An estimated 1,760 children die annually as a result of child abuse of which three-quarters (75.7%) of the children were younger than 4 years old¹. Infants (younger than 1 year) had the highest rate of fatalities among the group. Additionally, there were approximately 150,000 children who are permanently disabled each year in association with child abuse¹. Many of the serious injuries and fatalities could have potentially been prevented if clinicians and child protective services were able to better distinguish between injuries associated with abuse versus those caused by accidents. Missed cases of child abuse have been shown to be as high as 71%, where children were presented to hospitals for their injuries and not evaluated for abuse². Additionally, when perpetrators are charged with child abuse, little more than half of the cases move forward to prosecution as opposed to being screened out for reasons including the need for further investigation or insufficient evidence³. Therefore there is a need to provide clinicians, child protective services and law enforcement personnel with improved knowledge related to the types of injuries that are possible from common household accidents that are often falsely reported to be the underlying cause of injury in child abuse.

Bruising is an early sign of abuse, and can be an effective indicator of child abuse. Although not life threatening, bruising characteristics and bruising patterns (constellation of individual bruises throughout the body) provide a “roadmap” documenting a child’s exposure to impact. Previous studies have

relied upon the use of instrumented anthropomorphic test devices (ATD), or test dummies, to investigate injury risk in common childhood falls and accidents⁴⁻⁷. However, the ability to predict potential bruising locations occurring in association with falsely reported events in child abuse does not exist, and could prove useful in the distinction between abusive and accidental injuries.

In our study we propose to modify an existing pediatric ATD to allow for the prediction of potential bruising location in children during common household fall events that are often stated as false scenarios in child abuse. The scope of this project included the development of a “sensing skin” that was adapted to a commercial pediatric test dummy. This modified test dummy is capable of being used in mock laboratory experiments replicating common household injury events while the “sensing skin” measures and records levels of impact force and locations of impact on the human surrogate. This recorded data will provide a “roadmap” of the human surrogate’s contact exposure during a specific event and will identify the associated potential bruising roadmap for that specific event.

METHODS

System Overview

The surrogate bruising detection system was developed specifically for the 12 month old CRABI ATD (10 kg mass with a standing height of approximately 30 in) since bruising in this age group of children who are not independently mobile is often suggestive of abuse^{29,34}. Additionally there is a high rate of abuse

related fatalities in children aged 1 year or less¹. The conceptual model of the surrogate bruising detection system (Figure 11) consists of the following components:

- a pressure sensor integrated sensing skin,
- a data acquisition system, and
- a computerized body mapping image system.

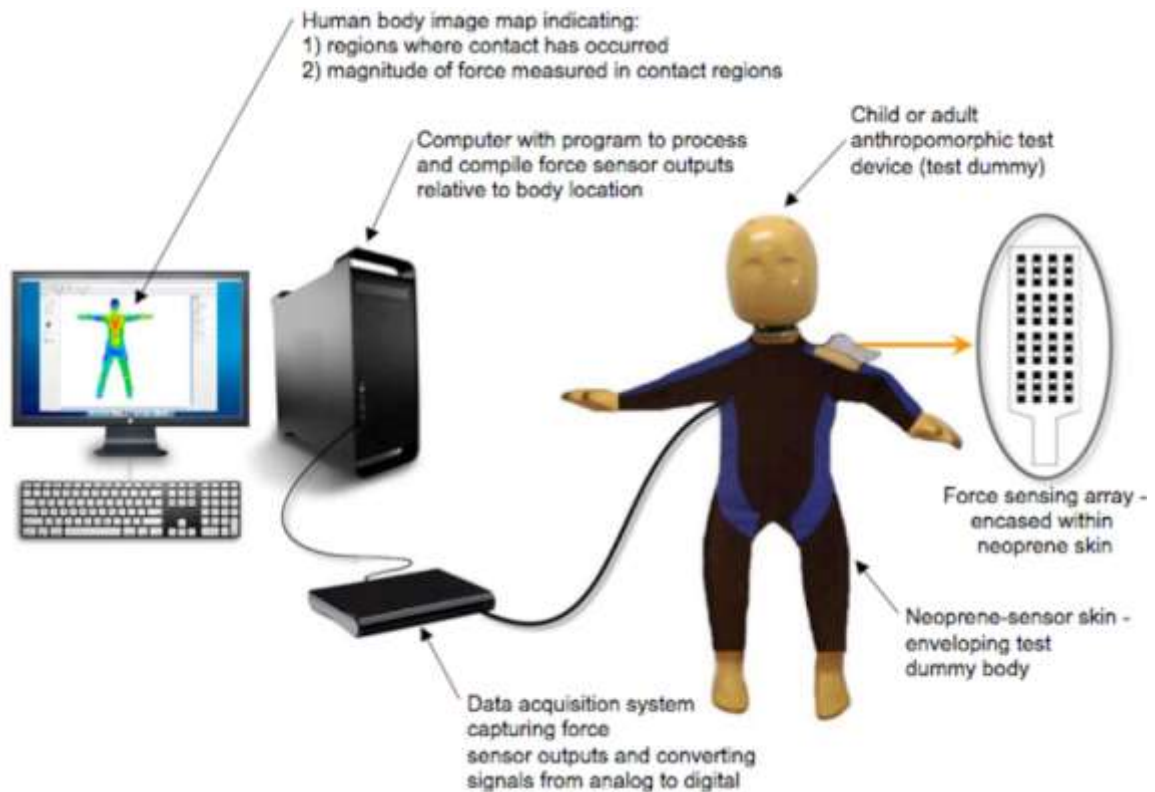


Figure 11. Conceptual model of surrogate bruising detection system (Patent No.: US 8,292,830 B2).

Sensor Overview

There are a wide range of force/pressure sensors available having various operating principles and functional ranges. Additionally, they can have different shapes and sizes, and could be constructed from a variety of materials. The majority of the sensors available are based on resistive, capacitive, piezoelectric or optical technologies. We opted to use resistive based sensors in our application because of their relatively simple operation and ability to operate satisfactorily in impact environments (shock resistance). The operating principle of the resistive sensor is based on the conversion of a change in physical pressure applied to the sensor, to a relative change in the sensor's electrical resistance. Mostly, resistive sensors measure an increase in applied force through a proportionate decrease in resistivity measured across the sensor electrodes. A typical resistive force sensor is made up of two parts. One part usually being a flexible polymer sheet that is either screen printed (thick film) or deposited (thin film) with conductive lines and the other part being a semi-conductive or pressure sensitive ink printed on a flexible substrate. These two layers placed over each other make up a force sensing resistor (FSR).

The ATD was divided into seven regions including the head, anterior torso, posterior torso, forearm, upper arm, thigh and shank; each requiring FSR coverage. Each section was individualized with a custom sensor array or matrix containing a varying number of sensor sizes and shapes depending on their location. This customized conductive layer was paired together with a semi-conductive layer (Sensitronics LLC, Bow, WA) to produce the FSR. These

customized FSR's were then integrated into a protective neoprene covering to form the sensing skin that could be easily adapted to the ATD's body segments. Each individual sensing region of the ATD that was equipped with a sensor matrix has a flat flexible cable (FFC) that serves as an individual wire lead for all sensors in that region to complete the connection to the data acquisition system.

Data Acquisition System (DAQ)

The data acquisition system collected and compiled the output from the sensing skin adapted to the ATD. The sensor matrices FFC's leading from each region of the ATD terminated on breakout boards that were wired to a connector block which in turn were connected to a DAQ card in the computer. Additionally, the resistive sensors in the sensing skin were connected to the DAQ through a voltage divider circuit to convert resistance to voltage; one sensor lead was connected to a power source and the other lead connected to ground, through a pull-down resistor. The points between the fixed pull-down resistor and the FSR served as the connection point to the analog input of the DAQ card.

Data acquisition hardware (National Instruments, Austin, Texas, U.S.) was used to capture and convert the analog sensor output. The multifunctional input/output data acquisition cards (NI, PCI-6225) acquired, conditioned and digitized the sensor output signals. The National Instruments PCI-6225 data acquisition card is capable of measuring 80 single ended analog channels at a 16 bit resolution and a sample rate of 250kS/s. A personal computer served as the platform for the data acquisition hardware.

Image Mapping

Graphical programming application software (Labview 2009, NI) was used to acquire, process, analyze, store and present sensor output in a meaningful format. This software provides algorithms and functions designed specifically for analysis and signal processing. A Virtual Instrument (VI) was developed to accomplish this objective. An active 3D (3-dimensional) body map image representing the ATD served as a graphical interface and was developed using Labview (National Instruments) software. The body image was discretely mapped to the sensors on the ATD such that active sensor outputs (those which have been impacted) and their locations were displayed on the computerized body map image. Sensor outputs in terms of force were color-coded, designating a pre-determined force range so as to aid in the quick overview of locations with high intensities of impact. The color contours/gradients were generated as a function of the sensor recorded force and distance from the sensor. The region at the center of the sensor represented the color equating to the recorded force value. As the distance increased from the sensor, the color gradient radially propagated outward, decreasing the color representative force value. This reduction was proportional to the distance from the sensor.

The three elements of the surrogate bruising detection system (sensing skin, DAQ, image mapping) were integrated into one functional unit with the capability to detect impact events, and present sensor outputs in a useful

computerized body map image that displays location of impact and level of impact force.

RESULTS

We designed individual custom sensor matrices for each of the seven regions of the ATD. However, to illustrate the design and development of the sensors we will limit our description to one of the seven regions of the ATD; the forearm.

Adapted Sensing Skin

Two-dimensional drawings of the sensor matrix and associated wiring terminating at a single point were prepared. The forearm section representing the conductive side of the sensor which consists of 8 individual sensors arranged to fit the contours of the ATD geometry is shown in Figure 12.

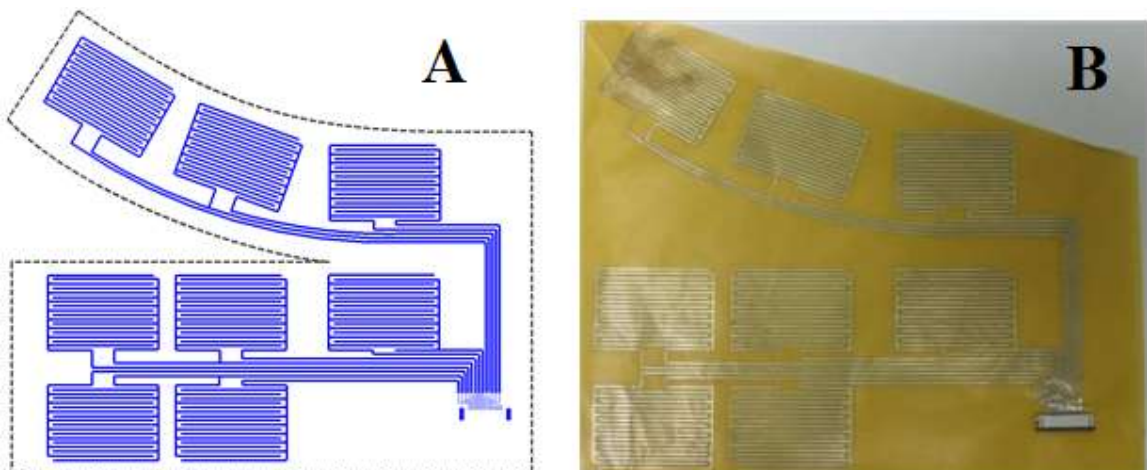


Figure 12 : The sensor matrix schematic incorporating 8 individual sensors and associated wiring that constitute the forearm sensor matrix (A). The sensor

design etched on copper clad laminate, constituting the conductive side of the forearm sensor matrix illustrating the individual sensors and associated leads coming together at the terminal point where the ZIF connector was soldered (B).

The sensor design pattern (Figure 3-A) was printed onto copper clad laminate (DuPont™ Pyralux®, FR 91130R) and then etched, generating the conductive side of the FSR. Following sensor fabrication, a zero insertion force (ZIF) connector was soldered to the matrix to facilitate easy attachment of a FFC lead that links the sensor matrix to the DAQ system (Figure 3-B). The copper clad sensor matrix was layered with the semi-conductive material (Sensitronics LLC, Bow WA) to form the force resistive sensors (FSR). This material has a resistance of $1M\Omega$, with standoff dots, that adds to the initial resistance of the sensor. The FSR was then sandwiched between two layers of neoprene that was cut in a pattern so as to conform to the ATD's forearm (Figure 13). A high level of friction between the neoprene and ATD surface, as well as the conforming pattern, serves to limit movement of the neoprene relative to the ATD when the sensing skin is adapted to the ATD.



Figure 13: The forearm sensor matrix enveloped in neoprene, ready to be adapted to the ATD.

Sensor Characteristics

Once the output voltage from the sensors was read via the Labview VI and represented on the computer display, a means of calibration was established to convert the sensor voltage output into the appropriate units of force by adjusting the sensitivity of the force sensor. There are several factors affecting the calibration as the sensor output voltage is proportional to the sensor supply voltage, voltage divider resistance, semi-conductive material resistance, sensor space (spacing) and trace (width). Furthermore, sensor output is influenced by location-specific characteristics such as the variation in ATD surface curvature/contour and non-uniformity in the underlying substrate thickness of the

ATD representative soft tissue. Varying a sensor's initial radius of curvature influences its unloaded voltage output, thereby introducing an offset that must be zeroed during calibration. Additionally, changes in underlying ATD surrogate soft tissue thickness has a direct influence on the stiffness of combined substrate underlying the sensor which could either decrease (softer ATD substrate) or increase (firmer ATD substrate) the sensor's registered load. When force is applied to a sensor on the ATD, there is a deflection in the ATD underlying representative soft tissue, leading to depression of the sensor, which varies the sensor's radius of curvature. The sensor output is dependent upon the extent of surrogate soft tissue deflection. Therefore it is essential to individually calibrate each sensor while properly positioned on the ATD to account for location-specific characteristics in the calibration curve.

The sensors' were calibrated (dynamically) while positioned on the ATD, using a force transducer to generate a specific load-voltage profile (Figure 14-A). Additionally, sensor repeatability was evaluated using a material testing system (MTS) (Figure 14-B) where sensors were subjected to loads of 10, 20 and 30 lbs while recording sensor output in order to compare sensor recorded and MTS applied loads. The force was administered on the sensor adapted to the forearm (approximate radius of curvature of 0.9 in) such that the ratio of force distribution area to sensor area was 0.25. The mean percent error recorded across the FSR measured load and the MTS measured load was 0.76%, 0.79% and 0.38% for the 10, 20 and 30 lbs, respectively. Figure 15 illustrates the loads exerted on the

sensor by the MTS versus the load measured by the FSR sensor during this testing.

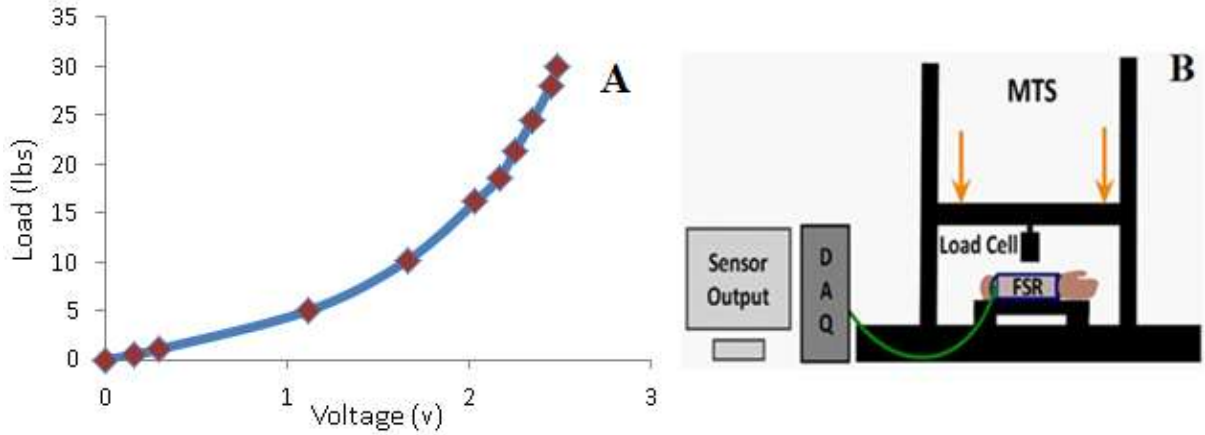


Figure 14: Load versus voltage calibration profile for the forearm sensor (A). FSR sensor repeatability testing schematic indicating a load applied to the sensing skin fitted on the ATD forearm (B).

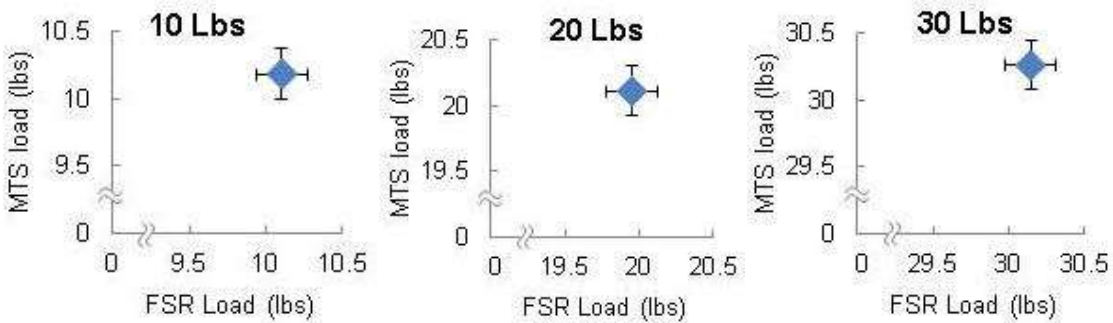


Figure 15: Loads of 10 lbs (n=6), 20 lbs (n=6) and 30 lbs (n=6) exerted by the MTS versus load measured by the FSR to demonstrate sensor repeatability (error bars show one standard deviation).

Although Figure 15 illustrates test data from 6 trials under 3 loading conditions for an individual sensor, this sensor is representative of all sensors implemented within the sensing skin given that FSRs use the same semi-conductive and conductive materials and have the same space and trace.

Computerized Body Mapping Image System

The calibration data was entered into the customized Labview VI developed to collect sensor data through the DAQ cards. Within the Labview VI, the sensor matrix output was represented on a 3D image of the ATD, to provide visual details of location and active sensor force readings. Figure 16-A illustrates compression (i.e. squeezing) of the forearm with varying color intensities equating to the level of force measured by the sensors. Additionally the ATD abdomen was dynamically impacted with a fist blow to illustrate the body mapping system's function (Figure 16-B).

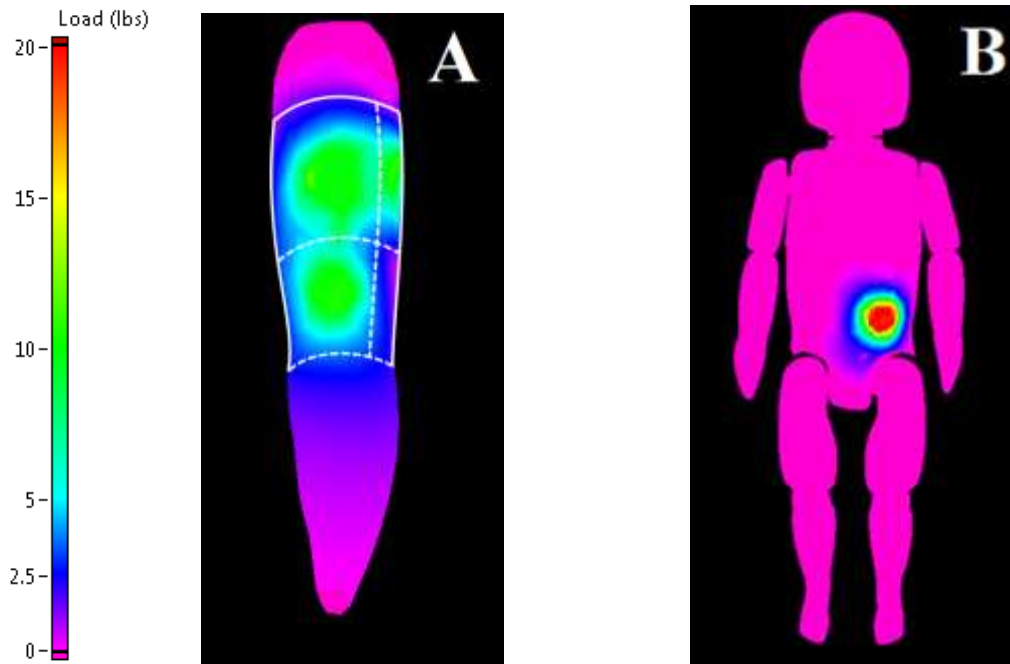


Figure 16: 3D body mapping images of the forearm (overlying the outline of individual sensors shown in white) (A) and complete ATD (B) capable of displaying varying colors dependent on the level of force imparted to specific regions of the body. Test results show peak force on the forearm sensor matrix associated with a squeezing action (A), and peak force on the abdominal region sensor matrix associated with a fist blow (B).

The same design process described for the sensor matrix of the forearm body region (ranging from custom FSR design and fabrication, to FSR calibration and finally sensor integration into the DAQ system for 3D-image sensor mapping) was repeated for all other remaining body regions of the ATD to complete the entire surrogate bruising detection system.

DISCUSSION AND CONCLUSION

ATD's or crash test dummies provide valuable data related to how the human body reacts to crashes and have contributed greatly to this cause. They have been designed primarily to measure response to acceleration, deflection, force and moments generated during a crash. However, the capability to assess the potential for soft tissue injuries such as the bruising has not been addressed by current ATD designs. The goal of our system was to provide an ATD adaptation with the capability to record locations of impact and measure contact force during simulated events. These recorded contact locations are regions where soft tissue injury such as bruising may occur. The only comparable soft tissue injury assessment device is the Facial Laceration Measurement System (FMLS) produced by Humanetics Innovative Solutions Inc. (Plymouth, MI). Our device differs from the FMLS in that it is capable of measuring and recording location of contact and force applied to any region of the body rather than solely the face.

Our system was designed so as to not inhibit the free motion of the joints or place any additional resistance on the ATD joints. This was achieved by limiting interference between the sensing skin and the moving components of the ATD. An additional goal was to assure that the inertial properties of the ATD were not altered. The total weight added to the ATD over the entire surface of coverage is approximately 1.4 lbs including all components of the sensing skin. When compared to the weight of the 12 month old ATD (22lbs) this equates to an

increase of approximately 6.4% evenly distributed over the coverage area which should not alter ATD dynamics as it relates to inertial characteristics.

In the diagnosis, investigation, and legal prosecution of child abuse cases, bruising patterns (constellation of individual bruises throughout the body) are often overlooked by child protective services, pediatricians, law enforcement personnel, biomechanics experts, and the judicial system since these injuries are typically non-life threatening. However, ignoring the incidence of bruising patterns is a missed opportunity to gain a better understanding of the environment that a child has been exposed to. Bruising provides a “roadmap” illustrating the child’s exposure to force application. Previous studies have shown that bruising patterns resulting from abuse are significantly different than those resulting from accidents^{31,39} and our bruising detection system will aid in further distinguishing biodynamic compatibility between the bruising pattern and stated cause. The surrogate bruising detection system has the potential to influence child abuse diagnosis, investigation and prosecution by contributing objective biomechanical data to the overall assessment of the child’s injuries.

Use of our device is expected to provide key personnel with objective data as to potential bruising locations that can be expected in common household accidents that are often provided as false histories in an effort to conceal child abuse. Conversely, use of the surrogate bruising detection system has the ability to provide objective data regarding potential bruising locations that can also serve to exonerate those who are innocent of alleged abuse. Thus, the surrogate bruising detection system provides an objective method to elucidate the

differences in potential bruising locations that can occur in abusive versus accidental trauma as a source of evidentiary data in the diagnosis and prosecution of child abuse.

Additional applications could include the assessment of soft tissue injury risk in automotive crash safety testing, as well as to simulate and evaluate abusive versus accidental soft tissue injuries in the elderly population, as bruising can also be a marker of elder physical abuse^{60,61}.

LIMITATIONS

The ATD has a total of 114 sensors that cover approximately 576 square inches. This implies an approximate sensor density of 0.2 sensors per square inch. The number of discrete sensing points was guided by a study that retrospectively reviewed bruising histories from the medical record of children aged 0 to 48 months that had been admitted to the Pediatric Intensive Care Unit with either accidental or abusive trauma in an effort to develop a bruising clinical decision rule⁶². In that study, all skin findings were recorded in a skin assessment database that allowed for region-specific documentation. Each entry consisted of the type of skin finding, body region of skin finding, and the number of discrete skin findings. In our bruising detection system, we chose a sensor density to allow us to distinguish contact points on the ATD with equally distinguishable spatial resolution for the different body regions as in the study by Pierce et al⁶². Although an increased sensor density would have resulted in an enhanced resolution in sensor recordings it would have required an increased number of

sensors, connectors, and associated wiring; all of which would increase the weight of the bruising detection system and thus the ATD. Additionally, a higher sensor density implies an increased number of input channels to the DAQ system, thereby increasing the complexity and cost of the device.

FSR sensor output is dependent on the ratio of force application area to sensor area. The sensors were calibrated at a 25% force application-sensor area ratio. However since it is difficult to predict how much of the sensor's active area will be contacted while using the system in experiments, there could be a small percent error in the output force recorded by the sensors. For example, we found that in altering the ratio of applied force contact area to active sensor area, from 25% to 75%, there was a maximum 3% error observed for constant loads of 10, 20 and 30 lbs. Therefore, this limitation must be considered when interpreting force output data recorded by the system.

The occurrence and severity of a bruise varies from person to person for a given application of forces given the many contributing factors that affect bruise development^{26,63,64}. Extrinsic factors such as the amount of force applied, rate of force application, and distribution of the force over larger/smaller areas are parameters that can affect the presence or absence of a bruise. Additionally, intrinsic factors related to the physiological and anatomical structures, such as architecture of the skin, soft tissue thickness, toughness of skin, fat content, vessel fragility, and presence and depth of underlying bone add to the complexity of this physiological event⁶⁴. Variables such as blood platelet levels, systemic blood pressure, vascular diseases and vasoactive or anticoagulant drug use in

addition to nutritional and allergy related disorders can have a great influence on the presence, absence and variability in intensity of bruise^{25,64-66}. This implies that the minimum load to cause bruising, the “bruising threshold”, varies across individuals. However it can be said with some degree of certainty that larger forces are associated with a greater potential for bruising. So instead of definitively asserting the presence of a bruise, we envision our device to be used as an investigative tool to determine potential bruising locations occurring within a body region under specific loading conditions.

The biofidelity of the CRABI ATD and in particular the soft tissue biofidelity is a limitation of our bruising detection system. The ATD surrogate tissue consists of a heat cured vinyl plastisol which is molded to mimic the contours of the body regions. There is urethane foam between the outer and inner layers of vinyl plastisol, which is compliant and is intended to represent the soft tissue of a child. The tissue biofidelity greatly influences force/pressure measured by our system as the sensor measured forces are proportional to the stiffness of the underlying ATD surrogate soft tissue. Also, since the CRABI ATD was primarily designed for measuring a child’s response to a high deceleration automotive crash environment, any testing conducted with the ATD in lower deceleration events (e.g. short distance falls) are limited by the biofidelity of the ATD. These limitations must be considered when using the ATD-adapted force sensing skin to assess bruising potential in falls.

CHAPTER IV:

POTENTIAL BRUISING PATTERNS ASSOCIATED WITH REARWARD FALLS IN CHILDREN

OVERVIEW

Children presenting multiple unexplained bruises can be an early sign of physical abuse. Bruising locations on the body can be an effective delineator of abusive versus accidental trauma. However, the ability to predict potential bruising locations associated with accidents (childhood falls) often used as falsely reported events in child abuse does not exist. In our study we used a 12-month old pediatric anthropomorphic test device (ATD) adapted with a custom developed force sensing skin to predict potential bruising locations during rearward falls from standing. The sensing skin measured and displayed recorded force data on a computerized body image mapping system when sensors were activated. Simulated rearward fall experiments were performed onto two different impact surfaces (padded carpet and linoleum tile over concrete) with two different initial positions (standing upright and posteriorly inclined) so that the ATD would fall rearward upon release. Findings indicated possibility of bruising in the posterior plane primarily within the occipital head and posterior torso regions.

INTRODUCTION

The United States is infamous as one of the worst among developed nations in its prevalence of child abuse. On average between four and seven child fatalities occur daily because of child abuse and neglect in the U.S.¹. Child abuse is a leading cause of fatality in children up to 4 years of age; an estimated 1,520 children are fatally injured annually as a result of child abuse¹. Infants (less than 1 year in age) are the most vulnerable to abuse and have the highest rate of fatalities of all age groups¹.

Bruising in children is visually apparent and is frequently an early manifestation of a child's abusive environment. Accidental bruising is infrequently observed in infants, due to their low degree of independent mobility⁶⁷. Bruising locations and bruising patterns (constellation of individual bruises throughout the body) provide a "roadmap" documenting a child's exposure to impact. Health care professionals and law enforcement officials often have to address the question of likelihood that a child's presenting injuries are compatible with history provided by the care giver. If injuries were distinguishable between accidental and abusive trauma, presenting abused children could be diverted from being reintroduced into their abusive environments which often results in further harm or death⁶⁸.

Previous studies have retrospectively highlighted differences in bruising patterns observed clinically, to provide a better understanding of skin findings in children that maybe at a high risk of abuse in their current

environment^{25,29,34,36,62,67,69,70}. However, the ability to predict potential bruising locations associated with falsely reported events (e.g. short distance falls) in child abuse does not exist and could prove useful in the distinction between abusive and accidental injuries.

In our study we used a bruising detection system to identify potential bruising patterns in simulated rearward falls from standing using a child surrogate representative of a 12-month old child (stage of early independent mobility). The bruising detection system consists of a pediatric anthropomorphic test device (ATD) adapted with a custom developed force sensing skin that is linked to display recorded force data on a computerized body mapping image system when the force sensors are activated⁷¹. Simulated rearward fall experiments were performed onto two different impact surfaces with two different initial positions, while recording ATD impact sites so as to predict potential bruising locations.

The purpose of this study is to provide a “roadmap” of the child surrogate’s contact exposure during specific fall events and to identify whether variations in the fall parameters (impact surface, initial position) lead to differences in impact locations. Our goal was characterize potential bruising locations or patterns associated with a common childhood fall.

METHODS

The surrogate bruising detection system (SBDS), consisting of the 12 month old CRABI ATD (10 Kg mass) fitted with a force sensing skin and associated data

acquisition hardware and analysis software, was used to predict potential bruising patterns in simulated fall scenarios. The sensing skin of the SBDS consists of 114 force sensors enveloping the surface of the ATD that is divided into seven regions including the head, anterior torso, posterior torso, upper arm (arm), lower arm (forearm), upper leg (thigh), lower leg (shank). Each region has individualized custom sensor arrays. Graphical programming software (Labview 2010; National Instruments, Austin, Texas) was used to acquire and display sensor output in a manner that relates sensor location to body region. Additional details of the SBDS and its individual components are described in earlier publications^{71,72}.

The SBDS was used to assess potential bruising locations on the body during a series of rearward fall experiments as this type of fall is commonly experienced by children who are in the early development stage of independent mobility.

Test Setup

The ATD was placed in an upright standing (orthostatic) position on ground level using a suspension system supported by a tripod with a manually operated release mechanism to allow the ATD to fall under the effect of gravity. The ATD has a standing height of 74.7cm (29.4 in). Fall experiments were conducted using two different initial conditions. The ATD was suspended to fall rearward upon release starting from two initial positions. The first initial position (Fig. 17) being a torso angle of 20 degrees (this was the minimum angle required to initiate repetitive rearward falls) and the second, 30 degrees to the vertical.

From now forward the 20 degree initial position will be referred to as the “upright” position and the 30 degree initial position will be referred to as the “inclined” position. The ATD’s CG height above ground level differed for each fall scenario (Table 6). In both fall scenarios the ATD’s feet were in contact with the ground at the start of the fall. To initiate a fall, the release mechanism was activated which released the ATD allowing it to fall rearward.



Figure 17: ATD in an upright initial position (scenario 1) for simulated rearward fall experiments

Prior to each fall, ATD joint angles were adjusted using a goniometer to ensure repeated positioning in all tests. Additionally, joint stiffness was calibrated to manufacturer specifications whereby the joints were tightened until the friction was just sufficient to support the weight of the limb against gravity. Two impact surfaces were evaluated for each fall scenario: 1) padded carpet over a wood subfloor and 2) linoleum tile over a concrete subfloor. The carpet surface consisted of a 1.3 cm (1/2 in) thick open loop carpet placed over 1.0 cm (3/8 in)

thick foam padding. The carpet and padding were placed over a 1.9 cm (3/4 in) thick plywood platform 183 cm x 91.5 cm (6 ft x 3 ft) built to standard building codes with 5.1 cm x 10.2 cm (2 in x 4 in) joists, spaced 40.6 cm (16 in) on center. 0.32 cm (1/8 in) linoleum tile was adhered to a concrete subfloor for the second impact surface scenario used in fall experiments.

Data Acquisition and Analysis

The SBDS's sensors consist of force sensing resistors whose outputs were fed to the data acquisition system through a voltage divider circuit to convert resistance to voltage. Data acquisition hardware (National Instruments, Austin, Texas) was used to capture and convert the analog sensor output. Multifunctional input/output data acquisition cards (PCI- 6225; National Instruments) acquired, conditioned and digitized the sensor output signals. A personal computer served as the platform for the data acquisition hardware.

Graphical programming software (Labview 2010; National Instruments, Austin, Texas) was used to acquire, process, analyze, store and present sensor output. An active 3D body map image representing the ATD served as a graphical interface; the ATD body image was discretely mapped to the sensors on the ATD such that active sensor outputs (those which have been impacted) and their locations were displayed on the computerized body map image. Sensor measured forces were color-coded, designating a pre-determined force range so as to provide a quick overview of body regions with high intensities of impact. A

filtering lower bound force of 4.5 N (≈ 1 lb) was used to establish the onset of contact between the ATD and impact surface.

Eight trials of each simulated rearward fall scenario (upright and posteriorly inclined initial positions) were conducted onto two different impact surfaces (padded carpet and linoleum) (Table 6). A total of 32 fall experiments were conducted.

Table 6: Evaluated fall scenarios, ATD center of gravity (CG) position and impact surfaces

Fall Type & Initial Position	CG Height (cm/in)	Surface Type
Rearward – Upright	46 (18)	Padded Carpet on Wood
		Linoleum Tile on Concrete
Rearward – Posteriorly Inclined	38 (15)	Padded Carpet on Wood
		Linoleum Tile on Concrete

Motion Capture

All falls were captured using a digital video camera (120 frames per second) to record overall fall dynamics. The camera was positioned so that the line of sight was perpendicular to the ATD sagittal plane. This allowed for qualitative assessment of fall dynamics.

Statistical Methods

A two-way analysis of variance (ANOVA) test was used to analyze impact forces on body regions to determine if initial position and impact surface factors led to significant differences. Additionally, post-hoc tests were conducted to further examine where significant differences existed ($p \leq 0.05$). Individual sensors were grouped by body region. Body regions were defined as head, anterior torso, posterior torso, left and right upper arm, left and right lower arm, left and right upper leg, and left and right lower leg.

RESULTS

Fall Dynamics

All fall scenarios generated contact in one body plane (posterior) and no other body planes came in contact with the impact surface.

Rearward Falls – Upright Initial Position

In the upright falls (scenario 1), the ATD fell after release into a squatting position with hips and knees flexed (200 ms – Fig. 18), then rotated rearward (posteriorly) about the feet. The first body region contacting the impact surface was the posterior pelvis (320 ms – Fig. 18), followed by the posterior aspect of the head and torso (450 ms – Fig. 18). Upon initial impact the ATD head and torso rebounded upward and rearward off the impact surface. This led to nearly

simultaneous secondary impact of the posterior head and torso (500 ms – Fig. 18). The body map images (Fig. 18) correspond to the video capture images describing areas of contact during the fall sequence. Since we were primarily concerned with the initial impact event, data associated with the secondary impact following rebound was not evaluated. Additionally, there were no observable differences in fall dynamics across surface type.

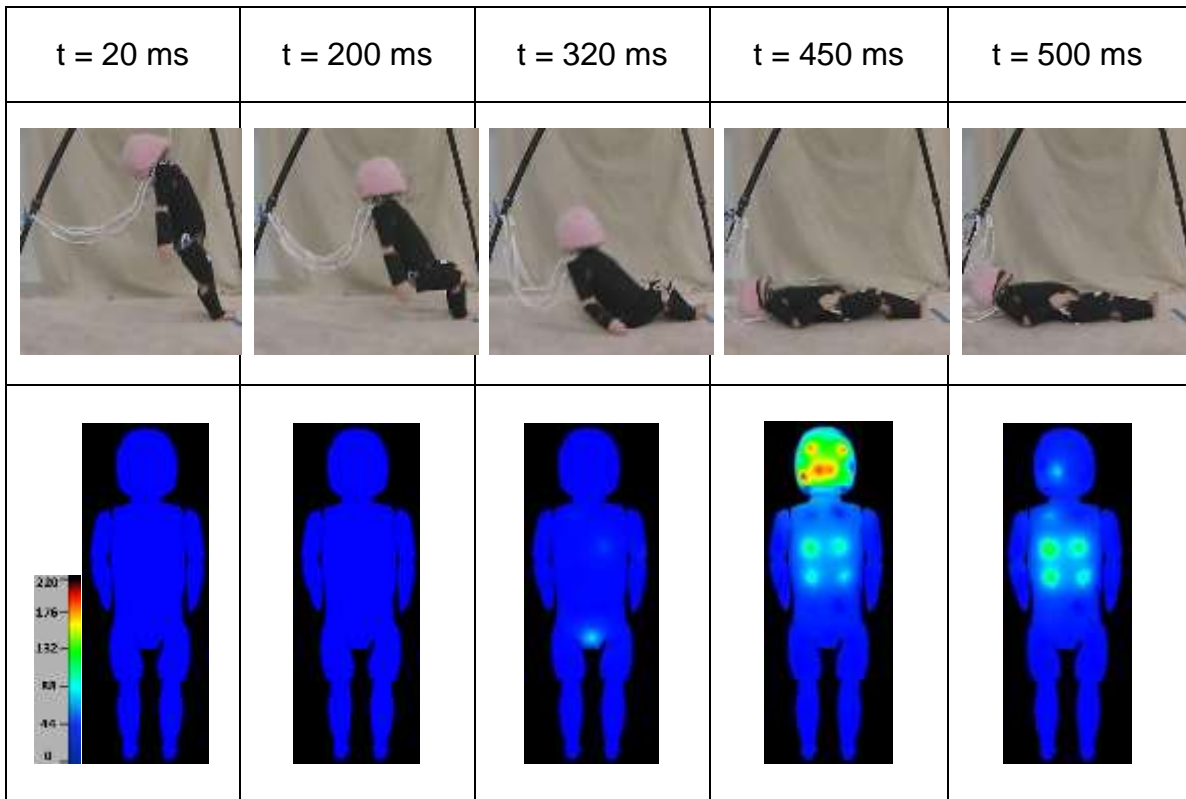


Figure 18: Frame sequences showing video capture of the upright initial position fall onto the carpet surface and SBDS body map images at corresponding time intervals. The body map images show the posterior ATD where the colors and intensities vary depending on the level of force (N) imparted to specific regions during the fall event.

Rearward Falls – Posteriorly Inclined Initial Position

In the inclined falls (scenario 2), the ATD torso fell downward flexing at the hip, followed by rearward rotation of the torso about the hip (hip extension). As the torso was rotating posteriorly about hip the neck extension occurred allowing the head to rotate posteriorly. The first body regions contacting the impact surface were the posterior pelvis and upper legs (200 ms – Fig. 19). The pelvis then rebounded, while the head and torso continued to rotate rearwards (350 ms – Fig. 19). Finally the occipital region of the head and posterior torso impacted the surface with the head leading the torso (450 ms – Fig. 19). Similar to the upright fall scenario, there were no visual differences in fall dynamics across surface type for the inclined falls. There was reasonable agreement between the body map images and video images of the fall sequence (Fig. 19).

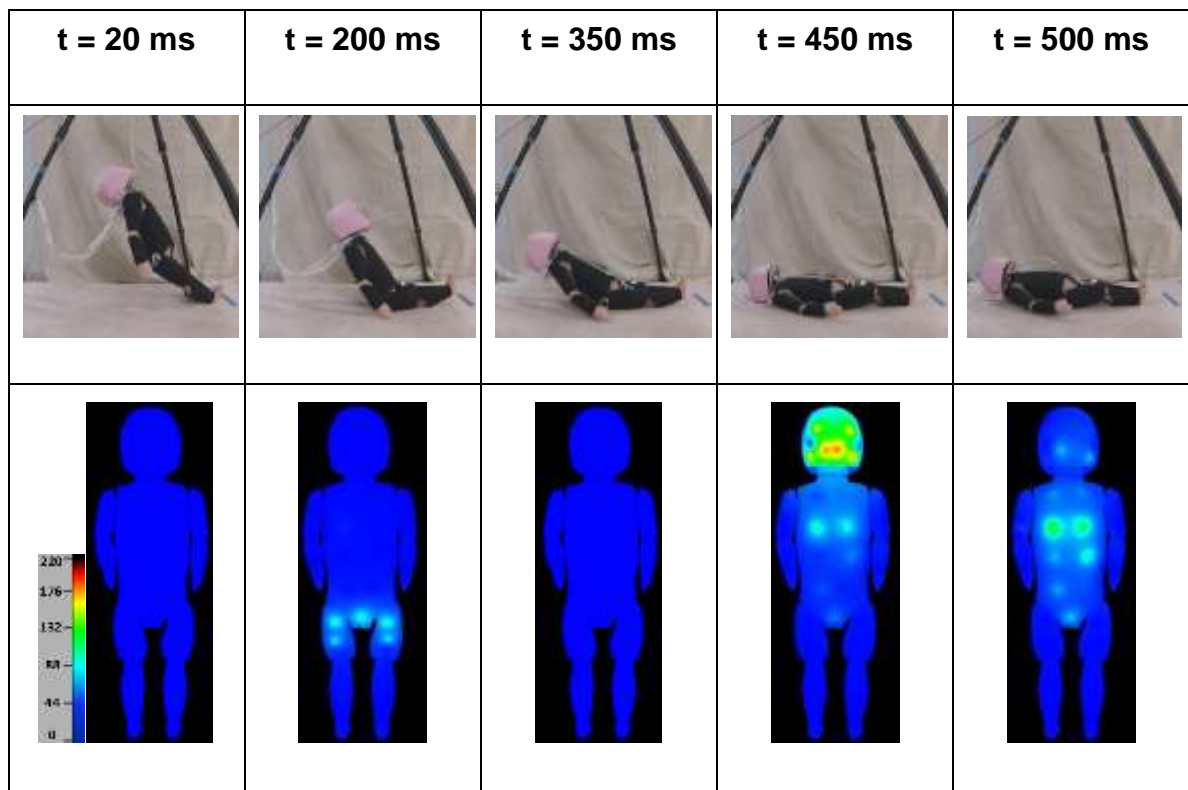


Figure 19: Frame sequences showing video capture of the inclined initial position fall onto the carpet surface and SBDS body map images at corresponding time intervals. The body map images show the posterior ATD where the colors and intensities vary depending on the level of force (N) imparted to specific regions during the fall event.

Contact Forces

The occipital region of the head and posterior torso were the two common body regions to contact the impact surface during all conducted falls. The mean peak impact force for the head (1995 N \pm 162) and posterior torso (1050 N \pm 154) were the highest in falls having an upright initial position onto the linoleum over concrete surface. The lowest mean peak impact force to the head (1050 N \pm 79) occurred during the falls having a posteriorly inclined initial position with impact onto the carpet over wood surface. The lowest mean peak impact force to the posterior torso (244 N \pm 61) occurred during falls with an upright initial position onto the carpet over wood surface (Table 7).

Table 7: Mean (8 trials) peak contact force (N \pm CI) for each body region in various fall scenarios

Body Region	Concrete Upright	Concrete Inclined	Carpet Upright	Carpet Inclined
Head	1995 ^a (\pm 162)	1397 (\pm 62)	1372 (\pm 90)	1050 ^a (\pm 79)
Anterior Torso	↓	↓	↓	↓
Posterior Torso	1050 ^a (\pm 154)	529 ^a (\pm 93)	244 (\pm 61)	291 (\pm 47)
Left Upper Arm	↓	↓	↓	↓

Body Region	Concrete Upright	Concrete Inclined	Carpet Upright	Carpet Inclined
Right Upper Arm	11 ^a (± 1)	↓	↓	↓
Left Lower Arm	16 ^b (± 5)	12 ^b (± 1)	↓	↓
Right Lower Arm	9 ^b (± 1)	12 ^b (± 1)	↓	↓
Left Upper Leg	↓	59 ^a (± 31)	↓	19 ^a (± 2)
Right Upper Leg	↓	71 ^a (± 38)	↓	22 ^a (± 3)
Left Lower Leg	20 ^b (± 11)	16 ^b (± 5)	↓	↓
Right Lower Leg	22 ^b (± 5)	12 ^b (± 6)	↓	↓

↓ – represents recorded forces that were below the established filtering lower bound of 5% of ATD body weight.

a – represents significant difference between designated cell and all other fall scenarios for a given body region.

b – represents significant differences between designated cell and other fall surface (for both initial conditions) for a given body region.

Head forces differed significantly across falls of varying initial position and impact surface type, $F(3,28) = 78.13$, $p < .001$, $\omega = 0.95$. Both main effects of position and surface for head force were statistically significant indicating that head force differs between falls onto concrete and carpet $F(1,28) = 118.49$, $p < .001$, $\omega = 0.89$ and between falls with an upright and inclined initial position $F(1,28) = 106.46$, $p < .001$, $\omega = 0.89$. The interaction effect of surface and position was also significant $F(1,28) = 9.59$, $p < .05$, $\omega = 0.51$, indicating that head force measured during impact onto different surfaces was influenced by initial position. Post-hoc Tukey's HSD tests indicated that head impact forces generated in both the concrete upright fall type and carpet inclined were

statistically significant from all other fall types ($p < .001$). However, the concrete inclined and carpet upright fall types did not differ significantly ($p > 0.05$).

Posterior torso forces differed significantly across falls of varying initial position and impact surface type, $F(3,28) = 79.56$, $p < .001$, $\omega = 0.95$. Both main effects of position and surface for posterior torso force were statistically significant indicating that posterior torso force differs between falls onto concrete and carpet $F(1,28) = 158.85$, $p < .001$, $\omega = 0.92$ and between falls with an upright and inclined initial position $F(1,28) = 32.82$, $p < .001$, $\omega = 0.73$. The interaction effect of surface and position was also significant $F(1,28) = 47.01$, $p < .05$, $\omega = 0.79$, indicating that posterior force measured for different impact surfaces is moderated by initial position. Post-hoc Tukey's HSD tests indicated that both the concrete upright and concrete inclined fall type were statistically significant from all other fall types ($p < .001$). However, the carpet upright and carpet inclined fall types did not differ significantly ($p > 0.05$).

Contact Regions

Linoleum over concrete

The regions of maximum recorded force by the SBDS for the upright and inclined reward falls onto linoleum on concrete surface show a difference in locations of impact (Fig. 20.). The occipital region of the head and the posterior torso reflect the majority of the impact forces with the lower leg and lower arm showing minor forces. The posterior regions of the upper legs only observed

contact in the inclined falls. The inclined falls appear to have no force imparted to the topmost region of the posterior torso in comparison to the upright falls.

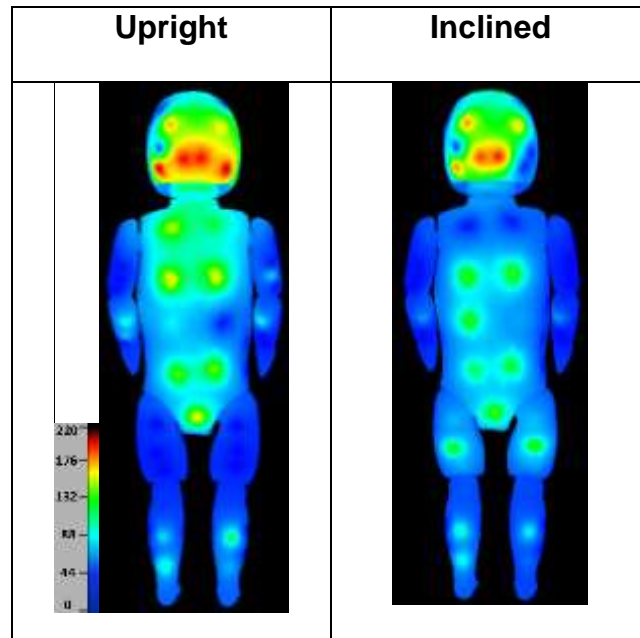


Figure 20: Maximum impact force across 8 trials for each initial position scenario as recorded by the SBDS for rearward falls onto linoleum over concrete surface. The body map images show the posterior ATD where the colors and intensities vary dependent on the level of force (N) imparted to specific regions during the fall event.

Carpet over wood

The regions of maximum recorded force by the SBDS for the upright and inclined reward falls onto carpet on wood surface show variation in locations of impact (Fig. 21.). The occipital region of the head and the posterior torso again reflect the majority of the impact forces, while the posterior regions of the upper legs only observed contact in the inclined falls. The inclined falls also appear to

have no force imparted to the topmost region of the posterior torso in comparison to the upright falls.

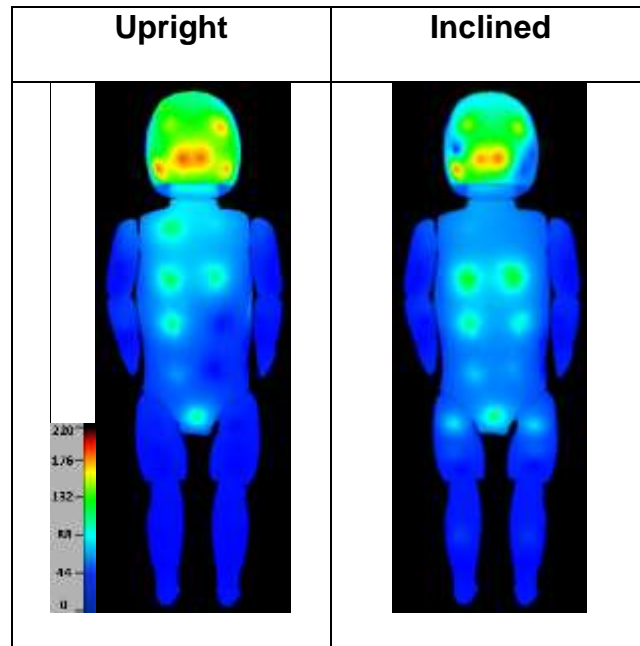


Figure 21: Maximum impact force in across 8 trials for each initial position scenario as recorded by the SBDS for rearward falls onto carpet on wood surface. The body map images show the posterior ATD where the colors and intensities vary dependent on the level of force (N) imparted to specific regions during the fall event.

DISCUSSION AND CONCLUSION

Dynamics

For the fall dynamics, we primarily analyzed the initial contact with the impact surface and any secondary or rebound impacts were disregarded. Prior studies^{7,73,74} have shown that differences in initial position, fall dynamics and impact surfaces in fall experiments using the CRABI 12 ATD have a notable

effect on recorded outcome measures. For this reason we chose to explore two initial positions and two impact surfaces in our fall experiments. There were observed differences in fall dynamics between the two initial positions (upright and inclined). In the upright falls, the ATD fell after release into a squatting position with hips and knees flexed, and then rotated rearward about the feet. These fall dynamics closely resemble the dynamics of a previous study by Thompson et al.⁷ where feet-first free falls from three fall heights were simulated using the CRABI 12 onto five impact surfaces to determine the influence of fall environment characteristics on head injury risk outcomes. In 46 cm (18 in) falls, Thompson et al.⁷ found similar ATD dynamics, where the first major impact with the ground surface occurred at the pelvis followed by the torso and then head.

Differences in fall dynamics between the two impact surfaces did not show any observable influence in our experiments. This may be as a result of the feet always being in contact with the floor surface from the start of the falls and lack of relative movement between the feet and surface in all experiments. The lack of relationship between impact surface and fall dynamics in our experiments is similar to the findings of Thompson et al.⁷ which revealed no differences in fall dynamics in 46 cm (18 in) falls onto 5 different impact surfaces (padded carpet, playground foam, linoleum over wood, linoleum over concrete, wood) having varying frictional properties.

Forces

The mean peak head impact force ($1995 \text{ N} \pm 162$) was the highest in falls having an upright initial position onto the linoleum over concrete surface and the lowest mean peak head impact force ($1050 \text{ N} \pm 79$) occurred during the falls having a posteriorly inclined initial position with impact onto the carpet over wood surface. Using the CRABI 12 ATD to assess head injury risk in experiments over three fall heights and five surfaces, Thompson et al.⁷ found falls onto linoleum over concrete and carpet over wood from 46 cm (18 in) generated peak resultant linear head accelerations of 89 g and 37 g respectively. Based upon the ATD head accelerations and head mass of 2.6 Kg (5.8 lb), calculated head impact forces for the Thompson et al.⁷ study result in $2305 \text{ N} (\pm 567)$ and $971 \text{ N} (\pm 299)$ for falls onto linoleum over concrete and carpet over wood respectively.

Prange et al.⁷⁵ dropped cadaveric pediatric head specimens ranging in age of 1, 3 and 11 days and the CRABI 6 month old ATD head from heights of 15 cm and 30 cm onto a flat anvil while measuring head accelerations on different regions of the head (vertex, occiput, forehead, right parietal, left parietal). The pediatric head impacts for the occipital region resulted in an average peak acceleration of 39 g and 55 g for the 15 cm and 30 cm fall heights, respectively. The ATD head drop impacts resulted in accelerations of 39 g and 62 g for the 15 cm and 30 cm heights, respectively. The CRABI 6 month old has a head mass of 2.1 Kg (4.6 lb) which results in a calculated head impact force of 817 N (184 lb) for the 15 cm (5.9 in) fall height and $1275 \text{ N} (\pm 286 \text{ lb})$ for the 30 cm (11.8 in) fall height.

Coats et al.⁷⁶ studied impact force and angular acceleration associated with low-height falls in infants. They developed an instrumented infant (1.5 month old) surrogate to measure the forces and 3D angular accelerations associated with falls from low heights (0.3–0.9 m) onto three impact surfaces - mattress, carpet pad, or concrete. The surrogate was dropped from a supine position with arms and legs extended to the sides of the body. Results of the study revealed peak head impact forces from surrogate drops onto concrete being significantly larger than those onto carpet ($p < 0.001$). The peak head impact force in the fall experiments was approximately 500 N for both 0.3 m (12 in) drops onto carpet and concrete surfaces and approximately 650 N and 1000 N for the 0.6 m (24 in) drop onto carpet and concrete respectively.

The head impact forces measured in our fall experiments in comparison to the studies described above are summarized in Table 8. Head forces associated with upright falls onto both impact surfaces in our experiments are in reasonable agreement with those reported by Thompson et al.⁷ for falls using the same ATD and initial position. The head impact forces determined using data from the Prange et al.⁷⁵ and Coats et al.⁷⁶ studies are generally lower than our findings for a few reasons. Prange et al.⁷⁵ conducted head drop tests on an anvil using a smaller ATD (CRABI 6) in comparison to our testing using the entire ATD (CRABI 12) dropped onto carpet and concrete. Coats et al.⁷⁶ used a custom designed ATD which is younger in age (1.5 months) to ours (12 months) and has a neck design that is less stiff than the CRABI 12 ATD neck. In addition to the reduced neck stiffness, the lighter mass of the head and different initial position (supine)

in Coats et al.⁷⁶ study reflect head forces that differ from our study. The head force in falls conducted by Thompson et al.⁷ are close in comparison to ours however it should be noted that those forces were calculated from measured head accelerations and head mass and are therefore approximates of actual head forces.

Table 8: Comparison of head impact forces, ATD head properties and initial conditions for various fall studies

	Our study CRABI 12	Thompson et al.⁷ CRABI 12	Prange et al.⁷⁵ CRABI 6	Coats et al.⁷⁶ 1.5 month ATD
Head force – carpet (N)	1050 – 1375	972 ^a	–	500 – 650
Head force – concrete (N)	1397 – 1995	2305 ^a	817 & 1275 ^{a, b}	1000
Head contact region	Occiput	Occiput	Occiput	Occiput ^c
Head mass (Kg)	2.6	2.6	2.1	1.0
ATD initial position	Inclined, Upright	Upright	Head drop	Supine
Fall height (cm)	38, 46	46	15, 32	30, 60, 90

^aForce calculated from measured acceleration and head mass.

^bDrops onto an anvil surface.

^cAssumed to be to the posterior aspect of the head (based on initial position) but not specified in study.

Contact Regions

Across all (n=32) trials in all fall scenarios, the occipital head and posterior torso were the common regions of impact in rearward falls. Considering the dynamics of a rearward fall, impact in those regions was expected. For falls onto carpet over wood, the common regions of impact for both initial positions were

the head and posterior torso. In addition to these common regions, sensors on the upper leg indicated impact for the inclined fall position. For falls onto linoleum over concrete, the common regions of impact for both initial positions were the head, posterior torso, lower arm and lower leg. In addition to these common regions, sensors on the upper leg indicated impact for the inclined position.

The commonality of impact to the upper legs in falls onto both surfaces for the inclined fall position is due to similar fall dynamics. In the inclined falls, the ATD fell into a seated position with legs fully extended on the ground, thus making contact on the upper leg region, whereas in the upright falls, the ATD rotated rearward while in a squat position onto his back thereby preventing contact of the upper legs.

When evaluating children with bruises in an effort to delineate between accidental and abusive trauma, the location, and pattern (constellation of individual bruises throughout the body) of bruising are especially important. Maguire et al.⁷⁷ conducted a review of current literature seeking to identify patterns of bruising that may be suggestive or diagnostic of abuse. The reviewed studies noted that bruises resulting from accidental trauma occurred predominantly on the anterior regions of the body, over bony prominences and were correlated to the child's level of independent mobility. In abused children the bruises tended to be larger and the most common sites were the face, neck, ear, head, trunk, buttocks, and arms.

Pierce, Kaczor et al.⁶² studied the skin findings (bruises, lacerations, etc.) of children ages 0-4 years that were admitted to the pediatric intensive care unit of a tertiary care children's hospital where cause of injury was identified through the trauma registry as abuse or accident. Each patient's age, and skin findings including bruising, body region of skin finding, and number of skin findings were recorded. A total of 95 patients were analyzed in the study; 42 patients were exposed to abusive trauma and 53 patients were exposed to accidental trauma. Differences in body regions with bruising were identified for children with abusive versus accidental trauma. The face, cheek, scalp, head, and legs had bruising in patients with abusive and accidental trauma; these regions did not delineate between accident and abuse. However, bruising to the ear, neck, hands, right arm, chest and buttocks regions were predictive of abuse. All bruising to the genitourinary area and hip occurred only in patients with abusive trauma

Kemp et al.⁷⁸ described the characteristics of bruising and the extent to which these differ between children (aged < 6 years) where abuse was confirmed and those where it was excluded in children with suspected physical abuse. Data was collected from 506 children; abuse was confirmed in 350 and excluded in 156 children. Results indicated that abused children were significantly more likely to have bruising than those where abuse was ruled out. Abused children also had significantly more bruises, more bruising sites and clustering of bruises than the group where abuse was excluded. Bruising to the left ear, cheeks, neck, trunk, front of thighs, upper arms, buttocks and genitalia were found significantly more frequently in abused children, than when abuse was ruled out.

When assessing body regions of impact during simulated falls, it is important to compare ATD morphology/geometric shape to that of an infant's morphology. While the CRABI 12 ATD represents the anthropometrics and mass distribution of a 12-month-old 50th percentile infant, its morphology (external shape/geometry) may vary somewhat from that of a 12-month-old 50th percentile infant. For example, the ATD morphology does not replicate soft tissue of the buttocks region; instead in our study, the proximal posterior upper leg region of the ATD represents the buttocks. The ATD head morphology provides a reasonable replica of a 12-month child when viewed (Fig. 22) but does not include ears, nose, lips and orbital region as individual features. However, we did not observe contact or impact to the facial region in our simulated falls. Also, the ATD head morphology does not represent the caudal most aspects of the occipital region or the mandible. Thus, it would not be possible to measure and record impact to these regions.



Figure 22: Lateral comparative overlay of 11-month-old child (3D reconstruction of CT imaging) and 12-month-old CRABI ATD (transparent; blue) highlighting morphological differences in head profile.

The impact regions recorded in our testing in comparison to the bruising locations found on children from relevant studies described above are summarized in Table 9.

Table 9: Comparison of potential bruising locations in our study to observed bruising in previous clinical studies

	Our study	Kemp et al.⁷⁸	Maguire et al.⁷⁷	Pierce et al.⁶²
Regions of Abusive Bruising	-	Cheek, ear, neck, trunk, head, front of thighs, upper arms	Head including face, front of body, ear, neck, trunk, arms, buttocks	All regions including torso, ear and neck
Regions of Accidental Bruising	^a Head occipital, posterior torso, posterior upper leg, posterior lower leg, posterior lower arm	Rear trunk, head	Knees, shins, head, forehead, hands, back, buttocks, forearm, foot and abdomen	All regions excluding torso, ear and neck

In our study we predominantly found impact to the head occipital region and posterior torso. The upper legs, lower legs and lower arms were impacted, however magnitudes of force were lower than those measured to the occipital and posterior torso regions. Compared to previous clinical studies describing bruising locations for a range of accident types, the head and posterior torso were found to be common regions of bruising^{77,78}. Parallel to Kemp et al.⁷⁸, Maguire et al.⁷⁷ and Pierce et al.⁶² we did not find impact or potential for bruising to the ears or neck. However, Kemp et al.⁷⁸ and Maguire et al.⁷⁷ did not report fall description, mechanism or injury causation. Thus, this limits direct comparisons to those studies as our experimental findings are specific to one fall scenario. The study by Pierce et al.⁶² did indicate cause of accidental trauma, however children in their study were admitted to the hospital's intensive care unit (ICU) and had severe injuries likely associated with high energy events unlike a

fall from standing height. A key distinction in this comparison is that the experimental falls identify all regions of contact with the impact surface during a specific, controlled fall scenario where a bruise could potentially develop, but not necessarily occur. Our experimental results do not predict bruising; rather only identify fall specific contact locations where potential bruising may occur.

LIMITATIONS

The biofidelity of the CRABI ATD and in particular the soft tissue biofidelity is a limitation of the SBDS. The ATD surrogate “soft tissue” consists of a heat cured vinyl plastisol that is layered with urethane foam between the outer and inner layers. The plastisol is compliant and molded to mimic the body contours representing “soft tissue”. SBDS sensor measured forces are proportional to the stiffness of the underlying ATD surrogate soft tissue; therefore soft tissue biofidelity greatly influences the measured forces. However, our primary goal was to determine points of contact during various injurious events and secondarily to assess relative levels of force imparted to different regions of the body. Thus, biofidelic limitations of the surrogate soft tissue do not prevent us from meeting our goals.

Also, since the CRABI ATD was primarily designed for measuring a child’s response to a high energy automotive crash environment, any findings from testing conducted with the ATD in lower deceleration events such as falls should be interpreted in light of biofidelity limitations. For example, the neck is somewhat

stiffer with limited range of motion designed for frontal impacts having little or no out of plane motion. The rubber elements that attach the limbs to the ATD torso are used in the hip and shoulder joints to provide the CRABI infant-like range of motion, but are an approximation of true infant biofidelity. In addition, joints of the shoulders, elbows, hips, and knees of the ATD are limited to motion primarily in the sagittal plane. Though ATD kinematics in our simulated falls occurred primarily in the sagittal plane, any out of plane motion may lead to inaccuracies in kinematics and force measures. Varying ATD joint stiffness could additionally alter fall dynamics thereby influencing impact locations and forces. Additionally, we were unable to implement sensors in the neck region of the ATD given its construction (segmented rubber and aluminum disks), but based on our experimental fall dynamics, the ATD neck had a low likelihood of contact/impact during falls.

The occurrence of a bruise varies from person to person for a given application of force based on many contributing factors that affect bruise development. Extrinsic factors include the amount of force applied, rate of force application, and distribution of the force over larger/smaller areas, intrinsic factors related to the physiological and anatomical structures include the architecture of the skin, soft tissue thickness, toughness of skin, fat content, vessel fragility, and presence and depth of underlying bone add to the complexity of this physiological event. Variables such as blood platelet levels, systemic blood pressure, vascular diseases and vasoactive or anticoagulant drug use in addition to nutritional and allergy related disorders can have a great influence on the

presence, absence and variability in intensity of a bruise. This implies that the minimum load to cause bruising, the “bruising threshold”, varies across individuals. However it can be said with some degree of certainty that larger forces are associated with a greater potential for bruising. So instead of definitively asserting the presence of a bruise, we are assessing potential bruising locations occurring within a body region under specific fall conditions.

While our findings predicted potential bruising locations in a rearward fall from standing using the SBDS, limitations described herein must be considered. The experimental falls identify all regions of contact with the impact surface during a specific, controlled fall scenario where a bruise could potentially develop, but not necessarily occur. Our experimental results do not predict bruising; rather only identify fall specific contact locations where potential bruising may occur. Despite these limitations, the capability to predict potential bruising locations or patterns is useful when attempting to determine compatibility between a stated cause and associated skin findings in forensic analyses.

CHAPTER V:

POTENTIAL BRUISING PATTERNS ASSOCIATED WITH BED FALLS IN CHILDREN

OVERVIEW

It is difficult to differentiate abusive from accidental injury in children as accidental falls are common occurrences in early childhood and falls are frequently stated as explanations in an effort to conceal abuse by a caregiver. Bruising injuries are one of the most common early signs of child abuse as bruising locations on the body can be an effective delineator of abusive versus accidental trauma. However, the ability to predict potential bruising locations associated with falsely reported fall events in child abuse does not exist. In our study we used a 12-month old pediatric anthropomorphic test device (ATD) adapted with a custom developed force sensing skin to predict potential bruising locations during bed falls. The sensing skin measured and displayed recorded force data on a computerized body image mapping system when sensors were activated. Simulated bed fall experiments were performed from two initial positions (facing forward and facing rearward) and two fall heights (24 in and 36 in) onto a padded carpet impact surface. Findings indicated possibility of bruising

in two planes with impact location primarily within the frontal, temporal and parietal head, anterior and posterior torso and upper arm and upper leg regions. There was significant similarity between our fall experiments and clinical findings in cases of accident bed falls and change table falls in terms of number of bruising regions and no significance between our experiments and clinical findings in abuse cases.

INTRODUCTION

Child abuse is a leading cause of fatality in children up to 4 years of age and infants (less than 1 year in age) are the most vulnerable to abuse and having the highest rate of fatalities of all age groups¹. Early detection of abuse from subtle injuries could help prevent those who are at risk from escalating abusive injuries. Unexplained bruising injuries in children are visually apparent and frequently an early manifestation of a child's abusive environment. Accidental bruising is infrequently observed in infants, due to their low degree of independent mobility⁶⁷. Bruising locations and bruising patterns (constellation of individual bruises throughout the body) provide a "roadmap" documenting a child's exposure to impact.

Falls from beds and other household furniture are common occurrences in children and sometimes result in injury but are also often used as false histories to conceal abuse^{4,73,76,79}. Clinicians often have to address the question of likelihood that a child's injuries are compatible with history provided by the care giver. Objective information about injury likelihood from household falls could

help distinguish between accidental and abusive trauma, thereby preventing abused children from being reintroduced into their abusive environments which often results in further harm or death⁶⁸.

Previous studies have retrospectively highlighted differences in bruising patterns observed clinically, to provide a better understanding of skin findings in children that maybe at a high risk of abuse in their current environment^{25,29,34,36,62,67,69,70}. However, the ability to predict potential bruising locations associated with falsely reported events such as common household furniture falls does not exist and could prove useful in the distinction between abusive and accidental injuries.

To identify potential bruising injuries and patterns in household furniture falls, we simulated falls from a horizontal surface representing a bed or change table. A bruising detection system⁷¹ was used to identify potential bruising patterns while simulating rolling off a bed surface using a child surrogate representative of a 12-month old. The bruising detection system consists of a pediatric anthropomorphic test device (ATD) adapted with a custom developed force sensing skin that is linked to display recorded force data on a computerized body mapping image system when the force sensors are activated. The effects of varying bed height and initial position on recorded impact regions predicting potential bruising locations was also examined.

The purpose of this study is to provide a “roadmap” of the child surrogate’s contact exposure during specific fall events and to identify whether variations in the fall parameters (initial height, initial position) lead to differences in impact

locations. Our goal was characterize potential bruising locations or patterns associated with a common household furniture falls and compare our findings to skin findings observed in clinical cases.

METHODS

The surrogate bruising detection system (SBDS), consisting of the 12 month old CRABI ATD (10 Kg mass) fitted with a force sensing skin and associated data acquisition hardware and analysis software, was used to predict potential bruising patterns in simulated fall scenarios. The sensing skin of the SBDS consists of 114 force sensors enveloping the surface of the ATD that is divided into seven regions including the head, anterior torso, posterior torso, forearm, upper arm, thigh and shank. Each region has individualized custom sensor arrays. Graphical programming software was used to acquire and display sensor output in a manner that relates sensor location to body region. Additional details of the SBDS and its individual components are described in earlier publications^{71,72}.

The SBDS was used to assess potential bruising locations on the body during a series of bed fall experiments as this type of furniture fall is commonly experienced by young children.

Test Setup

The ATD was placed in a side-lying position on the edge of a horizontal surface representing a couch, bed or change table (Fig. 23). A swinging

pendulum actuator supported by a tripod with a manually operated release mechanism was positioned at the ATD posterior mid-torso (approximate center of mass). The pendulum actuator provided a consistent initial force sufficient to initiate roll of the ATD from the bed surface and allow it to fall under the effects of gravity. Fall experiments were conducted using two different initial conditions and two different bed heights. The impact surface for all the falls was padded carpet.



Figure 23: CRABI anthropomorphic test device (ATD) in side-lying, facing forward initial position for bed fall experiments. The pendulum actuator providing the initial force to the posterior torso of the ATD is located behind the ATD.

Prior to each fall, ATD joint angles were adjusted using a goniometer to ensure repeated positioning in all tests (Table 10). Additionally, joint stiffness was calibrated to manufacturer specifications whereby the joints were tightened until the friction was just sufficient to support the weight of the limb against gravity. The impact surface evaluated for all fall scenarios was padded carpet over a

wood subfloor. The carpet surface consisted of a 1/2 in (1.3 cm) thick open loop carpet placed over 3/8 in (1.0 cm) thick foam padding. The carpet and padding were placed over a 3/4 in (1.9 cm) thick plywood platform 6 ft x 3 ft (183 cm x 91.5 cm) built to standard building codes with 2 in x 4 in (5.1 cm x 10.2 cm) joists, spaced 16 in (40.6 cm) on center.

Table 10: Initial joint angles for the side lying ATD

Joint location	Angle (degrees)
Right shoulder angle	135
Right elbow angle	110
Left shoulder angle	0
Left elbow angle	170
Hip angle (both)	130
Knee angle	100

Data Acquisition and Analysis

The SBDS's sensors consist of force sensing resistors whose outputs were fed to the data acquisition system through a voltage divider circuit to convert resistance to voltage. Data acquisition hardware was used to capture and convert the analog sensor output. Multifunctional input/output data acquisition cards (Resolution - 16 bit, Sample rate - 250kS/s) acquired, conditioned and digitized the sensor output signals. A personal computer served as the platform for the data acquisition hardware.

Graphical programming software (Labview 2010; National Instruments, Austin, Texas) was used to acquire, process, analyze, store and present sensor output. An active 3D body map image representing the ATD served as a graphical interface; the ATD body image was discretely mapped to the sensors on the ATD such that active sensor outputs (those which have been impacted) and their locations were displayed on the computerized body map image. Sensor measured forces were color-coded, designating a pre-determined force range so as to provide a quick overview of body regions with high intensities of impact. A filtering lower bound force of 4.5 N (≈ 1 lb) was used to establish the onset of contact between the ATD and impact surface.

Five trials of each of the four simulated bed fall scenario (facing forward and facing rearward positions for both fall heights of 24 in and 36 in) were conducted onto padded carpet for a total of 20 fall experiments (Table 11). A sample size calculation on previously collected data from rearward fall experiments revealed five trials to provide a power of 0.8 with a medium (0.25) effect size.

Table 11: Evaluated fall scenarios with surface height, ATD initial position and impact surface.

Fall Type & Height (trials)	Initial Position	Surface Type
Bed fall – 24 in (n= 5)	Facing forward	Carpet over wood
Bed fall – 24 in (n= 5)	Facing rearward	
Bed fall – 36 in (n= 5)	Facing forward	
Bed fall – 36 in (n= 5)	Facing rearward	

Motion Capture

All falls were captured using a digital video camera (120 frames per second) to record overall fall dynamics. The camera was positioned so that the line of sight was perpendicular to the ATD sagittal plane. This allowed for qualitative assessment of fall dynamics.

Statistical Methods

A two-way analysis of variance (ANOVA) test was used to analyze impact forces on body regions to determine if initial position and bed height factors led to significant differences. Additionally, post-hoc tests were conducted to further examine where significant differences existed ($p \leq 0.05$). Data was evaluated for normal distribution. Individual sensors were grouped by body region. Body regions were defined as head, anterior torso, posterior torso, left and right upper arm, left and right lower arm, left and right upper leg, and left and right lower leg.

RESULTS

Fall Dynamics

All fall scenarios indicated possibility of bruising in two planes with impact location primarily on the frontal, temporal and parietal head, anterior and posterior torso and upper arm and upper leg regions.

Facing Forward – 24 in bed height (FF24)

In the initial position the ATD was facing the edge of the bed such that the longitudinal (mid-sagittal plane) axis of the body was parallel with the ground (10 ms Fig.24). Subsequent to actuator-ATD contact, the ATD rolled forward about the edge of the bed surface (500 ms Fig. 24) longitudinally. During the free fall to the floor, the ATD continued to rotate about its longitudinal axis while simultaneously the head surpassed the feet just prior to impact (750 ms Fig. 24). The ATD impacted the floor surface on its lateral left with the left shoulder (the upper arm was impinged between the chest and floor) and left parietal head impacting at approximately the same time (790 ms Fig.24). Following the initial impact with the floor, the ATD rebounded upward off the floor before finally coming to rest (1000 ms Fig. 24).

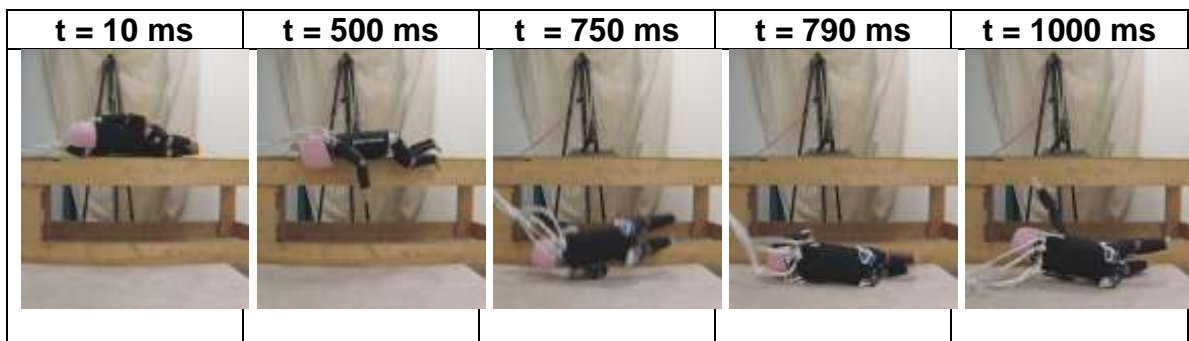


Figure 24: Frame sequences showing video capture of the FF24 bed fall onto the padded carpet surface at corresponding time intervals.

The SBDS body map image showing four views (anterior, posterior, left lateral and right lateral) highlighting the ATD to floor surface impact locations (Fig. 25) for the FF24 bed fall as shown in Fig. 24 (t = 790 ms). Since we were

primarily concerned with the initial impact event, data associated with the secondary impact following rebound was not evaluated.

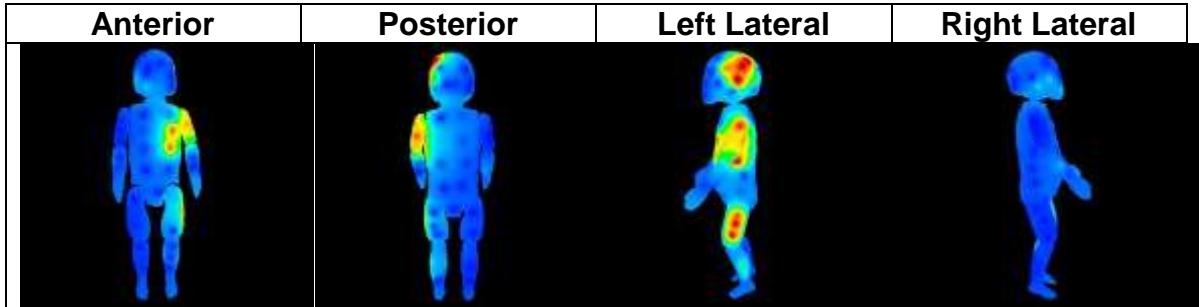


Figure 25: SBDS body map image corresponding to the FF24 bed fall impact where the colors and intensities vary depending on the level of force imparted to specific regions during the fall event

Facing Forward – 36 in bed height (FF36)

In the initial position the ATD was facing the edge of the bed such that the longitudinal (mid-sagittal plane) axis of the body was parallel with the ground (10 ms Fig. 26). Subsequent to actuator-ATD contact, the ATD rolled forward about the edge of the bed surface (500 ms Fig. 26) longitudinally. During the free fall to the floor, the ATD continued to rotate about its longitudinal axis while simultaneously the head surpassed the feet just prior to impact (875 ms Fig. 26). The ATD impacted the floor surface on its posterior side with the left posterior shoulder and parietal head at approximately the same time (875 ms Fig.26). Following the initial impact with the floor, the ATD rebounded upward off the floor before finally coming to rest (1000 ms Fig. 26).

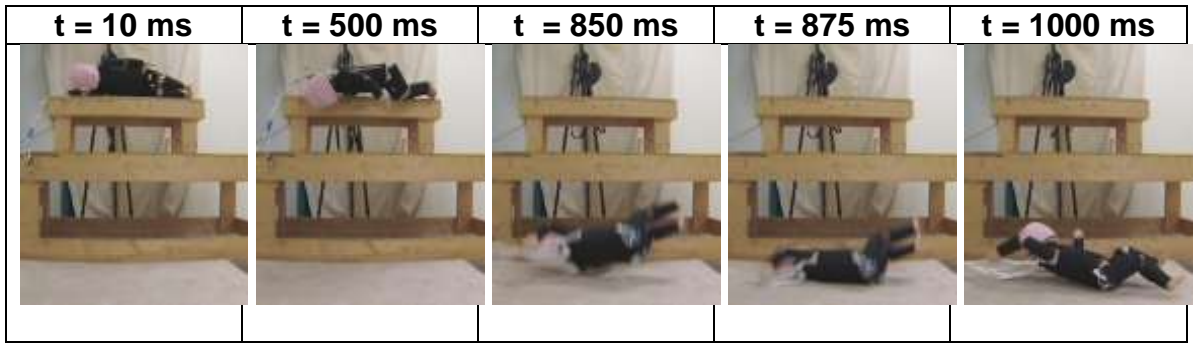


Figure 26: Frame sequences showing video capture of the FF36 bed fall onto the padded carpet surface at corresponding time intervals.

The SBDS body map image showing four views (anterior, posterior, left lateral and right lateral) highlighting the ATD to floor surface impact locations (Fig. 27) for the FF36 bed fall as shown in Fig. 26 (t = 875 ms). Secondary impact following rebound was not evaluated.



Figure 27: SBDS body map image corresponding to the FF36 bed fall impact where the colors and intensities vary depending on the level of force imparted to specific regions during the fall event

Facing Rearward – 24 in bed height (FR24)

In the initial position the ATD was facing away from the edge of the bed such that the longitudinal (mid-sagittal plane) axis of the body was parallel with the ground (10 ms Fig. 28). Subsequent to actuator-ATD contact, the ATD rolled rearwards about the edge of the bed surface (350 ms Fig. 28) longitudinally. During the free fall to the floor, the ATD continued to rotate about its longitudinal axis. The right arm was outstretched and leading the ATD followed by the legs and head which slightly trailed just prior to impact (565 ms Fig. 28). The ATD impacted the floor surface in a right anterior aspect with the right arm (the right lower arm was impinged between the chest and floor) followed by the legs, torso and right frontal head (625 ms Fig. 28). Following the initial impact with the floor, the ATD rebounded upward off the floor before finally coming to rest (1000 ms Fig. 28).

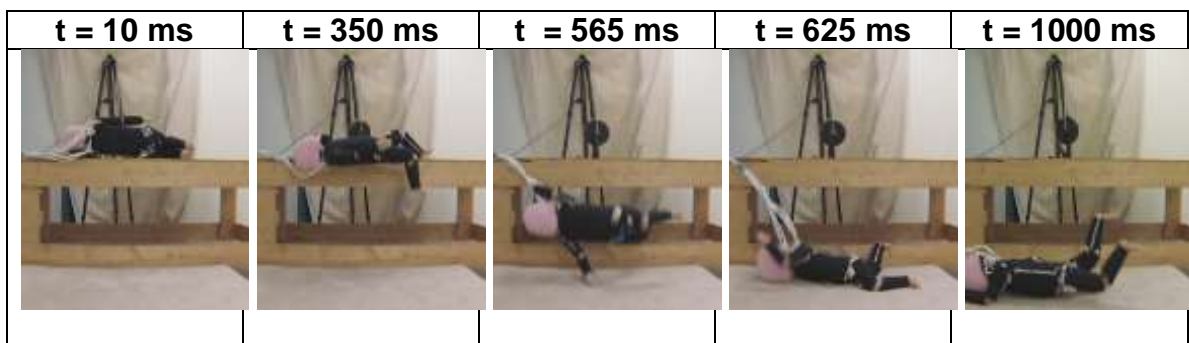


Figure 28: Frame sequences showing video capture of the FR24 bed fall onto the padded carpet surface at corresponding time intervals.

The SBDS body map image showing four views (anterior, posterior, left lateral and right lateral) highlighting the ATD to floor surface impact locations

(Fig.29) for the FR24 bed fall as shown in Fig. 28 ($t = 625$ ms). Since we were primarily concerned with the initial impact event, data associated with the secondary impact following rebound was not evaluated.

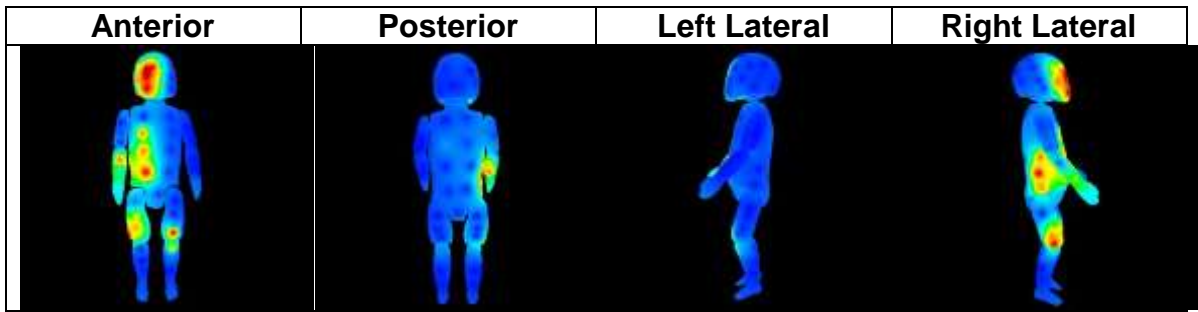


Figure 29: SBDS body map image corresponding to the FR24 bed fall impact where the colors and intensities vary depending on the level of force imparted to specific regions during the fall event

Facing Rearward – 36 in bed height (FR36)

In the initial position the ATD was facing away from the edge of the bed such that the longitudinal (mid-sagittal plane) axis of the body was parallel with the ground (10 ms Fig. 30). Subsequent to actuator-ATD contact, the ATD rolled rearwards about the edge of the bed surface (350 ms Fig. 30) longitudinally. During the free fall to the floor, the ATD continued to rotate about its longitudinal axis. The right arm was outstretched and leading the ATD followed by the legs and slightly trailed by the head just prior to impact (700 ms Fig. 30). The ATD impacted the floor surface in an anterior aspect with the right arm followed by the legs, torso and right frontal head (770 ms Fig.30). Following the initial impact with

the floor, the ATD rebounded upward off the floor before finally coming to rest (1000 ms Fig. 30).

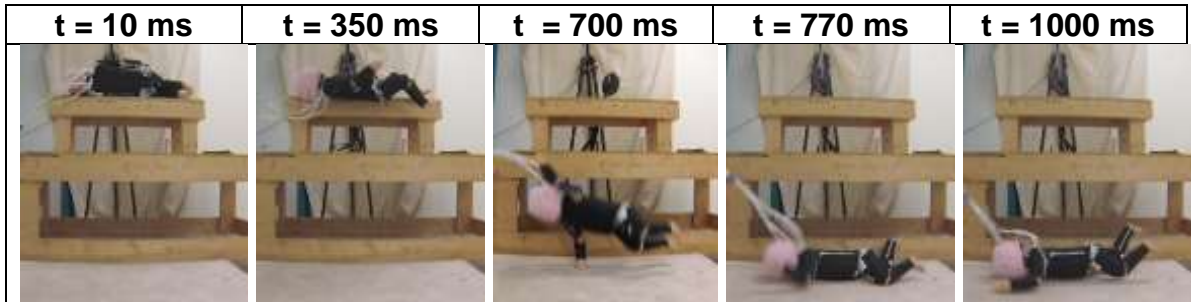


Figure 30: Frame sequences showing video capture of the FR36 bed fall onto the padded carpet surface at corresponding time intervals.

The SBDS body map image showing four views (anterior, posterior, left lateral and right lateral) highlighting the ATD to floor surface impact locations (Fig. 31) for the FR36 bed fall as shown in Fig. 30 (t = 770 ms). Secondary impact following rebound was not evaluated.

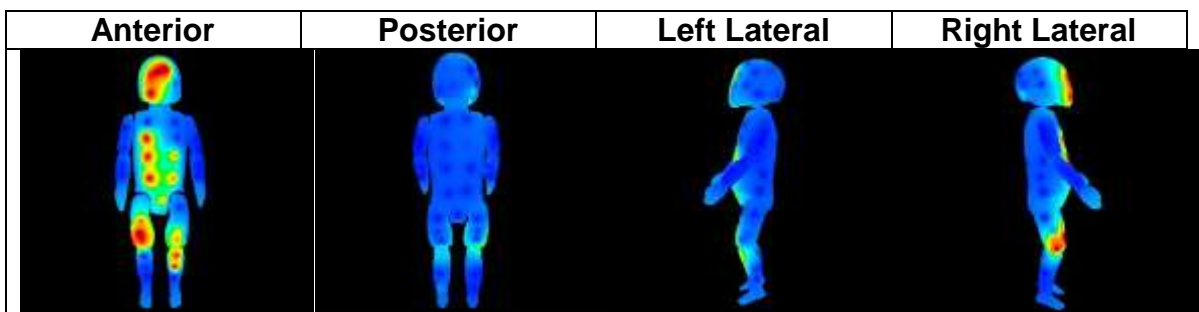


Figure 31: SBDS body map image corresponding to the FR36 bed fall impact where the colors and intensities vary depending on the level of force imparted to specific regions during the fall event

Contact Forces

The mean peak impact force for the head (2631 N \pm 100), anterior torso (1990 N \pm 63), right upper leg (2006 N \pm 293) and left lower leg (907 N \pm 167) were the highest in the FR36 falls. The mean peak impact force for the posterior torso (1945 N \pm 146) and left upper arm (1598 N \pm 118) were the highest in the FF36 falls. The mean peak impact force for the left upper leg (1249 N \pm 158) was the highest in the FF24 falls. The lowest mean peak impact force to the head (2045 N \pm 254) was in the FF24 falls (Table 12). A post hoc power analysis resulted in a power of 0.87 which demonstrates we maintained power based on the initial sample size analysis.

Table 12: Mean (5 trials) peak contact force (N \pm CI) for each body region in various fall scenarios

Body Region	FF24	FF36	FR24	FR36
Head	2045 ^b (\pm 254)	2510 (\pm 179)	2223 ^b (\pm 112)	2631 (\pm 100)
Anterior Torso	624 ^a (\pm 137)	↓	912 ^a (\pm 99)	1990 ^a (\pm 63)
Posterior Torso	606 ^a (\pm 70)	1945 ^a (\pm 146)	944 ^a (\pm 192)	↓
Left Upper Arm	1583 (\pm 112)	1598 (\pm 118)	↓	↓
Right Upper Arm	↓	↓	↓	↓
Left Lower Arm	↓	68 (\pm 73)	↓	↓
Right Lower Arm	44 (\pm 37)	↓	850 ^a (\pm 115)	↓
Left Upper Leg	1249 ^a (\pm 158)	424 (\pm 155)	336 (\pm 149)	399 (\pm 173)

Body Region	FF24	FF36	FR24	FR36
Right Upper Leg	↓	↓	1371 ^a (±194)	2006 ^a (±293)
Left Lower Leg	184 (±67)	↓	322 (±202)	907 ^a (±167)
Right Lower Leg	↓	↓	↓	↓

↓ – represents recorded forces that were below the established filtering lower bound of 5% of ATD body weight.

a – represents significant difference between designated cell and all other fall scenarios for a given body region.

b – represents significant differences between designated cell and other fall height (for both initial positions) for a given body region.

The head region recorded the highest levels of force in all falls when compared to other body regions. Additionally, since injuries to the head have the greatest consequences in terms of injury, we will primarily discuss the significance of head force on height and position factors. Head forces differed significantly across falls of varying fall heights and initial positions, $F(3,16) = 18.46$, $p < .001$, $\omega = 0.88$. Both main effects of height and position for head force were statistically significant indicating that head force differs between from 24 in and 36 in $F(1,16) = 49.42$, $p < 0.001$, $\omega = 0.83$ and between falls with an facing forward and facing rearward initial position $F(1,16) = 5.776$, $p < 0.05$, $\omega = 0.28$. The interaction effect of height and position was not significant $F(1,16) = 0.21$, $p > 0.05$, $\omega = 0.51$, indicating that head force measured during impact for a certain height was influenced by initial position. Post-hoc Tukey's HSD tests indicated that head impact forces generated by the 24 in fall heights were statistically significant from those in the 36 in fall heights for both initial conditions ($p < 0.05$).

However, the head forces generated for different initial positions for the same height did not differ significantly ($p > 0.05$).

Contact Regions

Facing Forward – 24 in and 36 in bed height

The regions of maximum recorded force (all 5 trials) by the SBDS for the 24 in (Fig. 32) and 36 in (Fig. 33) facing forward falls show a difference in locations of impact on the ATD. For the FF24 falls (Fig. 32), the left parietal region of the head, left upper arm and left upper leg reflect the majority of the contact forces with the impact surface. The left upper arm was trapped between the chest and floor and therefore we saw body contact between the medial aspect of the left upper arm and the chest. Additionally, the anterior plane, posterior plane and right lateral plane of the ATD recorded no contact with the floor.

In comparison, the FF36 falls highlight impact on the left lateral posterior and show no contact in the anterior and right lateral planes of the ATD. Therefore, in addition to the left parietal region of the head, left upper arm and left upper leg, there was contact to the occipital head and left posterior torso regions (Fig. 33).

Anterior	Posterior	Left Lateral	Right Lateral
----------	-----------	--------------	---------------

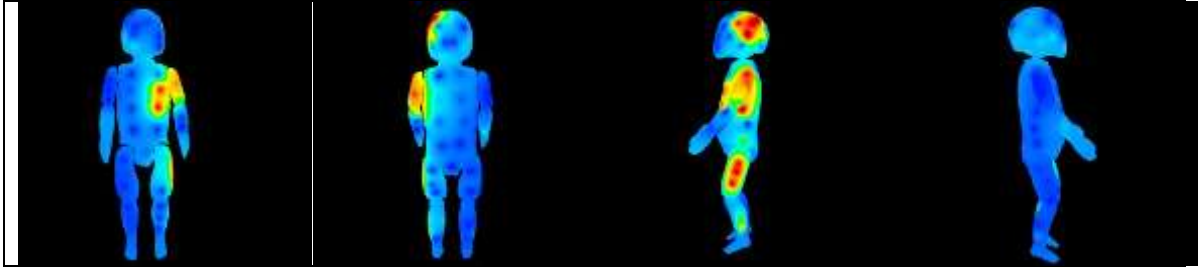


Figure 32: Maximum impact force across 5 trials as recorded by the SBDS for the FF24 fall scenario. The body map images show the anterior, posterior, left lateral and right lateral aspects of the ATD. The colors and intensities vary dependent on the level of force (N) imparted to specific regions during the fall event.

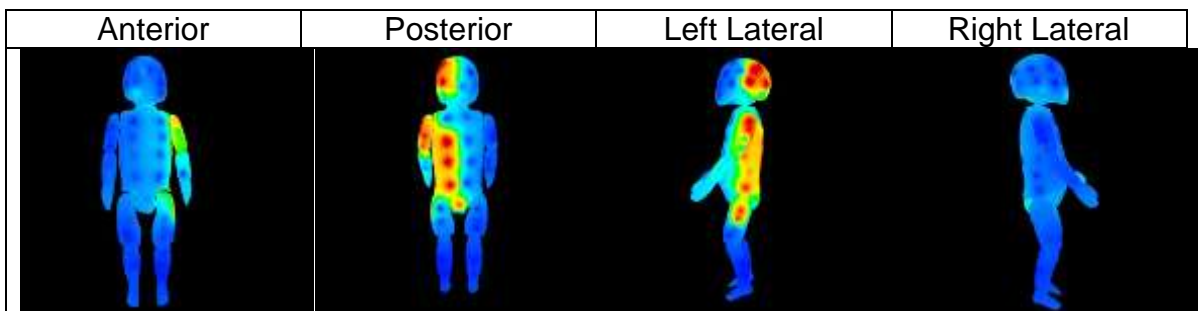


Figure 33: Maximum impact force across 5 trials as recorded by the SBDS for the FF36 fall scenario. The body map images show the anterior, posterior, left lateral and right lateral aspects of the ATD. The colors and intensities vary dependent on the level of force (N) imparted to specific regions during the fall event.

Facing Rearward – 24 in and 36 in bed height

The regions of maximum recorded force (all 5 trials) by the SBDS for the 24 in (Fig. 34) and 36 in and (Fig. 35) facing rearward falls show a difference in locations of impact on the ATD. For the FR24 falls (Fig. 34), the right frontal

region of the head and torso and right upper leg reflect the majority of the contact forces with the impact surface while the left upper leg and lower leg show minor forces. The right lower arm contact was from being impinged between the chest and floor surface. Additionally, the posterior plane, and left lateral plane of the ATD saw no contact with the floor.

In comparison, the FR36 falls highlight impact on the anterior plane of the ATD and show no contact in the posterior and left lateral planes. There was contact on the frontal region of the head, anterior torso, right and left upper leg and left lower leg (Fig. 35).

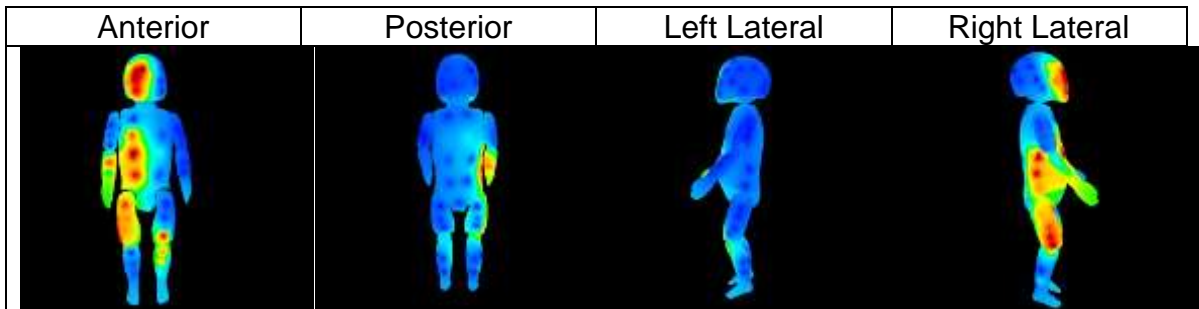


Figure 34: Maximum impact force across 5 trials as recorded by the SBDS for the FR24 fall scenario. The body map images show the anterior, posterior, left lateral and right lateral aspects of the ATD. The colors and intensities vary dependent on the level of force (N) imparted to specific regions during the fall event.

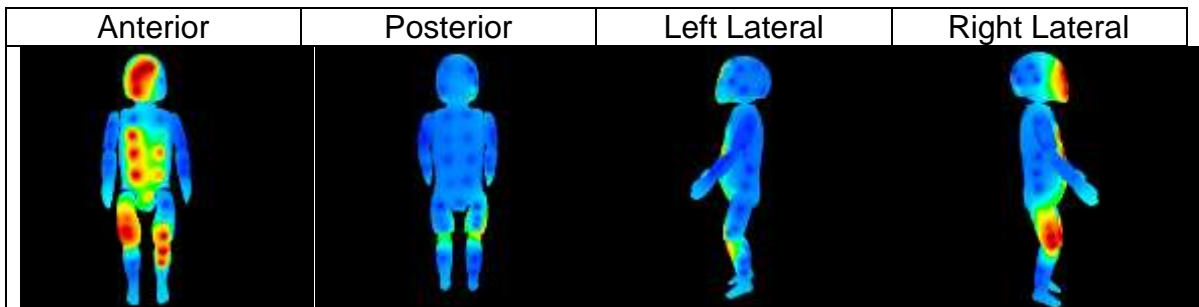


Figure 35: Maximum impact force across 5 trials as recorded by the SBDS for the FR36 fall scenario. The body map images show the anterior, posterior, left lateral and right lateral aspects of the ATD. The colors and intensities vary dependent on the level of force (N) imparted to specific regions during the fall event.

A synopsis of the experimental bed fall results highlighting body planes with and without contact and body regions with and without contact with the floor surface is shown in Table 13 and Table 14 respectively

Table 13: Overview of body planes with and without contact with the impact surface as observed in all conducted experimental falls.

Fall Type	Plane with Contact	Plane without Contact
FF 24	Anterior (left) L lateral	Posterior R lateral
FF 36	Posterior (right) L lateral	Anterior R lateral
FR 24	Anterior R lateral	Posterior L lateral
FR 36	Anterior R lateral	Posterior L lateral

Note: Individual sensor placement is not segregated along planes which implies that some sensors have coverage of multiple planes

Table 14: Overview of body regions with and without contact with the impact surface for all conducted experimental falls.

Fall Type	Region with Contact	Region without Contact
FF 24	L parietal head L anterior torso ^a L lateral torso L upper arm L upper leg L lower leg	Frontal head Occipital head R parietal head L posterior torso R anterior torso R posterior torso R lateral torso L lower arm R upper arm R lower arm R upper leg R lower leg
FF 36	L parietal head Occipital head L posterior torso L lateral torso L upper arm L upper leg L lower arm	Frontal head R parietal head L anterior torso R anterior torso R posterior torso R lateral torso R upper arm R lower arm R upper leg R lower leg L lower leg
FR 24	Frontal head R parietal head R anterior torso R lateral torso R upper leg L Upper Leg L Lower Leg R lower arm	Occipital head L parietal head R posterior torso L anterior torso L posterior torso L lateral torso R upper arm R lower leg L upper arm L lower arm

Fall Type	Region with Contact	Region without Contact
FR 36	Frontal head L anterior torso R anterior torso R upper leg L upper leg L lower leg	Occipital head R parietal head L parietal head L posterior torso R posterior torso R lateral torso L lateral torso R upper arm R lower arm L upper arm L lower arm R lower leg

a – contact due to body contact and not impact surface contact

The results show a difference in the regions of contact and no contact as well as the planes of contact and no contact when comparing initial position and fall height.

DISCUSSION AND CONCLUSION

We chose to explore two initial positions and two fall heights in our fall experiments since prior studies^{7,73,74} have shown that differences in initial position and fall height while conducting fall experiments using the CRABI 12 ATD have a notable effect on recorded outcome measures. Additionally, a bed fall height of 24 in closely represents household falls from a typical bed or couch while a 36 in fall height represents a typical change table height.

Dynamics

For the fall dynamics, we primarily investigated the initial contact with the impact surface and any secondary or rebound impacts were ignored. There were similarities and observed differences in fall dynamics between the two initial positions (facing forward and facing rearward) and the two fall heights (24 in and 36 in). The similarities in dynamics between falls with varying bed heights and similar initial position maintains close until the moment of impact. In the higher falls (36 in), the larger fall distance allows the ATD to rotate longitudinally for a longer time period prior to impact. These findings are similar to a study done by Thompson et al⁸⁰ that conducted a parametric sensitivity analysis on a validated computer model simulating a bed fall using a CRABI 12-month old. The model was used to investigate the influence of altering fall parameters on injury outcome measures. Thompson found that increasing or decreasing the bed height had an influence on fall dynamics and impact orientation.

The fall dynamics of the FF24 falls closely resemble the dynamics of a previous study by Thompson et al.⁷³ where bed fall experiments were simulated from a 24 in high horizontal surface using a CRABI – 12 month old onto five different impact surfaces. The initial position in the study was a side lying position similar to our facing forward position. The fall dynamics of the study closely resemble our study with rotation about the longitudinal axis while free falling to the ground and impacting with the head and left shoulder at approximately the same time.

Bertocci et al.⁴ simulated bed falls from a 27 in (0.68 m) high horizontal surface using a Hybrid II 3-year old ATD. The initial position in the Bertocci study was a side lying position similar to our facing forward position. Additionally, the fall dynamics were somewhat similar to ours prior to impact, however, possibly because of the size disparity in the Bertocci study ATD versus our ATD, their findings indicated the legs or pelvis of impacted the surface first where we noticed the shoulder and head first making contact in our experiments.

The differences in fall dynamics when comparing falls with varying initial position (FF and FR) and similar fall heights shows the ATD has a tendency to rotate longitudinally a greater amount for the FR falls compared to the FF falls. The approximate longitudinal rotation of the ATD from the initial position until the moment of impact with the floor for the FF falls was $\approx 180^\circ$ and $\approx 225^\circ$ for the 24 in and 36 in falls respectively. Alternatively the approximate longitudinal rotation of the ATD from the initial position until the moment of impact with the floor for the FR falls was $\approx 225^\circ$ and $\approx 270^\circ$ for the 24 in and 36 in falls respectively. This difference could be due to the orientation of the ATD's flexed legs. In the FF initial position the legs provide rotational rigidity, thereby reducing the overall rotational (about the longitudinal direction) force generated on the ATD when struck by the fall initiating impactor. In the FR falls the legs had minimal influence in reducing the generated rotational (about the longitudinal direction) force as they were in the opposite direction of the fall.

Forces

The mean peak head impact force ($2631 \text{ N} \pm 100$) was the highest in the 36 in falls with a facing rearward initial position and the lowest mean peak head impact force ($2045 \text{ N} \pm 254$) occurred in the 24 in falls with a facing forward initial position.

Several studies have investigated head injury risk in pediatric falls using varying representative ages of ATD's. Thompson et al.⁷³ conducted bed fall experiments from a 24 in high horizontal surface using a CRABI – 12 month old falling from a side lying position similar to our facing forward position. Thompson conducted the bed falls on five different impact surfaces and recorded an average linear head acceleration of 85 g for falls onto padded carpet. Based upon the ATD head accelerations and head mass of 2.6 Kg (5.8 lb) of the CRABI-12, calculated head impact forces for the Thompson⁷³ study result in 2170 N (± 140) for falls onto padded carpet over wood.

Coats et al.⁷⁶ studied impact force and angular acceleration associated with low-height falls in infants. They developed an instrumented infant (1.5 month old) surrogate to measure the forces and 3D angular accelerations associated with falls from low heights between 12 in and 36 in (0.3–0.9 m) onto three impact surfaces - mattress, carpet pad, or concrete. The surrogate was dropped from a supine position with arms and legs extended to the sides of the body. The peak head impact force in the fall experiments was approximately 650 N for the 0.6 m (24 in) drops and 1000 N for the 0.9 m (36 in) drops onto carpet surface.

Ibrahim et al.⁸¹ simulated falls using an 18-month-old surrogate that was dropped from heights of 0.3 m, 0.6 m and 0.9 m (12 in, 24 in and 36 in) onto carpet pad and concrete. The surrogate was suspended above the floor in a supine position with the head lower than the feet (to ensure the head made contact the ground before the torso) and allowed to free fall until impact. Peak estimated head impact force was approximately 3715 N (\pm 850) and 4570 N (\pm 285) for the 0.6 m and 0.9 m (24 in and 36 in) drops onto carpet pad respectively.

Bertocci et al.⁴ conducted bed falls from a 0.68 m (27 in) high horizontal surface using a Hybrid II 3-yearold ATD with a similar initial position as compared to our facing forward falls. The falls were conducted onto 4 impact surfaces including wood, padded carpet, linoleum and playground-foam. Results indicated linear head accelerations of approximately 160 g (\pm 60) for falls onto padded carpet. Based upon the ATD head accelerations and head mass of 2.7 Kg (6 lb) of the Hybrid II 3 Year Old Child Dummy, calculated head impact forces for the Bertocci et al. study result in 4237 N for falls onto padded carpet over wood.

The head impact forces measured in our fall experiments in comparison to the studies described above are summarized in Table 15. Head impact forces associated with 24 in facing forward falls in our experiments are in reasonable agreement with those reported by Thompson et al.⁷³ for falls using the same ATD, initial position and fall height. The head impact forces in Coats et al.⁷⁶ study are lower than our findings for a few reasons. Coats used a custom designed ATD reflecting a young infant which is younger in age (1.5 months) to ours (12 months) and has a neck design that is less stiff than the CRABI 12 ATD neck. In

addition to the reduced neck stiffness, the lighter mass of the head and different initial position (supine) in Coats study reflect head forces that differ from our study. Alternatively, the head impact forces from the Ibrahim et al.⁸¹ and Bertocci et al.⁴ studies are higher than our findings mainly because of the difference in ATD size. Ibrahim used a custom designed ATD which is older in age (18 months) to ours (12 months), in addition to a different initial position (supine free fall) than our experiments which simulated the entire fall event (rolling off the bed). The Bertocci et al.⁴ study also used an older ATD (Hybrid II 3 year old) which has greater mass (30 lbs) versus ours (20 lbs) which could account for the great head forces when compared to our findings. It should be noted that the head forces for the Thompson et al.⁷³ and Bertocci et al.⁴ studies were calculated from measured head accelerations and head mass and are therefore approximates of actual head forces.

Table 15: Comparison of head impact forces, ATD head properties and initial conditions for various fall studies

	Our study	Thompson et al.⁷³	Coats et al.⁷⁶	Ibrahim et al.⁸¹	Bertocci et al.⁴
Head Force – 24 in (N)	2045 – 2223	2170 ^a	650	3715	4237 ^a
Head Force – 36 in (N)	2510 – 2631	–	1000	4570	–
ATD Age	12 month	12 month	1.5 month	18 month	36 month
Head contact region	Frontal, Parietal, Occiput	Parietal ^b	Occiput	Occiput	Occiput ^b
Head mass (Kg)	2.6	2.6	2.1	1.0	2.7
Fall Type	Bed fall, Side lying, FF, FR	Bed fall, Side lying, FF	Supine, Free fall	Supine, Free fall	Bed fall, Side lying, FF

a – force calculated from measured acceleration and head mass.

b – assumed based on initial position and described fall dynamics but not specified in study.

Potential Bruising Regions

When assessing body regions of impact during simulated falls, it is important to compare ATD morphology/geometric shape to that of an infant's morphology. While the CRABI 12 ATD represents the anthropometrics and mass distribution of a 12-month-old 50th percentile infant, its morphology (external shape/geometry) may vary somewhat from that of a 12-month-old 50th percentile infant. For example, the ATD morphology does not replicate soft tissue of the

buttocks region; instead in our study, the proximal posterior upper leg region of the ATD represents the buttocks. The ATD head morphology provides a reasonable replica of a 12-month child (Fig. 36) but does not include ears, nose, lips and the eyes orbital region as individual features. Also, the ATD head morphology does not represent the caudal most aspects of the occipital region or the mandible. Thus, it was not possible to measure and record impact to these regions.

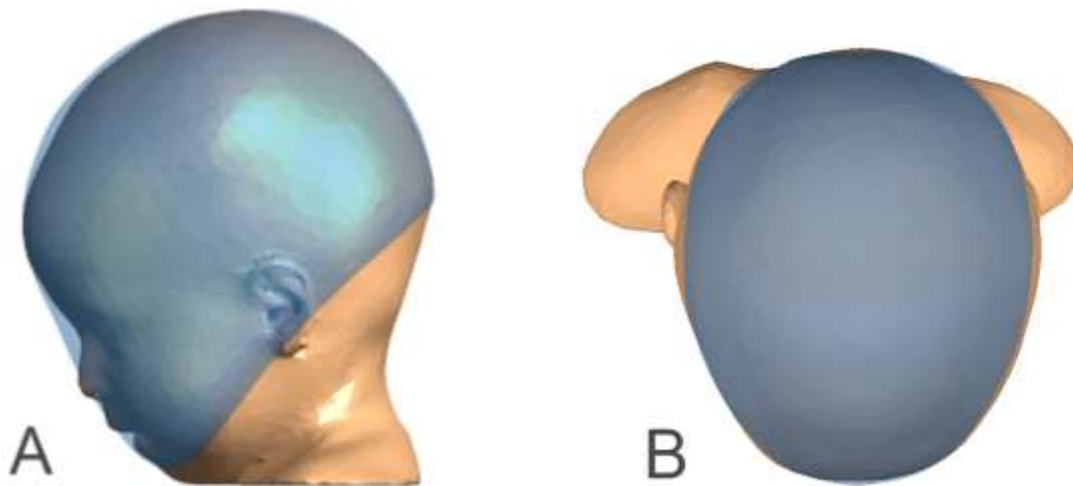


Figure 36: Lateral (A) and overhead (B) views of a comparative overlay of an 11-month-old child (3D reconstruction of CT imaging) and the 12-month-old CRABI ATD (transparent; blue) highlighting morphological differences in head profile.

A comparative overlay of an 11-month-old child (3D reconstruction of CT imaging) and the 12-month-old CRABI ATD highlighting approximate head sensor locations (shown in red) as comprised in the SBDS is shown in Fig. 37. It is important to note the approximate placement of the ears on the ATD head relative to the head sensor location (ear representative sensor shown as the red

square over the ears region in Fig. 37). Even though the 'ear representative sensor' is at the approximate location of the ear, the sensor size/area is relatively larger when compared to an actual ear (CT image in the overlay Fig. 37). This implies that loading at the far reaches of that sensor would still indicate bruising to the ear region. Our results indicate that in all the falls conducted (n = 20) the peak mean force recorded in the 'ear representative sensor' (red square representing the sensor over the ear region in Fig. 37) was $18 \text{ N} \pm 34$. Therefore bruising in the ear region is unlikely within the conditions of all our conducted bed falls.

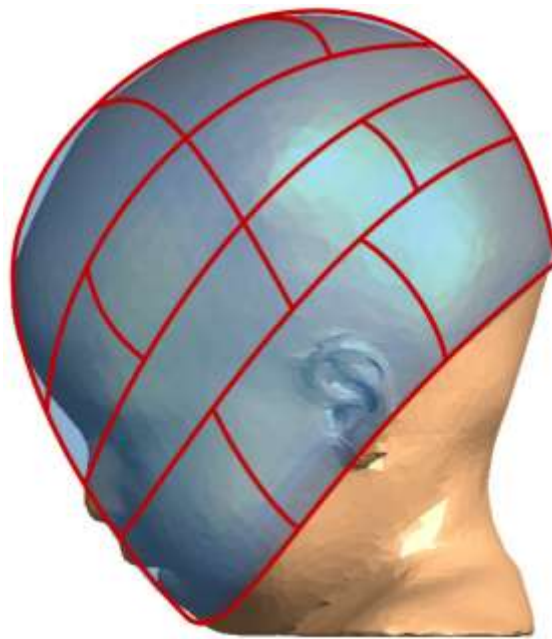


Figure 37: A comparative overlay of an 11-month-old child (3D reconstruction of CT imaging) and the 12-month-old CRABI ATD head (transparent; blue) highlighting approximate head sensor locations (red) as comprised in the SBDS.

Across all trials (n=20), we recorded contact within a maximum of two planes in any given scenario. Additionally, a consistent pattern emerged; the majority of contact regions and greater forces were recorded in one plane, with fewer regions of contact and decreased force exhibited in the second plane. Alternatively our findings suggest no possibility of bruising (as we saw no contact) in the two planes complementary to the impact planes for each fall scenario as highlighted in Table 13. It is pertinent to consider that the design of the boundaries/extremities of the individual sensors that make up the SBDS is not explicitly directed by the body planes. This implies that individual sensors cross over multiple planes and therefore could indicate impact in more than one plane even though the acting force was not directed at multiple planes. Additionally, the articulation of the extremities following the fall initiation and during the impact with the surface could influence locations of impact and consequently the planes of impact.

When assessing children with bruises, the location, and pattern (constellation of individual bruises throughout the body) of bruising is especially important in trying to delineate between accidental and abusive trauma. Several studies have investigated the distinction between bruising patterns in abused children versus those seen in accidental circumstances.

Maguire et al.⁷⁷ conducted a review of current literature seeking to identify patterns of bruising that may be suggestive of abuse. The reviewed studies noted that bruises resulting from accidental trauma occurred predominantly on the anterior regions of the body, over bony prominences and were correlated to the

child's level of independent mobility. In abused children the bruises tended to be larger and the most common sites were the face, neck, ear, head, trunk, buttocks, and arms.

Kemp et al.⁷⁸ described the characteristics of bruising and the extent to which these differ between children (aged < 6 years) where abuse was confirmed and those where it was excluded in children with suspected physical abuse. Data was collected from 506 children; abuse was confirmed in 350 and excluded in 156 children. Results indicated that abused children were significantly more likely to have bruising than those where abuse was ruled out. Abused children also had significantly more bruises, more bruising sites and clustering of bruises than the group where abuse was excluded. Bruising to the left ear, cheeks, neck, trunk, front of thighs, upper arms, buttocks and genitalia were found significantly more frequently in abused children, than when abuse was ruled out.

Pierce, Kaczor et al.⁶² studied the skin findings (bruises, lacerations, etc.) of children ages 0-4 years that were admitted to the pediatric intensive care unit of a tertiary care children's hospital where cause of injury was identified through the trauma registry as abuse or accident. Each patient's age, and skin findings including bruising, body region of skin finding, and number of skin findings were recorded. A total of 95 patients were analyzed in the study; 42 patients were exposed to abusive trauma and 53 patients were exposed to accidental trauma. Differences in body regions with bruising were identified for children with abusive versus accidental trauma. The face, cheek, scalp, head, and legs had bruising in patients with abusive and accidental trauma; these regions did not delineate

between accident and abuse. However, bruising to the ear, neck, hands, right arm, chest and buttocks regions were predictive of abuse. All bruising to the genitourinary area and hip occurred only in patients with abusive trauma.

The impact regions recorded in our testing in comparison to the bruising locations found on children from relevant studies described above are summarized in Table 16.

Table 16: Comparison of potential bruising locations in our study to observed bruising in previous clinical studies

	Our study	Kemp et al.⁷⁸	Maguire et al.⁷⁷	Pierce et al.⁶²
Regions of Abusive Bruising	-	Head, cheek, ear, neck, trunk, upper arms, front of thighs,	Head including face, front of body, ear, neck, trunk, arms, buttocks	All regions including torso, ear and neck
Regions of Accidental Bruising	^a Head, Torso, Left upper arm, Right lower arm, L & R upper leg, Left lower leg	Head, Rear trunk	Head, forehead, back, abdomen, forearms, hands, buttocks, knees, shins, foot	All regions excluding torso, ear and neck

a – recorded impact locations that could represent potential bruising locations and are only specific to one fall type (bed falls).

In our study we predominantly found impact to the head, torso, left upper arm, right lower arm, left and right upper legs and left lower leg. Compared to previous clinical studies describing bruising locations for a range of accident types, the head and posterior torso were found to be common regions of

bruising^{77,78}. In similarity to Kemp et al.⁷⁸, Maguire et al.⁷⁷ and Pierce et al.⁶² we found it unlikely to have bruising to the ears. However, Kemp et al.⁷⁸ and Maguire et al.⁷⁷ did not report detailed fall description, mechanism or injury causation. Thus this limits direct comparisons to those studies as our experimental findings are specific to bed fall scenarios.

Clinical Skin Findings in Accidental and Abuse Cases

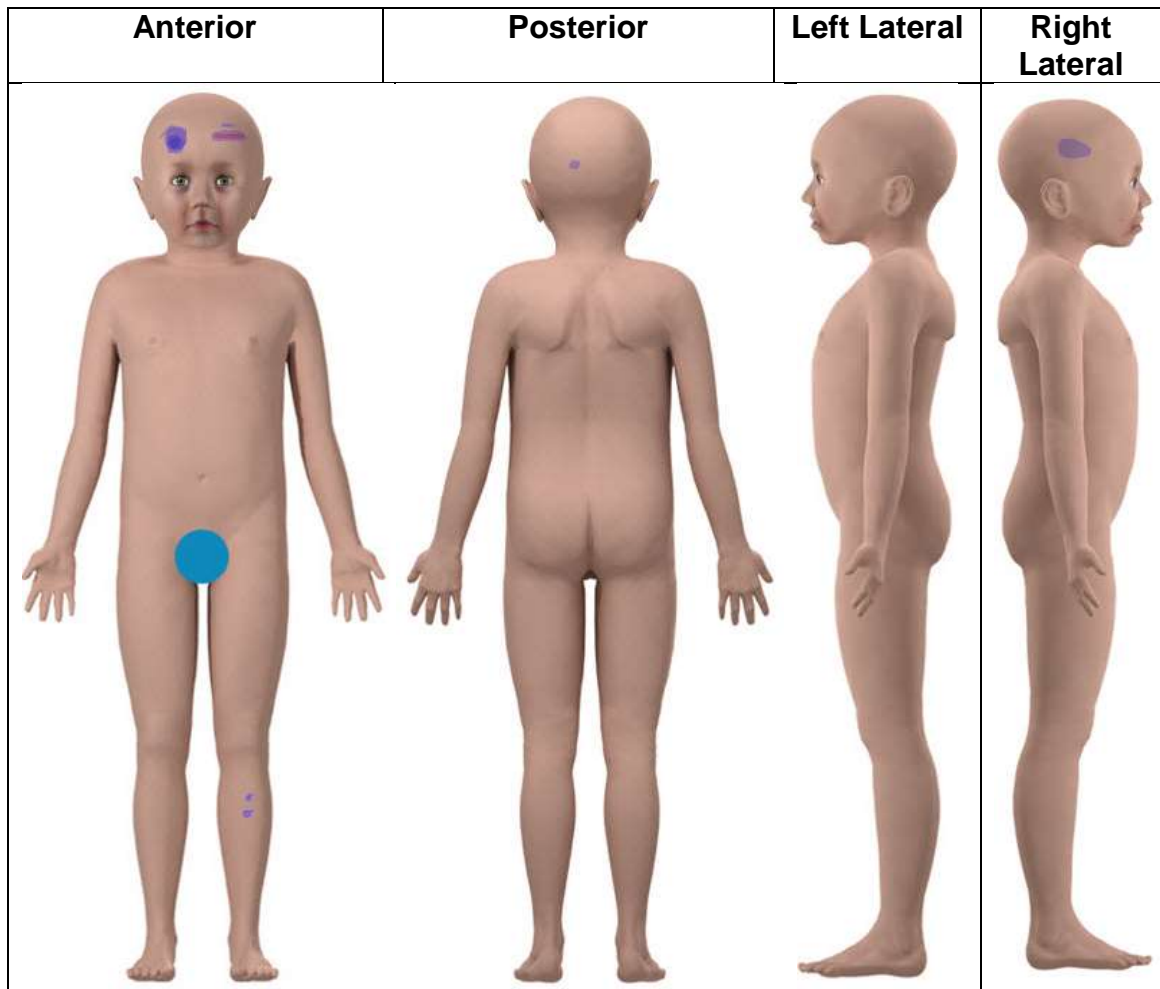
We evaluated clinical cases from the bruising clinical decision rule (BCDR) database⁶² and noted whether clinically documented bruised regions were contained within our experimentally predicted contact regions. A key distinction is that the experimental falls identify all regions of contact with the impact surface during a specific, controlled fall scenario where a bruise could potentially develop, but not necessarily occur. Our experimental results do not predict bruising; rather only identify fall specific contact locations where potential bruising may occur.

The BCDR database consists of clinical histories of children 0-4 years of age that were brought into the emergency room of a children's hospital (Chicago, Cincinnati and Pittsburg children's hospital) and had a bruise injury. The database does present selection bias as it is limited to families that decided to seek care after an injurious event. Each patient's age, and skin findings including total number of bruises, body location of bruising, bruising count, bruising planes and stated cause of injury, among many other variables were recorded in the BCDR database. Each case entered into the database was evaluated and

categorized by an expert panel to determine whether the case qualifies for one of five categories; *definite abuse*, *likely abuse*, *definite accident*, *likely accident* or *indeterminate*. Query results from the BCDR database included falls related to furniture falls in children 10-14 months of age. Through the assistance of Dr. Pierce and K. Kaczor⁶², multiple queries were performed on the BCDR database to gather case results that included bed falls, change table falls and abuse cases.

Clinical Cases – Bed Falls

This database query involved bed fall cases identified as *definite accident* or *likely accident* in children 10-14 months of age. Eight cases from a total of a hundred furniture fall cases fit our defined criteria. The cumulative skin findings observed in these cases highlight bruising to the frontal, occipital and right parietal head and the front of the left lower leg (Fig. 38). Also no bruises were seen in the anterior or posterior torso, upper extremities and the right upper and lower leg.



Images provided courtesy of Pierce MC and Kaczor K⁶²

Figure 38: Cumulative humagram highlighting skin findings from the BCDR database cases involving bed falls identified as *definite accident* or *likely accident* in children 10-14 months of age.

A direct comparison of clinical findings to our experimental results is not viable because the experimental results indicate contact regions where there is a **potential** for bruising rather than **actual** bruising locations. A clinical to experimental case by case comparison is also not possible as fall parameters (height, initial position, impact surface) in clinical cases are commonly insufficiently documented, and when documented, are not always accurately

witnessed accounts of the incident. Rather, we noted whether clinically documented bruised regions were contained within our experimentally predicted contact regions.

Bruising locations in clinical cases deemed accidental bed falls (n = 8) were contained within the regions contacted in the experimental falls (FF 24 and FR 24) with the exception of the occipital head (Table 17). The 24 inch experimental falls were simulating bed and couch falls and only two different initial positions were evaluated. Thus, a different initial position in experimental falls could have resulted in contact to the occipital region of the head.

Table 17: Regions with and without contact in experimental 24 inch facing forward and facing rearward falls, highlighting bruising locations recorded in clinical cases (shown as [#]) involving bed falls identified as *definite accident* or *likely accident* in children 10-14 months of age.

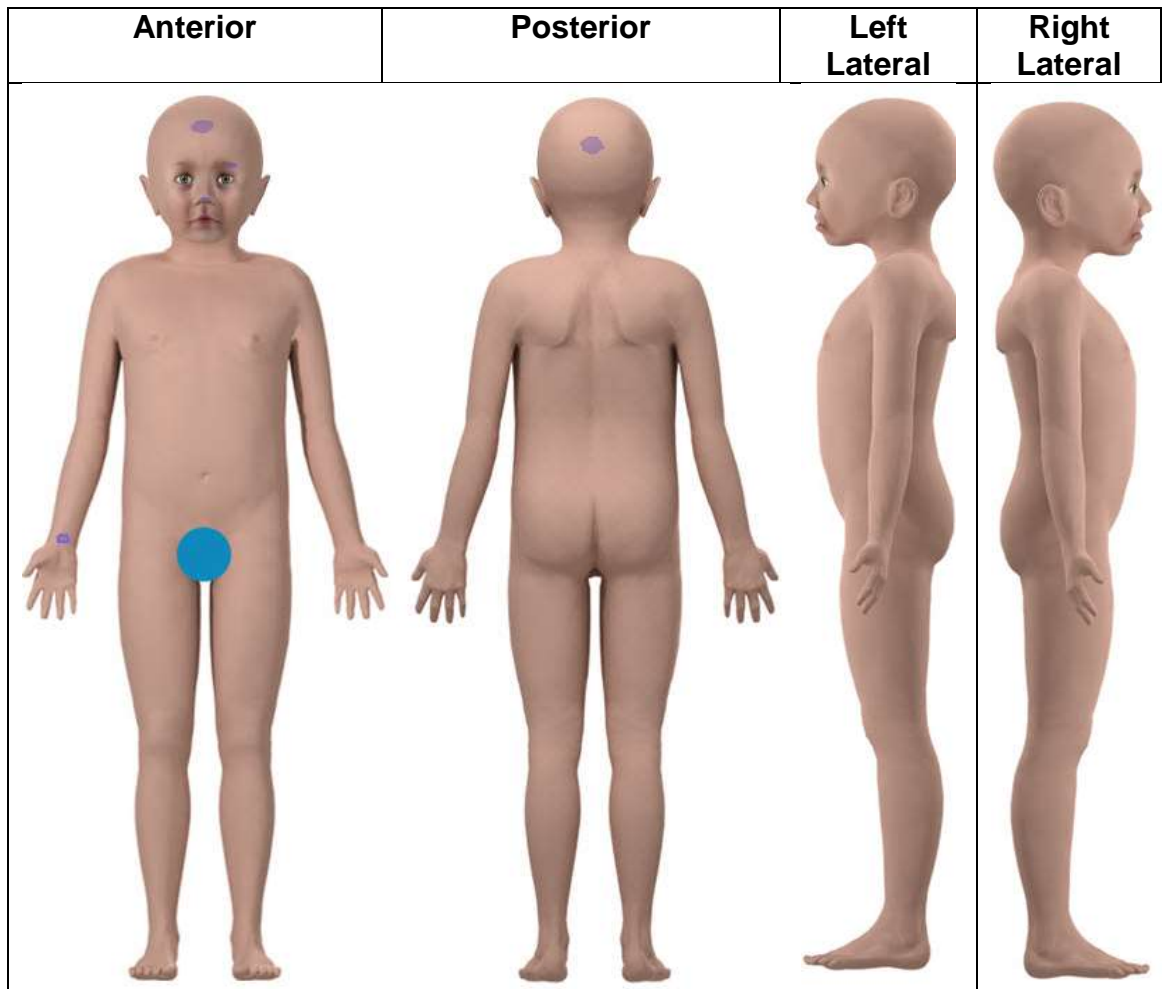
Fall Type	FF24 (n = 5)	FR24 (n = 5)
Regions with Contact	L parietal head L anterior torso L lateral torso L upper arm L upper leg L lower leg [#]	Frontal head [#] R parietal head [#] R anterior torso R lateral torso R upper leg L Upper Leg L Lower Leg [#] R lower arm

Fall Type	FF24 (n = 5)	FR24 (n = 5)
Regions without Contact	Frontal head [#] Occipital head [#] R parietal head [#] L posterior torso R anterior torso R posterior torso R lateral torso L lower arm R upper arm R lower arm R upper leg R lower leg	Occipital head [#] L parietal head R posterior torso L anterior torso L posterior torso L lateral torso R upper arm R lower leg L upper arm L lower arm

[#] indicates regions with a bruise, recorded in clinical cases involving accidental bed falls (n = 8)

Clinical Cases – Change Table Falls

This database query involved change table fall cases identified as *definite accident* or *likely accident* in children 10-14 months of age. Four cases from a total of a hundred furniture fall cases fit our defined criteria. The cumulative skin findings observed in these cases highlight bruising to the frontal and occipital head, and the right lower arm (Fig. 39).



Images provided courtesy of Pierce MC and Kaczor K⁶²

Figure 39: Cumulative humagram highlighting skin findings from the BCDR database cases involving change table falls identified as *definite accident* or *likely accident* in children 10-14 months of age.

Again, a direct comparison of clinical findings to our experimental results is not viable because the experimental results indicate contact regions where there is a **potential** for bruising rather than **actual** bruising locations. A clinical to experimental case by case comparison is also not possible as fall parameters (height, initial position, impact surface) in clinical cases are commonly insufficiently documented, and when documented, are not always accurately

witnessed accounts of the incident. Rather, we noted whether clinically documented bruised regions were contained within our experimentally predicted contact regions.

Bruising locations in clinical cases deemed accidental change table falls (n =4) were contained within the regions contacted in the experimental falls (FF 36 and FR 36) with the exception of the right lower arm (Table 18). The 36 inch experimental falls were simulating change table falls and only two different initial positions (facing forward and facing rearward) were evaluated. Thus, a different initial position in experimental falls could have resulted in contact to the right lower arm region.

Table 18: Regions with and without contact in experimental 36 inch facing forward and facing rearward falls, highlighting bruising locations recorded in clinical cases (shown as '#') involving change table falls identified as *definite accident* or *likely accident* in children 10-14 months of age.

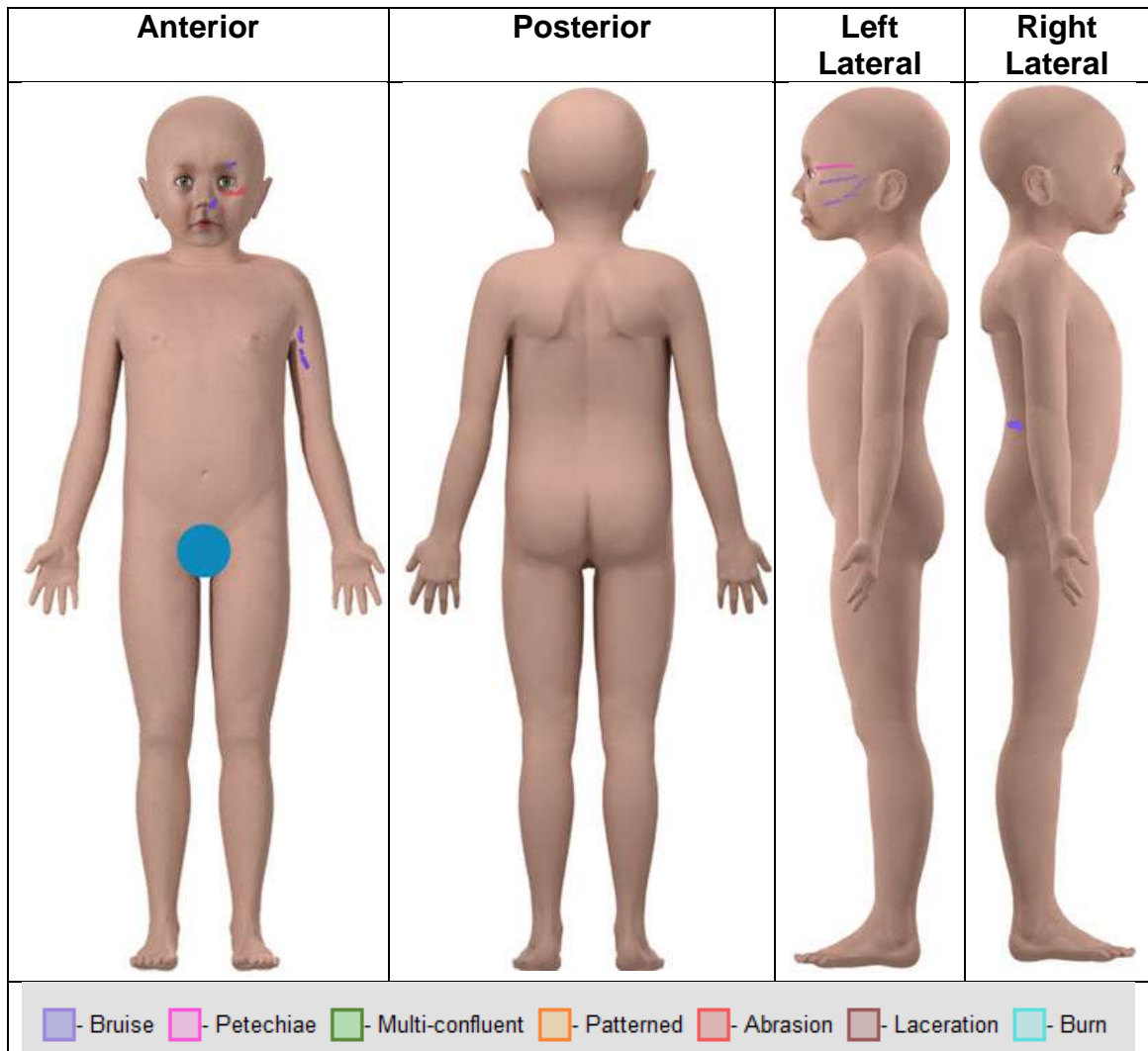
Fall Type	FF36 (n = 5)	FR36 (n = 5)
Regions with Contact	L parietal head Occipital head# L posterior torso L lateral torso L upper arm L upper leg L lower arm	Frontal head# L anterior torso R anterior torso R upper leg L upper leg L lower leg

Fall Type	FF36 (n = 5)	FR36 (n = 5)
Regions without Contact	Frontal head [#] R parietal head L anterior torso R anterior torso R posterior torso R lateral torso R upper arm R lower arm [#] R upper leg R lower leg L lower leg	Occipital head [#] R parietal head L parietal head L posterior torso R posterior torso R lateral torso L lateral torso R upper arm R lower arm [#] L upper arm L lower arm R lower leg

[#] indicates regions with a bruise in clinical cases involving accidental change table falls (n=4)

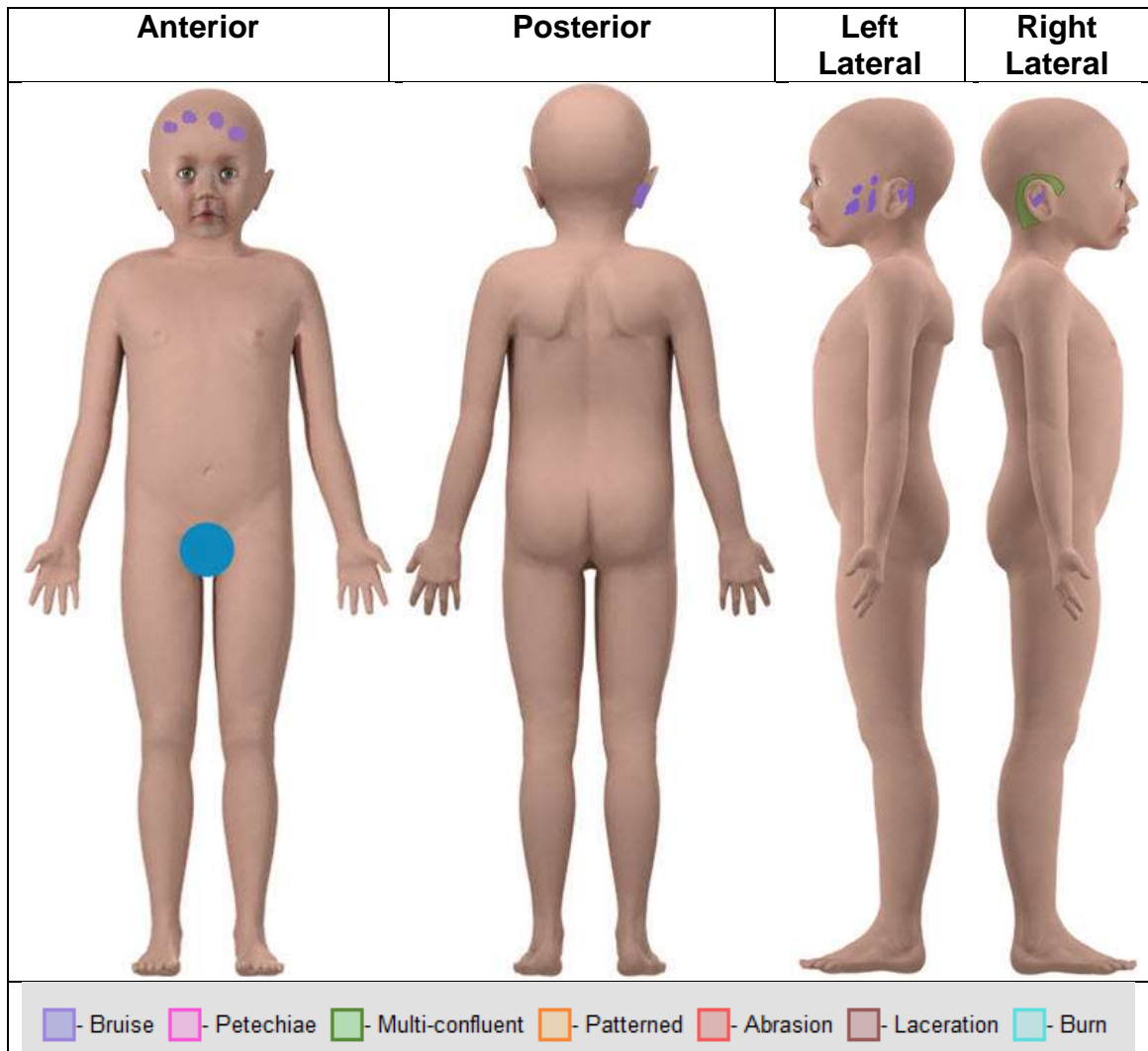
Clinical Cases – Abuse

This database query involved falsely stated furniture fall cases identified as *abuse* or *likely abuse* in children 10-14 months of age. Three cases from a total of a hundred furniture fall cases fit our defined criteria. The skin findings observed in these cases highlight multiple bruises to the frontal, left parietal and right parietal head, anterior, posterior, left and right torso, left and right upper arm and right upper leg (Fig. 40–A, Fig. 40–B, Fig. 40–C). A fundamental difference observed in abuse cases compared to accidental cases was bruises were scattered, and multiple in number per body region. Also, alternative skin findings (abrasions) in addition to bruises were presented as overlaid injuries in abuse cases. There also was bruising on the sole of the right foot (Case–C; not shown in Fig. 40–C) that was not considered in our observations.



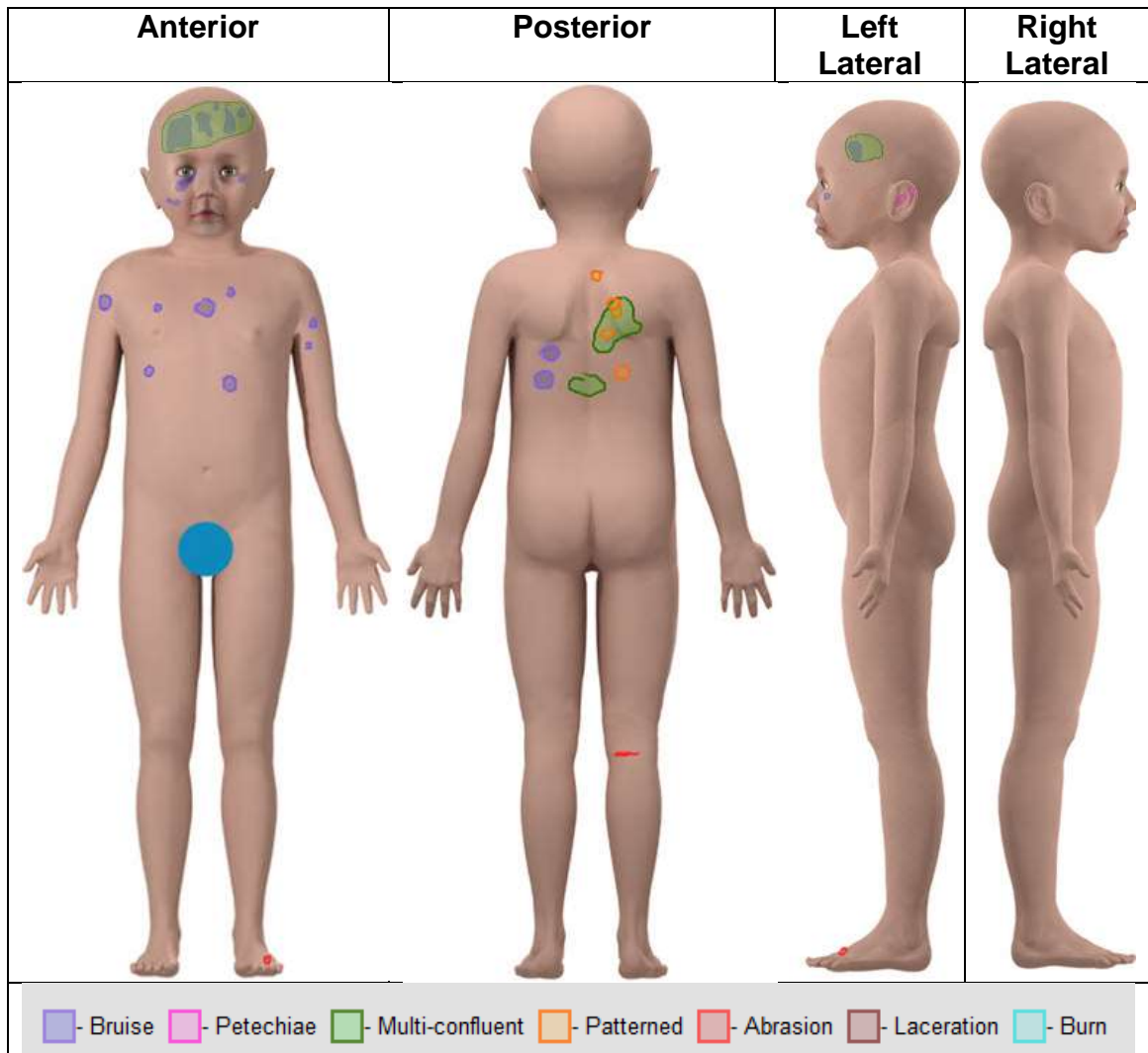
Images provided courtesy of Pierce MC and Kaczor K⁶²

Figure 40-A: Cumulative humagram highlighting skin findings from the BCDR database Case–A identified as *definite abuse* or *likely abuse* in a child 10-14 months of age. Legend - Bruise indicates discrete bruises. Petechiae describes red spots under the skin surface caused by intradermal hemorrhage. Multi-confluent indicates a bruised region where a discrete bruised area is difficult to identify; thus the area surrounding the bruised region was recorded. Patterned implies a distinct bruise imprint left by an impacting object.



Images provided courtesy of Pierce MC and Kaczor K⁶²

Figure 41–B: Humagram highlighting skin findings from the BCDR database Case–B identified as *definite abuse* or *likely abuse* in a child 10-14 months of age. Legend - Bruise indicates discrete bruises. Petechiae describes red spots under the skin surface caused by intradermal hemorrhage. Multi-confluent indicates a bruised region where a discrete bruised area is difficult to identify; thus the area surrounding the bruised region was recorded. Patterned implies a distinct bruise imprint left by an impacting object.



Images provided courtesy of Pierce MC and Kaczor K⁶²

Figure 42–C: Humagram highlighting skin findings from the BCDR database Case–C identified as *definite abuse* or *likely abuse* in a child 10-14 months of age. Legend - Bruise indicates discrete bruises. Petechiae describes red spots under the skin surface caused by intradermal hemorrhage. Multi-confluent indicates a bruised region where a discrete bruised area is difficult to identify; thus the area surrounding the bruised region was recorded. Patterned implies a distinct bruise imprint left by an impacting object

Abuse Case Histories Provided

History, Case–A: Unwitnessed fall where patient reportedly tried to climb from a bed onto a nightstand, then fell and hit their face on the nightstand.

History, Case–B: Patient reportedly fell from crib onto a carpeted area.

History, Case–C: Patient fell from bed, face-first onto a carpeted floor (3 to 4 ft fall height). Under a second caregiver, later that day patient fell out of the high chair and hit his head. Final confession of abuse by the second caregiver included shaking and throwing the patient.

Evaluation of Abusive Bruising Locations

Bruising locations in clinical cases with false histories of accidental furniture falls deemed abuse were beyond the regions of contact recorded in our experimental bed falls (Table 19). The abuse cases showed bruising on three or more body planes in multiple regions (Case–A had three planes of bruising, Case–B had four planes of bruising, Case–C had three planes of bruising). In contrast, our experimental falls recorded contact with the impact surface in only two planes for each fall type.

Table 19: Experimental results of the 24 inch facing forward and facing rearward falls, comparing regions with, and without contact highlighting bruising locations

(shown as '#') recorded in clinical cases involving furniture falls identified as abuse in children 10-14 months of age.

Fall Type	FF24 (n = 5)	FR24 (n = 5)
Regions with Contact	L parietal head [#] L anterior torso [#] L lateral torso L upper arm [#] L upper leg L lower leg [#]	Frontal head [#] R parietal head [#] R anterior torso [#] R lateral torso [#] R upper leg [#] L Upper Leg L Lower Leg [#] R lower arm
Regions without Contact	Frontal head [#] Occipital head [#] R parietal head [#] L posterior torso [#] R anterior torso [#] R posterior torso [#] R lateral torso [#] L lower arm R upper arm [#] R lower arm R upper leg [#] R lower leg [#]	Occipital head [#] L parietal head [#] R posterior torso [#] L anterior torso [#] L posterior torso [#] L lateral torso R upper arm [#] R lower leg [#] L upper arm [#] L lower arm

'#' indicates regions with a bruise in clinical cases involving accidental change table falls (n=4)

In conclusion, the SBDS was used to predict a “roadmap” of the child surrogate’s contact exposure during specific furniture fall events. Falls with varying parameters (initial height, initial position) did lead to differences in impact locations and forces in the head. This implies that initial height and initial position lead to differences in fall dynamics and impact orientation which lead to differences in bruising patterns and forces.

We evaluated clinical cases from the bruising clinical decision rule (BCDR) database and noted whether clinically documented bruised regions were contained within our experimentally predicted contact regions. Bruising locations in clinical cases deemed accidental bed falls (n = 8) and accidental change table falls (n = 4) were within the regions contacted in our experimental falls except for the occipital head and right lower arm respectively. Our experimental results do not predict bruising; rather only identify fall specific contact locations where potential bruising may occur. Additionally, bruising locations in clinical cases with false histories of furniture falls deemed abuse were beyond the regions of contact recorded in our experimental bed falls. This has important implications as it further reinforces that there are differences in bruising patterns between accidental falls and inflicted abuse.

LIMITATIONS

The biofidelity of the CRABI ATD and in particular the soft tissue biofidelity is a limitation of the SBDS. The ATD surrogate “soft tissue” consists of a heat cured vinyl plastisol that is layered with urethane foam between the outer and inner layers. The plastisol is compliant and molded to mimic the body contours representing “soft tissue”. SBDS sensor measured forces are proportional to the stiffness of the underlying ATD surrogate soft tissue; therefore soft tissue biofidelity greatly influences the measured forces. However, our primary goal was to determine points of contact during various injurious events and secondarily to assess relative levels of force imparted to different regions of the body. Thus,

biofidelic limitations of the surrogate soft tissue do not prevent us from meeting our goals.

Also, since the CRABI ATD was primarily designed for measuring a child's response to a high energy automotive crash environment, any findings from testing conducted with the ATD in lower deceleration events such as falls should be interpreted in light of biofidelity limitations. For example, the neck is somewhat stiffer with limited range of motion designed for frontal impacts having little or no out of plane motion. The rubber elements that attach the limbs to the ATD torso are used in the hip and shoulder joints to provide the CRABI infant-like range of motion, but are an approximation of true infant biofidelity. In addition, joints of the shoulders, elbows, hips, and knees of the ATD are limited to motion primarily in the sagittal plane. Though ATD kinematics in our simulated falls occurred primarily in the sagittal plane, any out of plane motion may lead to inaccuracies in kinematics and force measures. Varying ATD joint stiffness could additionally alter fall dynamics thereby influencing impact locations and forces. Additionally, we were unable to implement sensors in the neck region of the ATD given its construction (segmented rubber and aluminum disks), but based on our experimental fall dynamics, the ATD neck had a low likelihood of contact/impact during falls.

The occurrence of a bruise varies from person to person for a given application of force based on many contributing factors that affect bruise development. Extrinsic factors such as the amount of force applied, rate of force application, and distribution of the force over larger/smaller areas are parameters

that can affect the presence or absence of a bruise. Additionally, intrinsic factors related to the physiological and anatomical structures, such as architecture of the skin, soft tissue thickness, toughness of skin, fat content, vessel fragility, and presence and depth of underlying bone add to the complexity of this physiological event. Variables such as blood platelet levels, systemic blood pressure, vascular diseases and vasoactive or anticoagulant drug use in addition to nutritional and allergy related disorders can have a great influence on the presence, absence and variability in intensity of a bruise. This implies that the minimum load to cause bruising, the “bruising threshold”, varies across individuals. However it can be said with some degree of certainty that larger forces are associated with a greater potential for bruising. So instead of definitively asserting the presence of a bruise, we are assessing potential bruising locations occurring within a body region under specific fall conditions.

While our findings predicted potential bruising locations in a bed fall and change table fall from a side-lying position using the SBDS, limitations described herein must be considered. The experimental falls identify all regions of contact with the impact surface during a specific, controlled fall scenario where a bruise could potentially develop, but not necessarily occur. Our experimental results do not predict bruising; rather only identify fall specific contact locations where potential bruising may occur. However, the capability to predict potential bruising locations or patterns is useful when attempting to determine compatibility between a stated cause and associated skin findings in forensic analyses.

CHAPTER VI:

SUMMARY AND CONCLUSIONS

A summary of the results of our hypotheses testing are provided herein:

Hypothesis 1 – Different initial condition bed falls (height and position) will lead to differences in impact locations recorded in number of planes.

This hypothesis was tested through bed fall experiments conducted with the SBDS placed in different initial conditions (height and position) while recording impact locations as described in Chapter V. Impact planes were defined as a body plane that displayed any region of contact within the plane. There were four body planes (Anterior plane, posterior plane, left lateral plane and right lateral plane) defined for the surrogate. Results from all experimental bed falls ($n = 20$) recorded 2 planes of contact and 2 planes without contact. Therefore, there was no difference observed in the number of planes with impact when comparing height and position parameters in experimental bed falls.

Hypothesis 2 – Different initial condition bed falls (height and position) will lead to differences in impact locations recorded in number of body regions.

This hypothesis was tested through bed fall experiments conducted with the SBDS placed in different initial conditions (height and position) while

recording impact locations as described in Chapter V. Body regions were defined as one of eighteen (Frontal head, Occipital head, R parietal head, L parietal head, R anterior torso, R posterior torso, R lateral torso, L anterior torso, L posterior torso, L lateral torso, R upper arm, R lower arm, L upper arm, L lower arm, R upper leg, R lower leg, L upper leg, L lower leg). Results from the experiments indicate a difference in the number of body regions impacted between bed falls of different initial conditions, but this difference was not statistically significant ($p = 0.57$). There were six, eight, seven and six regions with impact for the FF24, FR24, FF36 and FR36 falls respectively. A chi square analysis done independently on comparing different fall parameters (comparing height and position) showed no significant difference ($p > 0.05$) implying that fall height and position had no significant difference on the number of impact regions.

Hypothesis 3 – During bed falls, impacts to the ear region will be less than 10%.

We were unable to test this hypothesis given the limitations of the head sensor pattern; the representative ear sensor has an area/size that is relatively larger compared to an actual ear, so it recorded loads from regions beyond a child's ear. Loading at the far reaches of this sensor would indicate potential bruising to the ear region which thereby prevents testing of this hypothesis.

Key Findings and Clinical Implications

The purpose of this study was to provide objective data regarding the potential bruising locations and bruising patterns in children in common household falls so as to aid clinicians in the distinction between abusive and accidental injuries. This study included three methodological components. In the first component we adapted an existing pediatric anthropomorphic test device (ATD) with custom developed force sensors integrated into a conformable skin. The sensors were coupled to a data acquisition system through which recorded force data was displayed on a computerized body mapping image system. The sensor outputs that make up the sensing skin have been shown to be repeatable under dynamic testing. The surrogate bruising detection system (SBDS) is the first patented tool capable of predicting potential bruising patterns when used in simulated events.

In the second component we utilized the SBDS to simulate rearward fall experiments that were performed onto two different impact surfaces (padded carpet and linoleum tile over concrete) with two different initial positions (standing upright and posteriorly inclined). Potential bruising regions and fall dynamics were investigated. Across all (n=32) trials in all rearward fall scenarios, the occipital head and posterior torso were the common regions of impact. The mean peak impact force for the head ($1995 \text{ N} \pm 162$) and posterior torso ($1050 \text{ N} \pm 154$) were the highest in falls having an upright initial position onto the linoleum over concrete surface. The lowest mean peak impact force to the head ($1050 \text{ N} \pm 79$) occurred during the falls having a posteriorly inclined initial position with

impact onto the carpet over wood surface. The lowest mean peak impact force to the posterior torso ($244 \text{ N} \pm 61$) occurred during falls with an upright initial position onto the carpet over wood surface. For falls onto carpet over wood, the common regions of impact for both initial positions were the head and posterior torso. In addition to these common regions, sensors on the upper leg indicated impact for the inclined fall position. For falls onto linoleum over concrete, the common regions of impact for both initial positions were the head, posterior torso, lower arm and lower leg. In addition to these common regions, sensors on the upper leg indicated impact for the inclined position. Compared to previous clinical studies describing bruising locations for a range of accident types, the head and posterior torso were found to be common regions of bruising^{77,78}. Parallel to literature^{78,77,62} we did not find impact or potential for bruising to the ears or neck which is not commonly seen as a location for bruising in accidental falls. A key distinction is that the experimental falls identify all regions of contact with the impact surface during a specific, controlled fall scenario where a bruise could potentially develop, but not necessarily occur. Our experimental results do not predict bruising; rather only identify fall specific contact locations where potential bruising may occur.

The final component utilized the SBDS to simulate bed fall and changing table fall experiments that were performed from two initial heights (24 inch and 36 inch) with two different initial positions (facing forward and facing rearward). Results from the experiments recorded a mean peak head impact force ($2631 \text{ N} \pm 100$) that was the highest in the 36 inch falls with a facing rearward initial

position and the lowest mean peak head impact force ($2045 \text{ N} \pm 254$) occurred in the 24 inch falls with a facing forward initial position. Head impact forces associated with 24 inch facing forward falls ($2045 \text{ N} \pm 254$) in our experiments were in reasonable agreement with those reported in literature ⁷³ (2170 N) for falls using the same ATD, initial position and fall height as our experiments. Across all trials ($n=20$), we recorded contact within a maximum of two planes in any given scenario. Additionally, a consistent pattern emerged; the majority of contact regions and greater forces were recorded in one plane, with fewer regions of contact and decreased force exhibited in the second plane. The experiments predicted differences in potential bruising locations in body regions based on initial conditions and fall heights.

The experimental falls identify all regions of contact with the impact surface during a specific, controlled fall scenario where a bruise could potentially develop, but not necessarily occur. Our experimental results do not predict bruising; rather only identify fall specific contact locations where potential bruising may occur. Bruising locations in clinical cases deemed accidental bed falls ($n = 8$) were contained within the regions contacted in the experimental falls (FF 24 and FR 24) with the exception of the occipital head. However, a different initial position in experimental falls could have resulted in contact to the occipital region of the head. Bruising locations in clinical cases deemed accidental change table falls ($n = 4$) were contained within the regions contacted in the experimental falls (FF 36 and FR 36) with the exception of the right lower arm. Again, a different initial position in experimental falls could have resulted in contact to the right

lower arm region. Bruising locations in clinical cases with false histories of accidental furniture falls deemed abuse were beyond the regions of contact recorded in our experimental bed falls. The abuse cases showed bruising on three or more body planes in multiple regions; our experimental falls recorded contact with the impact surface in only two planes for each fall type. This has important implications as it further reinforces that there are differences in bruising patterns between accidental falls and inflicted abuse.

The biofidelity of the CRABI ATD and in particular the soft tissue biofidelity could influence sensor measured forces and therefore potential bruising locations. The tissue stiffness is proportional to the forces measured by the SBDS. A more compliant soft tissue would better represent the soft tissue of a child and therefore for a given fall could produce lower forces.

Contact with an impact surface generates forces on the skin. The generation of a bruise at that location is influenced by the anatomic area subjected to the force. The areas of the body in which subcutaneous tissue and muscle directly lie over bone, such as the head, show bruises more readily due to the bone providing unyielding support to the compressed soft tissue. In contrast, areas such as the abdomen, buttocks, etc. have a lower potential to bruise from the same level of force because of the greater volume of tissue. The occurrence of a bruise varies from person to person for a given application of force based on many contributing factors that affect bruise development. Extrinsic factors such as the amount of force applied, rate of force application, and distribution of the force over larger/smaller areas are parameters that can

affect the presence or absence of a bruise. Additionally, intrinsic factors related to the physiological and anatomical structures, such as architecture of the skin, soft tissue thickness, toughness of skin, fat content, vessel fragility, and presence and depth of underlying bone add to the complexity of this physiological event. This implies that the minimum load to cause bruising, the “bruising threshold”, varies across individuals. Currently there is no established bruising threshold that provides a definitive answer on when bruising occurs based on recorded outcome measures. So instead of definitively asserting the presence of a bruise, we are assessing potential bruising locations occurring within a body region under specific fall conditions.

To our knowledge, the SBDS is the first tool capable of predicting potential bruising patterns during common household falls. The results of this study may aid clinicians by providing insight to better assess a child’s injuries for compatibility between the stated cause and presenting bruises in common household falls. Clinicians and child protective services should place more emphasis in detailed and accurate case histories that include parameters related to fall environment (height, surface, initial position) and fall dynamics as these factors affect the potential bruising locations.

Future work

The biofidelity of the CRABI ATD and in particular the soft tissue biofidelity could be improved upon to better represent the soft tissue properties of a child.

SBDS sensor measured forces are proportional to the stiffness of the underlying ATD surrogate soft tissue; therefore soft tissue biofidelity greatly influences the measured forces. Improvements in sensor density in the sensing skin of the SBDS could allow for more discrete sensing locations. A higher sensor resolution could translate to better distinction of contact within and around different body regions. Incorporating sensors within the sensing skin that could record additional outcome measure related to bruising prediction, such as applied pressure, soft tissue penetration depth, etc. could improve the potential bruising prediction capability. Additional outcome measures related to stress, impulse or energy could help in determining the prediction of a bruise.

Testing additional fall scenarios will provide a larger database of impact roadmap–event combinations for various falls and provide an indication of where potential bruising could occur for each specific event. Developing a computer simulation model representing a SBDS to predict potential bruising patterns will help investigate the influence of child and fall environment parameters on potential bruising patterns. A sensitivity analysis could describe the individual influence of child parameters (weight, height, joint stiffness) and fall parameters (fall height, initial position, impact surface) on bruising potential. We believe that in addition to protecting abused children, innocent families wrongly accused of abuse could also benefit from the outcomes of an event specific bruising prediction model.

REFERENCES

1. DHHS. Child maltreatment 2013. *US Department of Health and Human Services, Administration for Children and Families, Washington, DC* 2013.
2. Alexander R, Crabbe L, Sato Y, Smith W, Bennett T. Serial abuse in children who are shaken. *Archives of Pediatrics and Adolescent Medicine* 1990; **144**(1): 58-60.
3. Cross TP, Walsh WA, Simone M, Jones LM. Prosecution of child abuse: A meta-analysis of rates of criminal justice decisions. *Trauma, Violence, & Abuse* 2003; **4**(4): 323.
4. Bertocci GE, Pierce MC, Deemer E, Aguel F, Janosky JE, Vogeley E. Using test dummy experiments to investigate pediatric injury risk in simulated short-distance falls. *Archives of Pediatrics and Adolescent Medicine* 2003; **157**(5): 480-6.
5. Bertocci GE, Pierce MC, Deemer E, Aguel F, Janosky JE, Vogeley E. Influence of fall height and impact surface on biomechanics of feet-first free falls in children. *Injury* 2004; **35**(4): 417-24.
6. Deemer E, Bertocci G, Pierce MC, Aguel F, Janosky J, Vogeley E. Influence of wet surfaces and fall height on pediatric injury risk in feet-first freefalls as predicted using a test dummy. *Medical Engineering and Physics* 2005; **27**(1): 31-9.
7. Thompson AK, Bertocci G, Pierce MC. Assessment of head injury risk associated with feet-first free falls in 12-month-old children using an anthropomorphic test device. *The Journal of Trauma: Injury, Infection, and Critical Care* 2009; **66**(4): 1019.
8. CAPTA. Child Abuse Prevention and Treatment Act *United States Public Law 93-247 (S 1191)* 1974.
9. DHHS. Child maltreatment 2011. *US Department of Health and Human Services, Administration for Children and Families, Washington, DC* 2011.

10. NACHRI. Responding to Child Maltreatment, Survey Findings and Trends. *The National Association of Children's Hospitals and Related Institutions* 2008.
11. PCAA. Total Estimated Cost of Child Abuse and Neglect in the United States: The Statistical Evidence. *Prevent Child Abuse America, Chicago, IL* 2008.
12. Anda R. The Health and Social Impact of Growing Up with Adverse Childhood Experiences: The Human and Economic Costs of the Status Quo. *Review, Adverse Childhood Experiences (ACE) Study* 2008.
13. Touloukian RJ. Abdominal visceral injuries in battered children. *Pediatrics* 1968; **42**(4): 642-6.
14. Jackson G. Child abuse syndrome: the cases we miss. *British Medical Journal* 1972; **2**(5816): 756.
15. O'Neill Jr JA, Meacham WF, Griffin PP, Sawyers JL. Patterns of injury in the battered child syndrome. *The Journal of Trauma: Injury, Infection, and Critical Care* 1973; **13**(4): 332.
16. Diamond P, Hansen CM, Christofersen MR. Child abuse presenting as a thoracolumbar spinal fracture dislocation: A case report. *Pediatric Emergency Care* 1994; **10**(2): 83.
17. Ewing-Cobbs L, Kramer L, Prasad M, et al. Neuroimaging, physical, and developmental findings after inflicted and noninflicted traumatic brain injury in young children. *Pediatrics* 1998; **102**(2): 300-7.
18. Jenny C, Hymel KP, Ritzen A, Reinert SE, Hay TC. Analysis of missed cases of abusive head trauma. 1999; **281**(7): 621-6.
19. Benzel EC, Hadden TA. Neurologic Manifestations of Child Abuse. *Southern Medical Journal* 1989; **82**(11): 1347.
20. Smith SM, Hanson R. 134 battered children: a medical and psychological study. *British Medical Journal* 1974; **3**(5932): 666.
21. Myers JEB. Legal Issues in Child Abuse and Neglect Practice. 2 ed: SAGE; 1998.
22. Tjaden PG, Thoennes N. Predictors of legal intervention in child maltreatment cases. *Child abuse & neglect* 1992; **16**(6): 807-21.

23. Sedlak AJ, Schultz D, Wells SJ, Lyons P, Doueck HJ, Gragg F. Child protection and justice systems processing of serious child abuse and neglect cases. *Child abuse & neglect* 2006; **30**(6): 657-77.
24. Pressel DM. Evaluation of physical abuse in children. *American family physician* 2000; **61**(10): 3057.
25. Kaczor K, Clyde Pierce M, Makoroff K, Corey TS. Bruising and physical child abuse. *Clinical Pediatric Emergency Medicine* 2006; **7**(3): 153-60.
26. Wilson EF. Estimation of the age of cutaneous contusions in child abuse. *Pediatrics* 1977; **60**(5): 750-2.
27. Ellerstein NS. The cutaneous manifestations of child abuse and neglect. *Archives of Pediatrics and Adolescent Medicine* 1979; **133**(9): 906-9.
28. Caniano DA, Beaver BL, Boles Jr ET. Child abuse. An update on surgical management in 256 cases. *Annals of surgery* 1986; **203**(2): 219.
29. Maguire S, Mann MK, Sibert J, Kemp A. Are there patterns of bruising in childhood which are diagnostic or suggestive of abuse? A systematic review. *Archives of Disease in Childhood* 2005; **90**(2): 182-6.
30. Carpenter RF. The prevalence and distribution of bruising in babies. 1999; **80**(4): 363-6.
31. Dunstan FD, Guilda ZE, Kontos K, Kemp AM, Sibert JR. A scoring system for bruise patterns: a tool for identifying abuse. *Archives of Disease in Childhood* 2002; **86**(5): 330-3.
32. Labbé J, Caouette G. Recent skin injuries in normal children. *Pediatrics* 2001; **108**(2): 271-6.
33. Mortimer PE, Freeman M. Are facial bruises in babies ever accidental? *British Medical Journal* 1983; **58**(1): 75-6.
34. Sugar NF, Taylor JA, Feldman KW. Bruises in infants and toddlers: those who don't bruise rarely bruise. *Archives of Pediatrics and Adolescent Medicine* 1999; **153**(4): 399-403.
35. Tush BA. Bruising in healthy 3-year-old children. *Maternal-child nursing journal* 1982; **11**(3): 165-79.

36. Wedgwood J. Childhood bruising. *The Practitioner* 1990; **234**(1490): 598-601.
37. Lynch A. Child abuse in the school-age population. *The Journal of school health* 1975; **45**(3): 141.
38. Worlock P, Stower M, Barbor P. Patterns of fractures in accidental and non-accidental injury in children: a comparative study. *British Medical Journal* 1986; **293**(6539): 100.
39. Atwal GS, Ruttly GN, Carter N, Green MA. Bruising in non-accidental head injured children; a retrospective study of the prevalence, distribution and pathological associations in 24 cases. *Forensic Science International* 1998; **96**(2-3): 215-30.
40. De Silva S, Oates RK. Child homicide--the extreme of child abuse. *The Medical Journal of Australia* 1993; **158**(5): 300.
41. Naidoo S. A profile of the oro-facial injuries in child physical abuse at a children's hospital. *Child abuse & neglect* 2000; **24**(4): 521-34.
42. Barlow B, Niemirska M, Gandhi RP, Leblanc W. Ten years of experience with falls from a height in children. *Journal of pediatric surgery* 1983; **18**(4): 509.
43. Sussman SJ. Skin manifestations of the battered-child syndrome. *The Journal of pediatrics* 1968; **72**(1): 99.
44. Brinkman B, Puschel K, Matzsch T. Forensic dermatological aspects of the battered child syndrome. *Akt Dermatolol* 1979; **5**: 217-32.
45. Cory CZ, Jones MD. Can shaking alone cause fatal brain injury? A biomechanical assessment of the Duhaime shaken baby syndrome model. *Medicine, science and the law* 2003; **43**(4): 317-33.
46. Duhaime AC, Christian CW, Rorke LB. THE SHAKEN-BABY SYNDROME. *Southern Medical Journal* 1998; **91**(11): 1084.
47. Prange MT, Coats B, Duhaime AC, Margulies SS. Anthropomorphic simulations of falls, shakes, and inflicted impacts in infants. *Journal of neurosurgery* 2003; **99**(1): 143.

48. Hrysomallis C. Surrogate thigh model for assessing impact force attenuation of protective pads. *Journal of Science and Medicine in Sport* 2009; **12**(1): 35-41.
49. Desmoulin GT, Anderson GS. Method to investigate contusion mechanics in living humans. *Journal of Forensic Biomechanics* 2011; **2**(online): 1-10.
50. McBrier NM, Neuberger T, Okita N, Webb A, Sharkey N. Reliability and Validity of a Novel Muscle Contusion Device. *Journal of Athletic Training* 2009; **44**(3): 275.
51. Hamdy MK, Kunkle LE, Rheins MS, Deatherage FE. Bruised tissue III. Some factors affecting experimental bruises. *Journal of Animal Science* 1957; **16**(2): 496.
52. Nicholls HR, Lee MH. A survey of robot tactile sensing technology. *The International Journal of Robotics Research* 1989; **8**(3): 3.
53. Lee MH, Nicholls HR. Review Article Tactile sensing for mechatronics—a state of the art survey. *Mechatronics* 1999; **9**(1): 1-31.
54. Shimojo M, Namiki A, Ishikawa M, Makino R, Mabuchi K. A tactile sensor sheet using pressure conductive rubber with electrical-wires stitched method. *IEEE Sensors journal* 2004; **4**(5): 589-96.
55. Ohmura Y, Kuniyoshi Y, Nagakubo A. Conformable and scalable tactile sensor skin for curved surfaces. 2006; 2006. p. 1348-53.
56. Meyer J, Lukowicz P, Troster G. Textile pressure sensor for muscle activity and motion detection. 2006; 2006.
57. Sergio M, Manaresi N, Nicolini M, Gennaretti D, Tartagni M, Guerrieri R. A textile-based capacitive pressure sensor. *Sensor Letters* 2004; **2**(2): 153-60.
58. Inaba M, Hoshino Y, Nagasaka K, Ninomiya T, Kagami S, Inoue H. A full-body tactile sensor suit using electrically conductive fabric and strings. 1996; 1996.
59. Someya T, Sekitani T, Iba S, Kato Y, Kawaguchi H, Sakurai T. A large-area, flexible pressure sensor matrix with organic field-effect transistors for artificial skin applications. *Proceedings of the National Academy of Sciences of the United States of America* 2004; **101**(27): 9966.

60. Dyer C, Connolly M, McFeeley P. The clinical and medical forensics of elder abuse and neglect. In: Statistics CoN, ed. *Elder Mistreatment: Abuse, Neglect, and Exploitation in an Aging America*. Washington DC: National Academy Press; 2003: 339-81.
61. Lachs MS, Pillemer K. Elder abuse. *The Lancet* 2004; **364**(9441): 1263-72.
62. Pierce MC, Kaczor K, Aldridge S, O'Flynn J, Lorenz DJ. Bruising characteristics discriminating physical child abuse from accidental trauma. *Pediatrics* 2010; **125**(1): 67-74.
63. Maguire S, Mann MK, Sibert J, Kemp A. Can you age bruises accurately in children? A systematic review. *Archives of Disease in Childhood* 2005; **90**(2): 187-9.
64. Harris TL, Flaherty EG. Bruises and skin lesions. In: Jenny C, ed. *Child Abuse and Neglect: Diagnosis, Treatment and Evidence*. Canada: Elsevier Saunders; 2011: 237-51.
65. Khair K, Liesner R. Bruising and bleeding in infants and children-a practical approach. *British Journal of Haematology* 2006; **133**(3): 221.
66. Langlois NEI, Gresham GA. The ageing of bruises: A review and study of the colour changes with time. *Forensic Science International* 1991; **50**(2): 227-38.
67. Feldman KW. The bruised premobile infant: should you evaluate further? *Pediatr Emerg Care* 2009; **25**(1): 37-9.
68. Petska HW, Sheets LK, Knox BL. Facial bruising as a precursor to abusive head trauma. *Clinical pediatrics* 2013; **52**(1): 86-8.
69. Kemp C. Child abuse or accident? *AAP News* 1999; **15**(7): 2-d-3.
70. Sheets LK, Leach ME, Koszewski IJ, Lessmeier AM, Nugent M, Simpson P. Sentinel injuries in infants evaluated for child physical abuse. *Pediatrics* 2013; **131**(4): 701-7.
71. Dsouza R, Bertocci G. Design and development of a force sensing skin adapted to a child surrogate to identify potential bruising locations. *TECHNOLOGY* 2014; **02**(01): 49-54.

72. Bertocci G, inventor Soft tissue impact assessment device and system patent US 8292830 B2. 2008 Oct 23, 2012.
73. Thompson A, Bertocci G, Pierce MC. Assessment of injury potential in pediatric bed fall experiments using an anthropomorphic test device. *Accident; analysis and prevention* 2013; **50**: 16-24.
74. Thompson AK, Bertocci GE. Paediatric bed fall computer simulation model development and validation. *Computer methods in biomechanics and biomedical engineering* 2013; **16**(6): 592-601.
75. Prange MT, Luck JF, Dibb A, Van Ee CA, Nightingale RW, Myers BS. Mechanical properties and anthropometry of the human infant head. *Stapp car crash journal* 2004; **48**: 279-99.
76. Coats B, Margulies SS. Potential for head injuries in infants from low-height falls. *Journal of neurosurgery Pediatrics* 2008; **2**(5): 321-30.
77. Maguire S, Mann M. Systematic reviews of bruising in relation to child abuse-what have we learnt: an overview of review updates. *Evidence-based child health : a Cochrane review journal* 2013; **8**(2): 255-63.
78. Kemp AM, Maguire SA, Nuttall D, Collins P, Dunstan F. Bruising in children who are assessed for suspected physical abuse. *Arch Dis Child* 2014; **99**(2): 108-13.
79. Pitone ML, Attia MW. Patterns of injury associated with routine childhood falls. *Pediatr Emerg Care* 2006; **22**(7): 470-4.
80. Thompson A, Bertocci G. Pediatric bed fall computer simulation model: parametric sensitivity analysis. *Medical engineering & physics* 2014; **36**(1): 110-8.
81. Ibrahim NG, Margulies SS. Biomechanics of the toddler head during low-height falls: an anthropomorphic dummy analysis. *Journal of neurosurgery Pediatrics* 2010; **6**(1): 57-68.

APPENDIX A

Commercial Sensor Static Testing

Sensitronics square sensor with green spacers



- Sensor dimensions: 32 mm x 32 mm, Thickness = 0.35 mm
- Resistance Range – 3 M ohms to 0.15 K ohms
- Sensor rise time – 0.1 sec

Static Load (lbs) over 0.75 in ²	Applied Pressure (psi)	Recorded Pressure (psi)	% Error
0.125	0.166	0.0	100.00 %
1.000	1.330	2.0	-50.38 %
3.125	4.166	4.2	-0.82 %
5.125	6.830	6.5	4.83 %
6.125	8.000	7.8	2.50 %
8.125	10.660	10.2	4.32 %

Sensitronics square small sensor



- Sensor dimensions: 12 mm x 14 mm, Thickness = 0.27 mm
- Resistance Range – 3 M ohms to 0.15 K ohms
- Sensor rise time – 0.1 sec

Static Load (lbs) over 0.125 in ²	Applied Pressure (psi)	Recorded Pressure (psi)	% Error
0.125	1	0	100.00 %
1.000	8	4	50.00 %
3.125	25	28	-12.00 %
5.125	41	41	0.00 %
6.125	49	49	0.00 %
8.125	65	50	23.08 %

Sensitronics circular sensor with green spacers



- Sensor dimensions: 35 mm dia.,
Thickness = 0.35 mm
- Resistance Range – Infinite ohms
to 0.5 K ohms
- Sensor rise time – 0.1 sec

Static Load (lbs) over 0.75 in ²	Applied Pressure (psi)	Recorded Pressure (psi)	% Error
0.125	0.166	0.00	100.00 %
1.000	1.330	2.00	-50.38 %
3.125	4.166	5.42	-30.10 %
5.125	6.830	7.00	-2.49 %
6.125	8.000	7.90	1.25 %
8.125	10.660	9.20	13.70 %

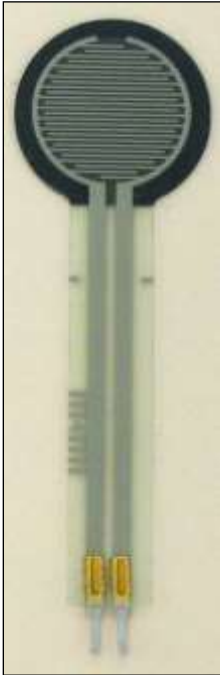
Sensitronics circular sensor small



- Sensor dimensions: 5 mm dia.,
Thickness = 0.55 mm
- Resistance Range – 6.2 M ohms
to 45 K ohms
- Sensor rise time – 0.1 sec

Static Load (lbs) over 0.05 in ²	Applied Pressure (psi)	Recorded Pressure (psi)	% Error
0.125	2.5	0	> 100.00 %
1.000	20.0	0	> 100.00 %
3.125	62.5	65	-4.00 %
5.125	102.0	55	46.08 %
6.125	122.0	110	9.84 %
8.125	162.5	140	13.85 %

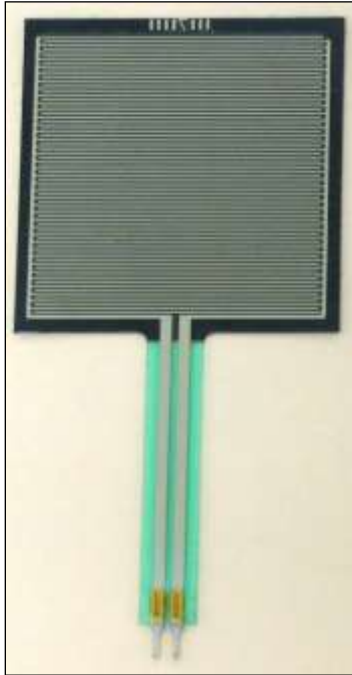
Troseen circular sensor large



- Sensor dimensions: 18.5 mm dia., Thickness = 0.57 mm
- Resistance Range – Infinite ohms to 0.6 K ohms
- Sensor rise time – 0.1 sec

Static Load (lbs) over 0.75 in ²	Applied Pressure (psi)	Recorded Pressure (psi)	% Error
0.125	0.166	0.7	-321.69 %
1	1.33	3.5	-163.16 %
3.125	4.166	8.2	-96.83 %
5.125	6.83	9.4	-37.63 %
6.125	8	9.9	-23.75 %
8.125	10.66	10.6	0.56 %

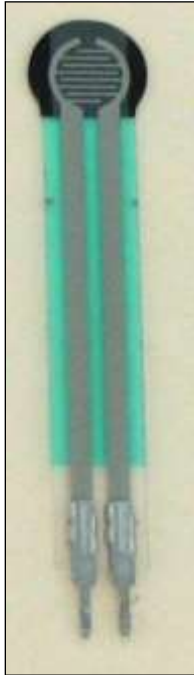
Troseen square sensor



- Sensor dimensions: 43.7 mm x 43.7 mm, Thickness = 0.57 mm
- Resistance Range – Infinite ohms to 125 ohms
- Sensor rise time – 0.1 sec

Static Load (lbs) over 0.75 in ²	Applied Pressure (psi)	Recorded Pressure (psi)	% Error
0.125	0.166	2.2	-1225.30 %
1	1.33	4.2	-215.79 %
3.125	4.166	8.0	-92.03 %
5.125	6.83	9.5	-39.09 %
6.125	8	9.7	-21.25 %
8.125	10.66	10.5	1.50 %

Troseen circular sensor small



- Sensor dimensions: 8 mm diam.,
Thickness = 0.4 mm
- Resistance Range – Infinite ohms
to 2.75 K ohms
- Sensor rise time – 0.1 sec

Static Load (lbs) over 0.12 in ²	Applied Pressure (psi)	Recorded Pressure (psi)	% Error
0.125	1.04	1.4	-34.62 %
1.000	8.33	8.0	3.96 %
2.125	21.87	19.0	13.12 %
3.125	26.00	30.0	-15.38 %
6.125	51.00	37.0	27.45 %
8.125	67.70	37.0	45.35 %

Distance lab square fabric pressure sensor



- Sensor dimensions: 50 mm x 40 mm, Thickness = 4.5 mm
- Resistance Range – Infinite ohms to 4.35 K ohms for single layer of velostat
- Sensor rise time – 0.1 sec

Static Load (lbs) over 0.75 in ²	Applied Pressure (psi)	Recorded Pressure (psi)	% Error
0.125	0.166	1.4	> -100.00 %
1	1.33	2.6	-95.49 %
3.125	4.166	2.6	37.59 %
5.125	6.83	3.0	56.08 %
6.125	8	3.0	62.50 %
8.125	10.66	3.0	71.86 %

APPENDIX B

Dynamic Testing of Commercial Sensors and In-House Milled Sensors

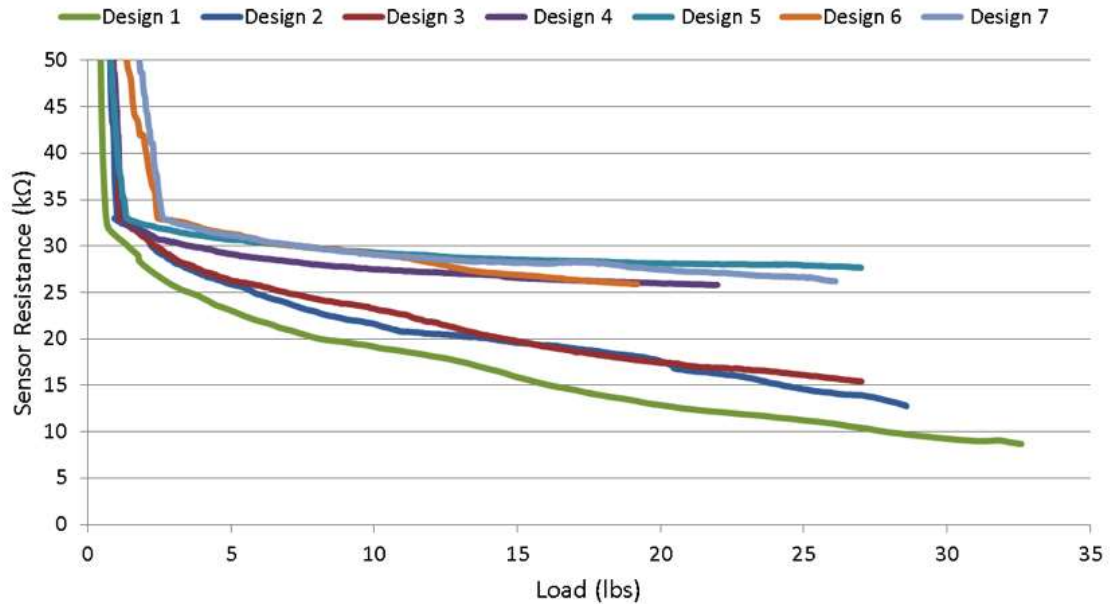


Figure B1. Dynamically applied load versus sensor resistance profiles: in-house milled conductive side different space and trace designs joined with 500 kΩ semi-conductive material. Design 1 (green profile) represents the finest space and trace, while Design 7 (blue profile) represents the coarsest space and trace. Design 1 provided the most desirable response given its ability to output resistances that can be differentiated across the range of loads applied.

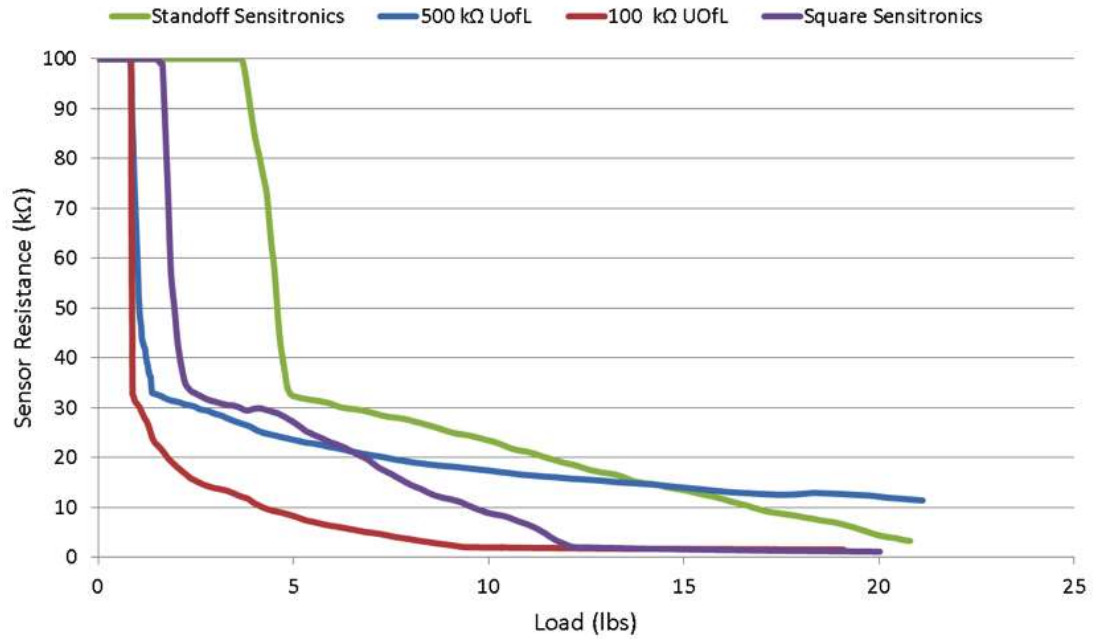


Figure B2. Dynamically applied load versus sensor resistance profiles for select commercial FSR sensors and in-house milled conductive side (U of L; Design 1 – finest space and trace) joined with two different semi-conductive materials. The standoff spacers on the Sensitronics sensor (green profile) enabled the sensor to delay activation upon the application of load.

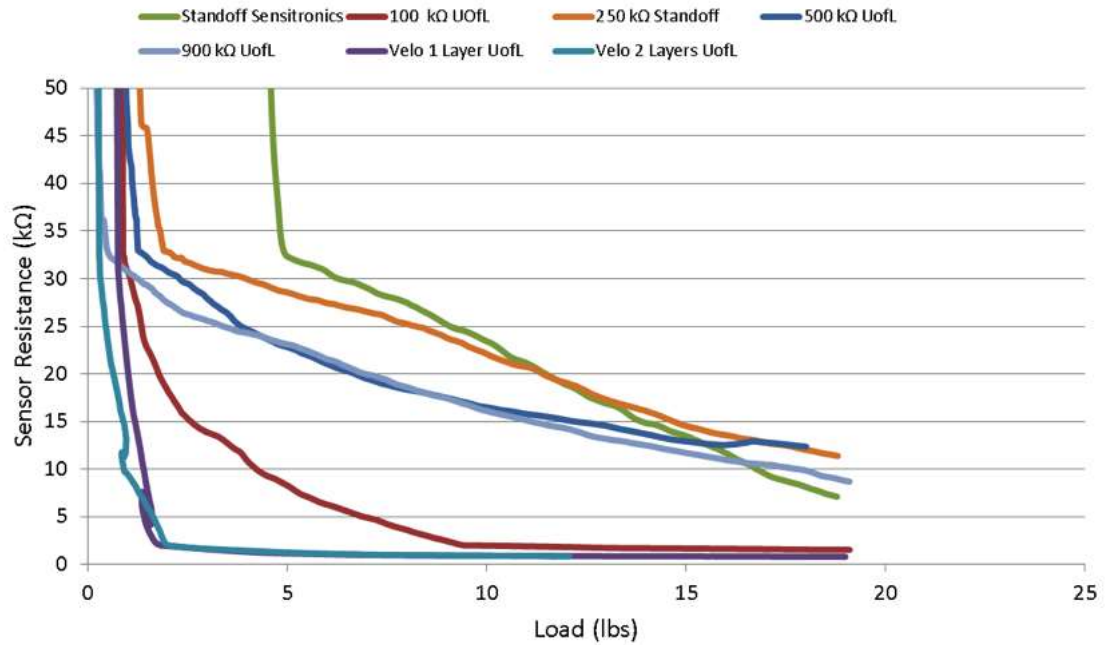


Figure B3. Dynamically applied load versus sensor resistance profiles: semi-conductive materials evaluation when joined with in-house milled conductive side (U of L; Design 1 – finest space and trace) compared to Sensitronics (commercial) sensor with standoff spacers. The 250 K-ohm semi-conductive material produced the most desirable output given its resistance output that can be discriminated across the range of loads applied.

APPENDIX C

Photolithographic Process to Generate Integrated Sensor Matrix

The steps involved in the photolithographic process to create the conductive side of an FSR are as follows:

- Photomask - design and cutting - The photomask consists of a square glass plate that has a film of metal emulsion on one side. The mask is fabricated by means of an electron beam that cuts the metal layer from the glass leaving behind the shape of the design pattern (Figure C1).

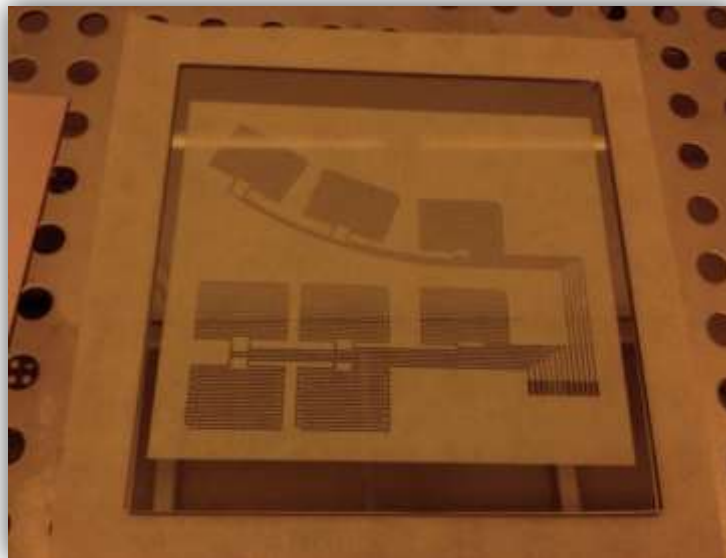


Figure C1: The glass photomask with our forearm sensor matrix pattern.

- Copper substrate – DuPont's Pyralux Copper Clad Laminate – AP9131; double sided, with a dielectric thickness of 3 mil and a copper thickness of 35 μm .
 - Cleaning – The copper substrate was cleaned with acetone to remove any waxes or oils that may be coating the surface.
 - Photoresist application - Shipley 1827 photoresist was applied to the copper substrate using the rotating process to obtain a uniform thickness (Figure D2).



Figure C2: Copper substrate positioned within rotating machine tub after application of the photoresist.

- Soft Baking – The photoresist-coated copper substrate was removed from the rotating device and placed on a hotplate at 115 degrees C for approximately 90 seconds to allow the photoresist coating film to dry (Figure C3).



Figure C3: Photoresist coated copper substrate placed on the hot plate for soft baking.

- Mask alignment and exposure – The copper substrate was aligned with and positioned beneath the photomask, and then exposed to UV radiation for 35 seconds (Figure C4). This process alters the chemical properties of the photoresist that is not protected by the photomask, thereby producing a pattern transfer from the photomask to the photoresist onto the copper substrate.



Figure C4: Glass photomask aligned over the photoresist coated copper substrate prepared for UV exposure.

- Development – The photoresistive layer on the copper substrate was developed using MF-319 developer. The copper substrate is soaked in the developer for approximately 45-50 seconds while constantly agitating the mixture (Figure C5). The substrate was examined after development to ensure that exposed photoresist has been properly developed.

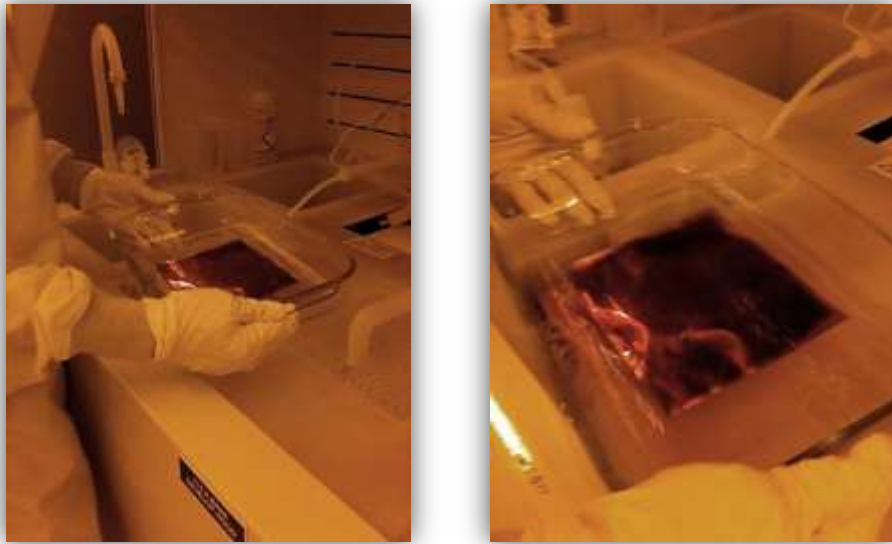


Figure C5: Developing the photoresist using MF-319 developer. The copper substrate is soaked in the developer which removes the photoresist that was exposed to UV light.

- Copper Etching – The copper substrate was then placed in ferric chloride solution (FeCl_3) so as to etch away the copper that was not protected by the photoresist pattern (Figure C6). The FeCl_3 bath had to be constantly agitated and etching times varied from 120 to 150 mins.



Figure C6: Ferric Chloride used for etching the copper clad laminate in the clean room.

It is in this last step of copper etching that we experienced problems with losing portions of the protective photoresist and therefore introducing discontinuity in our pattern. We believe it is the extended time period that it takes this pattern to etch that is responsible for the intermittent loss of pattern in the photoresist. We have attempted to use various methods of reducing the pattern's FeCl exposure time with similar unacceptable results (Figure C7).

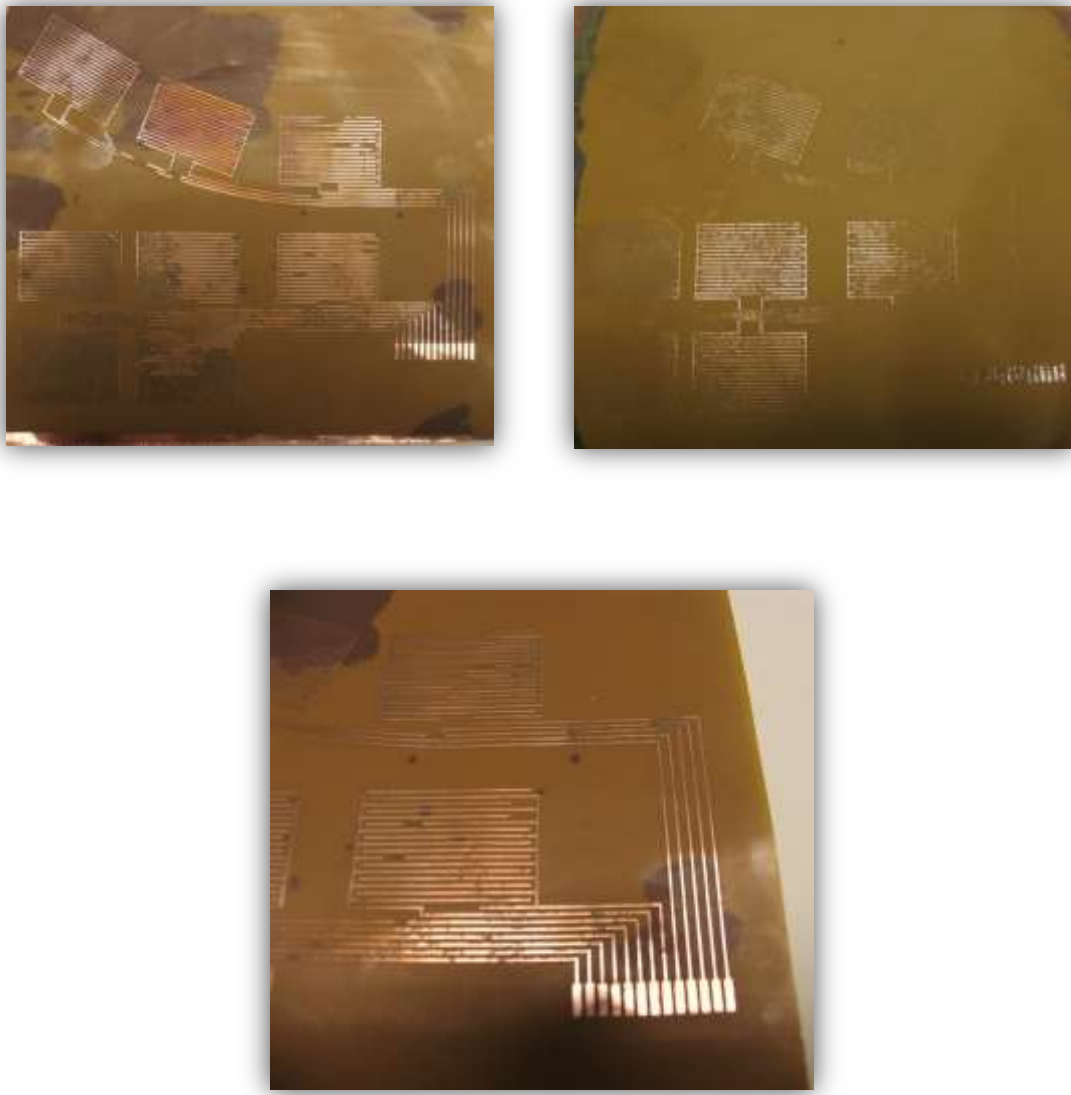


Figure C7: Various trials of etched sensor matrix patterns showing the lack of continuity in some of the traces due to under-etching of copper pattern.

CURRICULCUM VITA

NAME	POSITION TITLE		
<p>Raymond Dsouza, MS raymond.dsouza@louisvilled.edu 502-852-0279</p>	<p>Research Engineer Injury Risk Assessment & Prevention Bldg. B 110 500 S. Preston St Louisville - 40202</p>		
EDUCATION/TRAINING	DEGREE	YEAR(S)	
University of Pune, India Mechanical Engineering	BE	2004	
University of Louisville, KY Mechanical Engineering	MS	2008	
University of Louisville, KY Mechanical Engineering	PhD	2015*	

*Expected graduation date

A. POSITIONS AND HONORS:

Positions and Employment

Jan 2003 – Oct 2004

Stress Analysis Engineer, Onward Technologies Pvt. Ltd., Pune, India

Jan 2005 – July 2005

Quality Engineer, Network Security Solutions Ltd., Pune, India

Sept 2005 – Dec 2005

Student Assistant, Mechanical Engineering Dept., University of Louisville,
Louisville, KY

Aug 2008 – Dec 2008

Forensic Biomechanics Research Assistant, Biomechanical Consultants of California,
Davis, CA

Jan 2006 – Nov 2009

Graduate Research Assistant, Injury Risk Assessment and Prevention
Laboratory (iRAP), University of Louisville, Louisville, KY

Nov 2009 – Current

Research Engineer, Injury Risk Assessment and Prevention Laboratory
(iRAP), University of Louisville, Louisville, KY

Honors

2012 First place poster, Kentucky Innovation & Entrepreneurship Conference,
Louisville, KY

2012 Second place poster, Engineering Exposition, University of Louisville,
Louisville, KY

2008 First place poster, Engineering Exposition, University of Louisville,
Louisville, KY

2007 University of Louisville Fellowship Award

2006 Golden Key International Honor Society

Skills

Computer crash simulation and validation, Dynamic sled testing, Finite element analysis,
Structural dynamics, Motion capture, Kinematics analysis, Design engineering, Data
acquisition design and data analysis, Sensor design and fabrication, System
programming.

Technically skilled in the following software:

Crash Simulation Software: MADYMO, PC Crash, ATB 3i, Dynaman

Solid Modelers: Solid Works, Pro-Engineer, Solid Edge, CATIA V5, AutoCad &
AUTOLISP

System Design/Programming: Labview, Matlab/Simulink, C/C++, Visual C

B. SELECTED PEER-REVIEWED PUBLICATIONS

Peer-reviewed Journal Papers:

1. Dsouza, R., Bertocci, G., Potential bruising patterns associated with rearward falls in children. Under review, Annals of Biomedical Engineering, 2015.
2. Dsouza, R., Bertocci, G., Design and development of a force sensing skin adapted to a child surrogate to identify potential bruising locations. Technology, Vol 02(01): 49, 2014
3. Dsouza R, Bertocci G, Development and Validation of a Computer Crash Simulation Model of an Occupied Adult Manual Wheelchair Subjected to a Frontal Impact. Medical Engineering & Physics, Vol 32(3), 272-279, 2010

Peer-reviewed Conference Proceedings (Select):

1. Dsouza R, Bertocci G, Design and Development of a Surrogate Bruising Detection System to Describe Bruising Patterns in Children, Poster Presentation at the Kentucky Innovation & Entrepreneurship Conference in Louisville, 2012 - Awarded 1st place for best poster presentation
2. Dsouza R, Bertocci G, Design and Development of a Surrogate Bruising Detection System to Describe Bruising Patterns in Children, Poster Presentation at the Engineering Exposition 2012, University of Louisville - Awarded 2nd place for best poster presentation
3. Dsouza R, Bertocci G, Design and Development of a Surrogate Bruising Detection System to Describe Bruising Patterns in Children, presented at the Biomechanics Symposium 2012, Ohio state University
4. McDonnell G, Dsouza R, Bertocci G, Tiernan J, Simms C, The Influence of Pelvic-Belt Angle on Wheelchair Occupant Injury Risk: A Simulation Study, IRCOBI Conference, Trinity College, Dublin, Ireland, Sept 2012
5. McDonnell G, Dsouza R, Bertocci G, Tiernan J, Simms C, The Influence of Shoulder and Pelvic-Belt Floor Anchorage Location on Wheelchair Occupant Injury Risk: A Simulation Study, IRCOBI Conference, Trinity College, Dublin, Ireland, 2013

6. Dsouza R, Bertocci G, Development and Validation of a Computer Crash Simulation Model of an Occupied Adult Manual Wheelchair Subjected to a Frontal Impact, Proceedings of the Annual RESNA 2008 Conference, June 2008
7. Dsouza R, Bertocci G, van Roosmalen L, Effect of Manual Wheelchair Caster Stiffness and Energy Absorption on Wheelchair-Occupant Kinematics during a Frontal Impact, Proceedings of the Annual RESNA 2007 Conference, June 2007
8. Dsouza R, Bertocci G, Wheelchair Seat Loading Associated with a Motor Vehicle Frontal Impact, Poster Presentation at Engineering-Expo, University of Louisville, 2007 – Awarded 1st Place for best poster presentation
9. Dsouza R, Uppal R, Stress Analysis of Housing for Planetary Gear Reduction System of a Tractor, Presented at the Seminar for Mechanical Engineers, India, MESCOE 2004 - 1st Place Winner for best presentation
10. Dsouza R, Lohar T, Design, Classification and Applications of Freewheel Clutches, Presented at the Seminar for Mechanical Engineers, India, MESCOE 2003